BASKENT UNIVERSITY
INSTITUTE OF SCIENCE AND ENGINEERING
DEPARTMENT OF ELECTRICAL AND ELECTRONICS ENGINEERING
MASTER OF SCIENCE IN ELECTRICAL AND ELECTRONICS ENGINEERING

DESIGN OF A FLIGHT TEST INSTRUMENT SYSTEM FOR MEASURING AND ANALYZING OF VIBRATION SIGNALS ON A HELICOPTER

BY

SİNAN AKBAŞ

MASTER OF SCIENCE THESIS

ANKARA – 2025

BASKENT UNIVERSITY
INSTITUTE OF SCIENCE AND ENGINEERING
DEPARTMENT OF ELECTRICAL AND ELECTRONICS ENGINEERING
MASTER OF SCIENCE IN ELECTRICAL AND ELECTRONICS ENGINEERING

DESIGN OF A FLIGHT TEST INSTRUMENT SYSTEM FOR MEASURING AND ANALYZING OF VIBRATION SIGNALS ON A HELICOPTER

BY

SİNAN AKBAŞ

MASTER OF SCIENCE THESIS

ADVISOR

DOÇ. DR. SELDA GÜNEY

ANKARA – 2025

BASKENT UNIVERSITY

INSTITUTE OF SCIENCE AND ENGINEERING

This study which was prepaid by Sinan AKBAŞ, for the program of Master of Science in Electrical and Electronics Engineering, has been approved in partial fulfillment of the requirements for the degree of MASTER OF SCIENCE in Electrical and Electronics Engineering Department by the following committee.

Date of Thesis Defense: 29 / 01 / 2025

Thesis Title: DESIGN OF A FLIGHT TEST INSTRUMENT SYSTEM FOR MEASURING AND ANALYZING OF VIBRATION SIGNALS ON A HELICOPTER

Examining Cımmittee Members	**Signature**
Prof. Dr. Hamit ERDEM, Baskent University	…………………..
Doç. Dr. Selda GÜNEY, Baskent University	…………………..
Dr. Lecturer Member Koray AÇICI, Ankara University	…………………..

APPROVAL

Prof. Dr. DİLEK ÇÖKELİLER SERDAROĞLU

Director, Institute of Science and Engineering

Date : … / … / 2024

BAŞKENT ÜNİVERSİTESİ

FEN BİLİMLER ENSTİTÜSÜ

YÜKSEK LİSANS TEZ ÇALIŞMASI ORİJİNALLİK RAPORU

Tarih: 29/01/2025

Öğrencinin Adı, Soyadı: Sinan AKBAŞ

Öğrencinin Numarası: 22120194

Anabilim Dalı: Elektrik-Elektronik Mühendisliği Anabilim Dalı

Programı: Elektrik-Elektronik Mühendisliği Yüksek Lisans Programı

Danışmanın Unvanı/Adı, Soyadı: Doç. Dr. Selda GÜNEY

Tez Başlığı: Helikopterdeki Titreşim Sinyallerinin Ölçülmesi ve Analizi için Uçuş Test Cihazı Tasarımı

Yukarıda başlığı belirtilen Doktora tez çalışmamın; Giriş, Ana Bölümler ve Sonuç Bölümünden oluşan, toplam 105 sayfalık kısmına ilişkin, 29/01/2025 tarihinde tez danışmanım tarafından Turnitin adlı intihal tespit programından aşağıda belirtilen filtrelemeler uygulanarak alınmış olan orijinallik raporuna göre, tezimin benzerlik oranı % 15'dir. Uygulanan filtrelemeler:

1. Kaynakça hariç
2. Alıntılar hariç
3. Beş (5) kelimeden daha az örtüşme içeren metin kısımları hariç

"Başkent Üniversitesi Enstitüleri Tez Çalışması Orijinallik Raporu Alınması ve Kullanılması Usul ve Esaslarını" inceledim ve bu uygulama esaslarında belirtilen azami benzerlik oranlarına tez çalışmamın herhangi bir intihal içermediğini; aksinin tespit edileceği muhtemel durumda doğabilecek her türlü hukuki sorumluluğu kabul ettiğimi ve yukarıda vermiş olduğum bilgilerin doğru olduğunu beyan ederim.

Öğrenci İmzası: ………………….

ONAY

Tarih: 29/01/2025

Öğrenci Danışmanı

Doç. Dr. Selda GÜNEY

ACKNOWLEDGEMENTS

I would like to thank Deico Engineering, which made a great contribution to the emergence of this thesis, and I would like to express my sincere gratitude to Assoc. Dr. Selda Güney.

ÖZET

Sinan AKBAŞ

HELİKOPTERDEKİ TİTREŞİM SİNYALLERİNİN ÖLÇÜLMESİ VE ANALİZİ İÇİN UÇUŞ TEST CİHAZI TASARIMI

Başkent Üniversitesi Fen Bilimleri Enstitüsü

Elektrik-Elektronik Mühendisliği Anabilim Dalı

2025

Uçak titreşimlerinin sağlığı ve izlenmesi güvenlik açısından çok önemlidir. Güvenli uçuşu sürdürmek için helikopter titreşim seviyelerinin minimumda tutulması gerekir. Bu nedenle titreşim sinyali analizi ve titreşim seviyelerini ölçen sistemler aviyonik sektöründe oldukça önemli konulardır.

Bu tez kapsamında veri toplama amaçlı Uçuş Test Cihazı (UTC) sistemi tasarlanmıştır. Tasarlanan UTC sistemi güç modülü, denetleyici modülü, analog giriş modülü ve arka panel modülünden oluşmaktadır. Güç modülü, giriş gücünü sistem gereksinimlerine göre istenilen seviyelere dönüştürür. Denetleyici modülü, üzerinde FPGA bulunması nedeniyle hesaplamalardan ve iletişimden sorumludur. Analog giriş modülü, sensörlerle arayüz oluşturmaktan, sinyal koşullandırmadan ve titreşim sinyallerinin örneklenmesinden sorumludur. Arka panel tüm modülleri bir araya getirecek şekilde tasarlanmıştır.

Çalışma aynı zamanda titreşim sinyali analizini de içermektedir. Titreşim seviyesini ve fazını belirlemek için farklı yaklaşımlar yapıldı. Öncelikle titreşim büyüklüğünün belirlenmesi için FFT uygulaması yapılmış, faz hesaplaması için ise çeşitli dijital filtreler tasarlanarak sisteme uygulanmıştır. Geliştirilen algoritmalar laboratuvar ortamında sabit titreşim üreteci cihazı ile doğrulanmış, daha sonra titreşim seviyesini ölçmek için helikopterden ölçümler yapılmıştır. Sonuçların karşılaştırılması amacıyla helikopter deneylerinde hazır raf (COTS) cihazı kullanılmış olup, sonuçlar ve karşılaştırmalar paylaşılmıştır. Daha sonra çeşitli makine öğrenme algoritmaları (SVM, GPR, doğrusal regresyon vb. gibi) titreşimin hem büyüklüğü hem de faz tahmini için eğitilmiştir. Bu algoritmalar için simülasyon sonuçları paylaşılmış ve değerlendirilmiştir.

ANAHTAR KELİMELER: Sinyal işleme, Makine öğrenmesi, Donanım tasarımı, Uçuş test cihazı, Algoritma geliştirme, Titreşim sinyalleri.

ABSTRACT

Sinan AKBAŞ

DESIGN OF A FLIGHT TEST INSTRUMENT SYSTEM FOR MEASURING AND ANALYZING OF VIBRATION SIGNALS ON A HELICOPTER

Baskent University Science Institute

Electrical and Electronics Engineering

2025

Health and monitoring of aircraft vibrations are crucial to safety. To maintain safe flying, helicopter vibration levels should be kept at a minimum. Therefore, vibration signal analysis and systems that measure vibration levels are very important topics in the avionics industry.

In the scope of this thesis, Flight Test Instrument (FTI) system is designed for data acquisition purposes. Designed FTI system consists of power module, controller module, analog input module and backplane module. The power module converts input power to desired levels according to system requirements. The controller module is responsible for calculations and communication due to having an FPGA on board. The analog input module is responsible for interfacing with the sensors, signal conditioning, and sampling the vibration signals. The backplane is designed for combining all the modules together.

The study also contains vibration signal analysis. In order to determine the vibration level and phase different approaches were made. First of all, for determining vibration magnitude, FFT implementation has been made, and for the phase calculation several digital filters were designed and implemented into the system. Algorithms that are developed have been verified in laboratory environments with a constant vibration generator device then measurements from a helicopter had been taken in order to measure the vibration level. To compare the results a commercial of the shelf (COTS) device was used in helicopter experiments and the results and comparisons have been shared. Afterward, several machine learning algorithms (such as SVM, GPR, linear regression etc.) are trained for vibration both magnitude and phase prediction. Simulation results have been shared and evaluated for these algorithms.

KEYWORDS: Signal Processing, Machine Learning, Hardware Design, Flight Test Instrument, Algorithm Development, Vibration Signals.

TABLE OF CONTENTS

ACKNOWLEDGEMENT i
ÖZET ii
ABSTRACT iv
TABLE OF CONTENTS vi
TABLE OF TABLES viii
TABLE OF FIGURES ix
SYMBOLS AND ABBREVIATIONS xiii
1. INTRODUCTION 1
1.1. Thesis Outline 3
2. RELATED WORKS 6
3. MATERIALS AND METHODS 9
3.1. SENSORS 9
3.2. ANALOG INPUT MODULE 11
3.2.1. Signal conditioning and AA filter block 11
3.2.2. ADC Block 40
3.2.3. FPGA block 56
3.3. CONTROLLER MODULE 61
3.3.1. Communication interfaces and module features 61
3.4. Power Module 64
3.4.1. Power requirements of system 64
3.4.2. Designed power module specifications 65
3.5. Implementation Of Digital Design, Software and Algorithms on FPGA 66
3.5.1. Signal processing algorithms 66
3.5.2. Regression methods 69
3.5.3. Programmable logic side 73
3.5.4. Processing Subsystem Side 74
3.5.5. Experimental setup 74
4. DISCUSSION AND RESULTS 85
4.1. Result of Signal Processing Algorithms 85
4.1.1. Case 1: Result of lab device studies 85

4.1.2. Case 2: Result of helicopter studies..87
4.2. Result of Machine Learning Algorithms..89
4.2.1. Case 1: Result of lab device studies..89
4.2.2. Case 2: Result of helicopter studies..93
5. CONCLUSION AND FUTURE WORK 103
REFERENCES..105

TABLE OF TABLES

Page

Table 4.1. Result of Vibration Signal of Lab Device 85
Table 4.1. Continues 86
Table 4.1. Continues 87
Table 4.2. Horizontal Vibration Measurement on Helicopter Taken from Designed FTI System 88
Table 4.3. Horizontal Vibration Measurement Taken from COTS Device 88
Table 4.4. Vertical Vibration Measurement Taken from Designed FTI System 89
Table 4.5. Vertical Vibration Measurement Taken from COTS Device 89
Table 4.6. Vibration Magnitude Results of the Trained Models 90
Table 4.7. Vibration Phase Results of the Trained Models 91
Table 4.8. Helicopter Measurement Vibration Magnitude Results Due to Lab Device Data Training 94
Table 4.9. Helicopter Measurement Vibration Phase Results Due to Lab Device Data Training 95
Table 4.10. Helicopter Measurement Vibration Magnitude Results Due to New Trained Model Including Helicopter Data 96
Table 4.11. Helicopter Measurement Vibration Phase Results Due to New Trained Model Including Helicopter Data 97
Table 4.12. Specification Comparision Between COTS device and Designed FTI System ... 100

TABLE OF FIGURES

Page

Figure 1.1. Signal Processing Overview 5
Figure 1.2. Machine Learning Overview...5
Figure 2.1. Data Acquisition Stages 6
Figure 2.2. Classification of Different Signal Processing Algorithms Used in Vibration Signal Analysis 7
Figure 3.1. Block Diagram of Overall System Overview 9
Figure 3.2. Analog Input Module Block Diagram 11
Figure 3.3. Data Flow Chart 12
Figure 3.4. RC Low Pass Filter 12
Figure 3.5. Simple Active Filter 13
Figure 3.6. RC and RL Passive Filter 14
Figure 3.7. RC and RL High Pass Filter 15
Figure 3.8. Series and Parallel Resonant Band Pass Filter 16
Figure 3.9. Series and Parallel Resonant Band Stop Filter 16
Figure 3.10. Active Filter Circuitry 17
Figure 3.11. Fourth Order Two Stages Butterworth Low Pass Filter with 0 dB Gain 19
Figure 3.12. Magnitude Response of Fourth Order Two Stages Butterworth Low Pass Filter.20
Figure 3.13. Phase Response of Fourth Order Two Stages Butterworth Low Pass Filter[.......20
Figure 3.14. Phase Delay of Fourth Order Two Stages Butterworth Low Pass Filter 21
Figure 3.15. Fourth Order Two Stages Butterworth Low Pass Filter with 10 dB Gain 21
Figure 3.16. Magnitude Response of Fourth Order Two Stages Butterworth Low Pass Filter with 10 dB Gain 22
Figure 3.17. Phase Response of Fourth Order Two Stages Butterworth Low Pass Filter with 10 dB Gain 22
Figure 3.18: Phase Delay of Fourth Order Two Stages Butterworth Low Pass Filter with 10 dB Gain...23
Figure 3.19. Third Order Two Stages Chebyshev Low Pass Filter 25
Figure 3.20. Magnitude Response of Third Order Two Stages Chebyshev Low Pass Filter 25
Figure 3.21. Phase Response of Third Order Two Stages Chebyshev Low Pass Filter 26

Figure 3.22. Phase Delay of Third Order Two Stages Chebyshev Low Pass Filter..................26
Figure 3.23. Magnitude Response of Third Order Two Stages Chebyshev Low Pass Filter with 10 dB Gain 27
Figure 3.24. Phase Response of Third Order Two Stages Chebyshev Low Pass Filter with 10 dB Gain 27
Figure 3.25. Phase Delay of Third Order Two Stages Chebyshev Low Pass Filter with 10 dB Gain..28
Figure 3.26. Sixth Order Three Stages Bessel Low Pass Filter with 0 dB Gain 30
Figure 3.27. Magnitude Response of Sixth Order Three Stages Bessel Low Pass Filter with 0 dB Gain 30
Figure 3.28. Phase Response of Sixth Order Three Stages Bessel Low Pass Filter with 0 dB Gain..31
Figure 3.29. Phase Delay of Sixth Order Three Stages Bessel Low Pass Filter with 0 dB Gain 31
Figure 3.30. Sixth Order Three Stages Bessel Low Pass Filter with 10 dB Gain 32
Figure 3.31. Magnitude Response of Sixth Order Three Stages Bessel Low Pass Filter with 10 dB Gain 32
Figure 3.32. Phase Response of Sixth Order Three Stages Bessel Low Pass Filter with 10 dB Gain..33
Figure 3.33. Phase Delay of Sixth Order Three Stages Bessel Low Pass Filter with 10 dB Gain 33
Figure 3.34. Ideal Continuous to Discrete Time Converter C/D..35
Figure 3.35. Sampled Discrete x[n] of x(t) 35
Figure 3.36. A Original Signal's Spectrum 37
Figure 3.37. B Spectrum of Impulse Train (Sampling Function) 37
Figure 3.38. C Sampled Signal’s Spectrum with $\Omega s > 2\Omega N$ 38
Figure 3.39. D Sampled Signal’s Spectrum with $\Omega s < 2\Omega N$ 38
Figure 3.40. Designed 10th Order 5 Stage Butterworth Low Pass Filter with 10kHz Cut off, stop band at 20kHz with a -60dB gain 39
Figure 3.41. Magnitude Response of Designed Butterworth Filter 39
Figure 3.42. Phase Response of Designed Butterworth Filter...40

Figure 3.43. ADC Architectures, Resolution, Sample Rates and Applications 41
Figure 3.44. Basic Successive Approximation (SAR) ADC Block Diagram 42
Figure 3.45. Typical Timing Diagram of the SAR ADC [17]...43
Figure 3.46. Algorithm of Successive Approximation ADC Explained with Binary Weighing 44
Figure 3.47. Modern SAR ADC Block Diagram 45
Figure 3.48. Effects of the Four Different Concepts That is Taken Advantage of by the Sigma-Delta ADCs 46
Figure 3.49. First Order Sigma-Delta ADC 47
Figure 3.50. Second Order Sigma-Delta Modulator and Comparison of Noise Characteristics 48
Figure 3.51. 6-bit Subranging ADC Block Diagram 49
Figure 3.52. Missing Codes Caused by Non-Linear N1 sub-ADC or Mismatch at the Gain Stage of the Architecture 50
Figure 3.53. Basic Block Diagram of the 6-bit Subranging ADC with Error Correction 51
Figure 3.54. Block Diagram of Pipelined Architecture with Error Correction Logic 52
Figure 3.55. Timing of a pipelined ADC with 65 MSPS Sampling Rate................................53
Figure 3.56. Passband Response of ADS1278 55
Figure 3.57. TDM Mode All Channels Enabled 56
Figure 3.58. Internal Structure of the FPGA 57
Figure 3.59. ZYNQ 7000 Architecture...59
Figure 3.60. Pseudo Code of Measuring and Analysis Process 60
Figure 3.61. Block Diagram of Communication Interfaces 61
Figure 3.62. Block Diagram of Ethernet Interface 62
Figure 3.63. Communication Data Flow Chart Between the Modules and Host PC 64
Figure 3.64. Magnitude Response of Digital Lowpass Filter...68
Figure 3.65. Group Delay of Digital Lowpass Filter...69
Figure 3.66. Constant Vibration Generator 75
Figure 3.67. Top View Constant Vibration Generator 76
Figure 3.68. Raw Data of the Vibration Signal 77
Figure 3.69. Vibration Signal in Frequency Domain 78

Figure 3.70. Filtered Signal 79
Figure 3.71. Velocimeter Raw Data Taken from Helicopter 80
Figure 3.72. Designed Digital Bandpass Filter for Helicopter 81
Figure 3.73. Group Delay of Digital Filter for Helicopter 82
Figure 3.74. Filtered Vibration Signal of Helicopter 83
Figure 3.75. FFT Plot of Aircraft Measurement 84
Figure 4.1. MSE, RMSE and MAE of Trained Models Case 1 92
Figure 4.2. Predicted vs Actual Graph of Matern 5/2 GPR for the Trained Model of Magnitude Prediction 92
Figure 4.3. Predicted vs Actual Graph of Exponential GPR for the Trained Model of Phase Prediction 93
Figure 4.4. MSE, RMSE and MAE of Trained Models Case 2.1 95
Figure 4.5. MSE, RMSE and MAE of Trained Models Case 2.2 97
Figure 4.6. Predicted vs Actual Graph of Rational Quadratic GPR for the Trained Model of Magnitude Prediction 98
Figure 4.7. Predicted vs Actual Graph of Matern 5/2 GPR for the Trained Model of Phase Prediction 98
Figure 4.8. Balance Chart of a Helicopter 100
Figure 4.9. Designed FTI System 101
Figure 4.10. Designed FTI System Overview 102

SYMBOLS AND ABBREVIATIONS

AA	Anti-Aliasing
ADC	Analog to Digital Converter
AMD	Advance Micro Devices
BW	Band Width
C/D	Continuous to Discrete
CH	Channel
CMOS	Complementary Metal Oxide Semiconductor
COTS	Commercial Of The Shelf
DAC	Digital to Analog Converter
DAQ	Data Acquisition
dB	Decibel
DC	Direct Current
DFT	Discrete Fourier Transform
DSP	Digital Signal Processing
EEPROM	Electrically Erasable Programmable Read Only Memory
FFT	Fast Fourier Transform
FIFO	First In First Out
FIR	Finite Impulse Response
FPGA	Field Programmable Gate Array
FTI	Flight Test Instrument
GPR	Gaussian Process Regression
HHT	Hilbert Huang Transform
IC	Integrated Circuit
IDE	Integrated Development Environment
IIR	Infinite Impulse Response
IPS	Inch Per Second
JTAG	Joint Test Application Group
KSPS	Kilo Sample Per Second
LDV	Lazer Doppler Velocimeter
MAE	Mean Absolute Error
MCU	Micro Controller Unit
MDI	Medium Dependent Interface
MEMS	Micro Electromechanical System
MSB	Most Significant Bit
MSE	Mean Square Error
MSPS	Mega Sample Per Second
PC	Personal Computer
PCM	Pulse Code Modulation
PL	Programmable Logic
PS	Processing Subsystem
PSD	Power Spectral Density
RGMII	Reduced Gigabit Media Independent Interface
RMSE	Root Mean Square Error

RMS	Root Mean Square
RPM	Revolutions Per Minute
SAR	Successive Approximation
SHA	Sample and Hold
SOC	System On Chip
SPI	Serial Peripheral Interface
SVM	Support Vector Machine
STFT	Short Time Fourier Transform
TCP/IP	Transmission Control Protocol / Internet Protocol
VHDL	Very High-Speed Integrated Circuit Hardware Description Language
WT	Wavelet Transform
WVD	Wigner Ville Distribution

1. INTRODUCTION

Vibration can be described as a mechanical phenomenon characterized by oscillatory motion around a reference point or equilibrium position. It is created by involving the repetitive back-and-forth movement of an object or system about a central point or axis. This motion can occur in various forms, including linear (straight-line), rotational (circular), or a combination of both.

Vibration can reveal in different frequencies, amplitudes, and directions, depending on the nature of the system generating it. It can be caused by external forces acting on a system, internal mechanical or structural properties, or interactions between components within the system.

In engineering and physics, vibration is studied extensively because the performance, stability, and reliability of mechanical systems are affected by vibration enormously. It can have both beneficial and detrimental effects depending on the context [1]:

- **Beneficial Effects:** In some cases, controlled vibration is desirable and can serve useful purposes. For example, vibration is utilized in machinery such as engines, turbines, and pumps to facilitate proper functioning, enhance efficiency, and prevent stalling or resonance.
- **Detrimental Effects:** Excessive or uncontrolled vibration can be problematic and lead to various issues, including mechanical wear, fatigue, instability, and structural damage. In applications such as aerospace, automotive, and manufacturing, minimizing unwanted vibration is crucial for the safety, performance, and longevity of equipment.

Understanding the causes and characteristics of vibration, as well as techniques for its analysis, control, and mitigation, is essential for engineers and designers across numerous industries to ensure the reliability and efficiency of mechanical systems [2].

The long-term negative impact of vibration on machines can be significant and can lead to several detrimental consequences, including;

- **Mechanical Wear and Fatigue:** The wear and tear of machine components such as bearings, gears, shafts, and other moving parts can be accelerated by continuous vibration. This mechanical wear can lead to increased friction, surface damage, and ultimately, component failure due to fatigue.
- **Reduced Operational Life Span:** The cumulative effects of vibration-induced wear and fatigue can significantly shorten the operational lifespan of machines. Components may fail prematurely, necessitating frequent repairs or replacements, which can increase maintenance costs and downtime.
- **Decreased Efficiency and Performance:** Vibrations can impair the efficiency and performance of machines by causing misalignments, imbalances, and loss of precision in moving parts. This can lead to decreased productivity, energy inefficiency, and compromised output quality in manufacturing processes.
- **Structural Damage and Deterioration:** Excessive vibration can cause structural damage to machine frames, housings, and support structures. Over time, this can lead to cracks, deformation, or other forms of deterioration, compromising the overall integrity and safety of the equipment.
- **Safety Hazards:** Vibrations can create safety hazards for operators and nearby personnel, particularly in high-risk environments such as construction sites, industrial facilities, or transportation vehicles. Uncontrolled vibration can cause machinery to malfunction, leading to accidents, injuries, or even fatalities.
- **Environmental Impacts:** Vibrations transmitted through the ground or surrounding structures can also have environmental impacts, such as noise pollution or structural vibrations that affect nearby buildings or infrastructure.
- **Increased Maintenance Costs:** Dealing with the consequences of vibration-related damage requires regular maintenance, inspections, and repairs, all of which incur additional costs for equipment owners and operators. Addressing vibration issues proactively through preventive maintenance measures can help mitigate these costs in the long run.

Overall, the long-term negative impact of vibration on machines underscores the importance of implementing effective vibration monitoring, control, and mitigation strategies to maintain equipment reliability, safety, and longevity. This includes measures such as proper machine design, maintenance of optimal operating conditions, periodic inspections, and the use of vibration isolation or damping techniques where applicable.

Flight test instrumentation, on the other hand, is known as a system of sensors and equipment mounted on aircraft. Data collection during test flights is its goal. Instrumentation used in flight tests is crucial to the creation of new aircraft models. New aircraft must be tested before they can be certified. This testing procedure includes the use of flight test equipment [3].

Sensors are one of the many parts that make up flight test equipment. Transducers and other sensors are positioned throughout the aircraft. Airspeed, altitude, temperature, pressure, acceleration, vibration, and structural strain are among the factors that they are intended to assess in relation to flight [4].

Flight test instrumentation consists of sensors and a data acquisition system. This is basically the instrumentation system's brain for a flying test. The data acquisition system transforms the data as the sensors gather it. Data from the sensors is converted into a digital representation by the data acquisition system. After the data is in a digital format, the data acquisition system will either store it locally or send it to a remote destination [3].

After clarifying the vibration and its long-term negative effects on machines also, the flight test instrument systems, in this thesis, will be focused on helicopter vibration sources and its measurement and detection techniques.

1.1. Thesis Outline

FTI (Flight Test Instruments) systems are basically measurement and data acquisition devices that are used in avionic vehicles. The main purpose of these systems; is monitoring and recording specific data in the field of production, maintenance, and repair processes. In order to do so, FTI systems contain a lot of transducers, and sensors such as; air pressure sensors, velocity meters, accelerometers, fuel pressure sensors, cameras, etc.

The main compound of the FTI system is the data acquisition unit. This part of the system contains a lot of analog circuitry and analog to digital converter (ADC) channels in order to sample and monitor the desired data. Therefore, in data acquisition (DAQ) units there are several types of signal conditioning and filtering circuitries for each different type of sensor.

After the desired data is conditioned and sampled by analog circuitry, it is fed through to the digital part of the system which is the controller unit of the FTI system. The controller unit of the system mostly contains FPGA-based (Field Programmable Gate Array) designs but when the older designs are analyzed, one can see that it was common to use MCU-based (Micro Controller Unit) controller designs.

The last but essential part of the FTI System is the power modules. All the transducers, sensors, DAQ modules, and controller units require different levels of power trials in order to perform their duties. The avionic vehicle environment is very noisy due to different complex devices and mechanical structures. FTI power modules are obligated to supply clean power to the other compounds of the FTI systems [4].

In the concept of the thesis, an FTI system consisting of the power module, analog input module, controller module and backplane module to bring them all together is designed. Afterward, signal processing algorithms for vibration level and phase detection are developed and implemented on the designed system.

Finally, machine learning algorithms are used in MATLAB environment to compare with the signal processing algorithms. Comparison is done due to evaluation metrics such as; RMSE (Root Mean Square Error), MSE (Mean Square Error) and MAE (Mean Absolute Error).

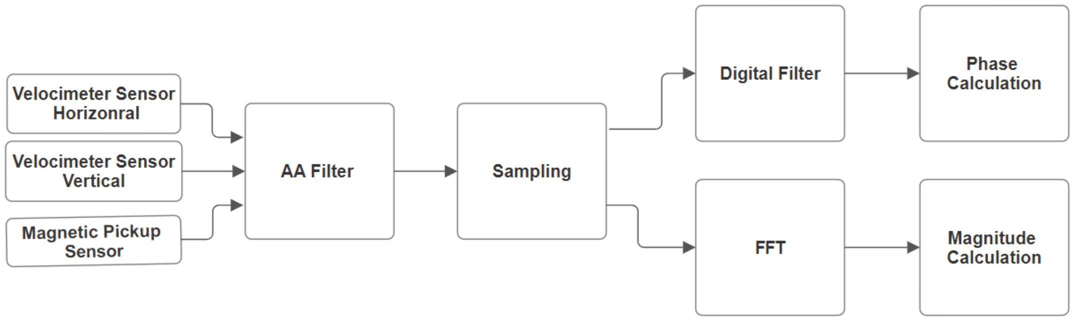

Figure 1.1: Signal Processing Overview

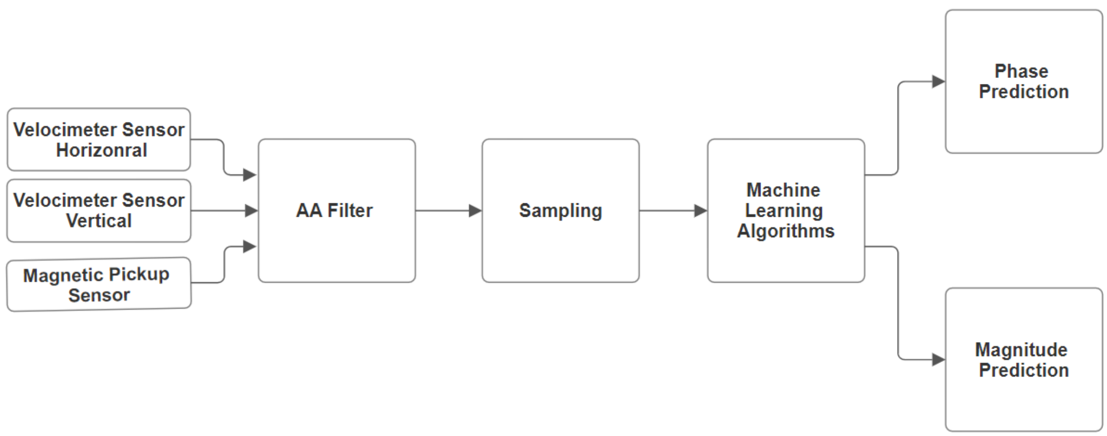

Figure 1.2. Machine Learning Overview

2. RELATED WORKS

The main purpose of the vibration signal analysis is to prevent the failure of the mechanical components. While operating a motion most of the mechanical parts are faced with vibration especially systems that include motors and rotors. Due to this reasoning, a lot of studies have been made in the area of vibration monitoring and vibration signal level detection. Therefore, there are different approaches for determining the vibration level.

In the research of Mohamad Hazwan, Mohd Ghazali, and Wan Rahiman, they summarized the sensor types, data acquisition device features, and also signal processing algorithms that are essential to determine the vibration and analyze the vibration signal. The data acquisition device and vibration signal analyzer concept are given as a block diagram as follows;

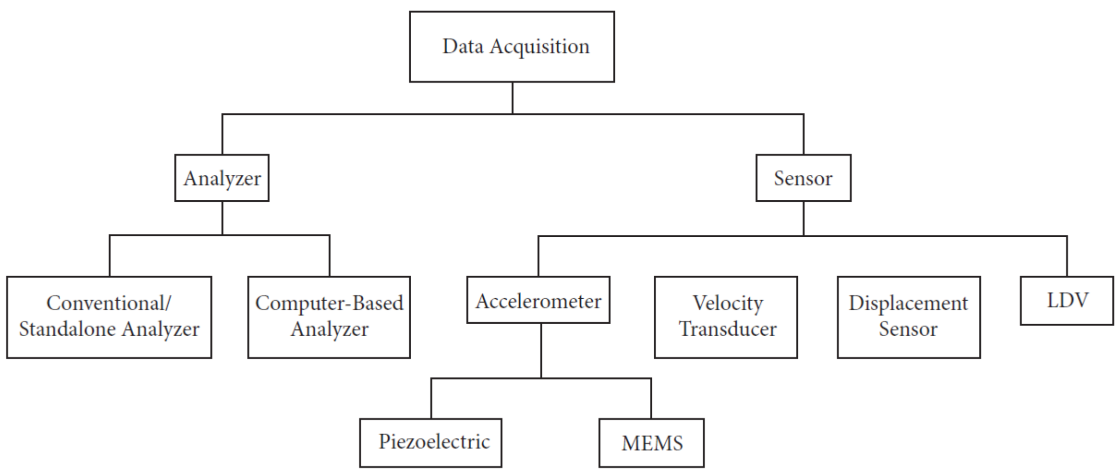

Figure 2.1. Data Acquisition Stages [5]

Vibration signals can be sampled by using different types of sensors. The sensor selection depends upon design requirements. Sensor types used in vibration signal analysis convert mechanical information into electrical signals. The research states that four types of sensors can be used for vibration analysis which are accelerometers, velocimeters, displacement sensors, and laser Doppler velocimeters (LDV). Then, an analyzer device is necessary according to the selected sensor type. An analyzer device is a device that contains amplifiers, filters, and ADCs. Data passes through analog circuitry in order to be sampled and fed through the processing unit. After the data acquisition, vibration signals should be analyzed and feature extractions must be done due to different algorithms. In this research, different types of signal processing algorithms are discussed. The classification of signal processing algorithms is shown below;

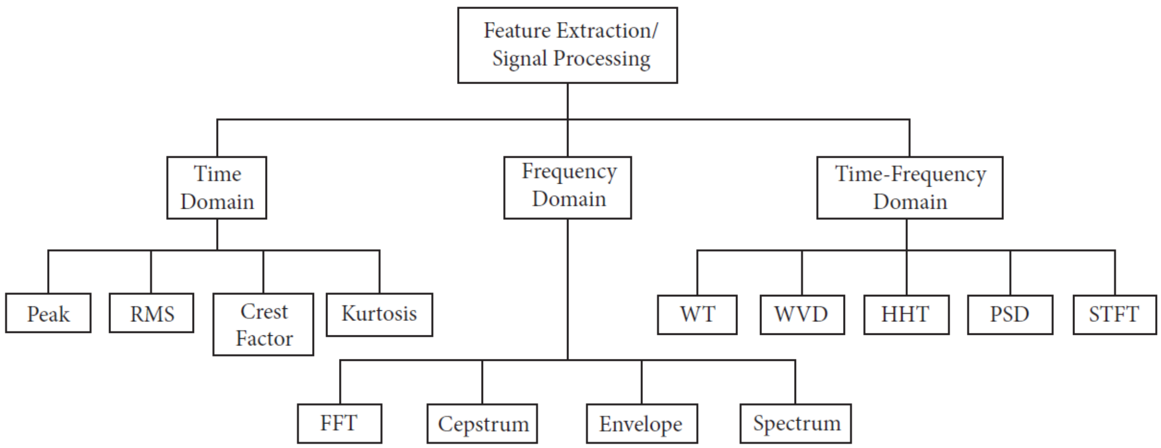

Figure 2.2. Classification of Different Signal Processing Algorithms Used in Vibration Signal Analysis [5]

They have researched more than 100 articles to gather different approaches together and determine which type of algorithm, sensor or device is better in which condition [5].

In the book Vibration Signal Analysis Techniques by Donald R. Houser, mechanical phenomena of vibration and vibration signal detection techniques are given in detail. For the time domain analysis, the book suggests; mean square values, probability density function, correlation function and time averaging methods for diagnostics. For the frequency domain analysis, the book suggests; power spectral density, cross-power spectral density and spectral correlation. In the digital domain, book suggests FFT implementation for vibration signals [1].

Another research was done by combining FFT and DWT (Discrete Wavelet Transform) on an FPGA-based signal processing unit. The idea behind this implementation is to make use of features of both FFT and DWT. Since FFT can predict the exact frequency of the periodic vibration, the specific band of frequency can be examined by DWT. In this study, besides the vibration signal fault on the rotating motor also wanted to be determined. Due to this concern, time domain analysis is implemented for vibration magnitude detection, FFT analysis is implemented to acknowledge vibration increase at a certain frequency, DWT analysis is implemented for the detection of a motor with two broken bars and lastly, FFT and DWT combined analysis is implemented on FPGA based signal processing unit for detecting other faults besides increase in vibration levels [7].

In this study, the FFT approach is used to determine the magnitude of the vibration level. In helicopters, the vibration signal is periodic and occurs at the frequency of the RPM of the rotor. For the phase calculation of the vibration signal time domain analysis is conducted due its simplicity and fitness of the application. After implementing these algorithms on an FPGA-based data acquisition device which is also designed for this thesis study, machine learning algorithms will be evaluated with compared to signal processing algorithms.

3. MATERIALS AND METHODS

In this part of the thesis, sensors that is used for vibration data sampling, designed FTI system and its specifications, developed algorithms and their implementations are given in detail. As it can be seen from the Figure 4.1, two types of sensor are used for data collection: the first sensor type is velocimeter which is used for both vertical and horizontal vibration and the second sensor type that is used is magnetic pick-up. Magnetic pick-up is used for tracking the vibration signal's period. These sensors are interfacing with the analog input module's channels. After data is being sampled by ADC, then digital data is sent to controller module in order to been processed and analyzed. After the vibration signal's magnitude and phase values are extracted from raw signal, these values are sent to user PC via ethernet interface.

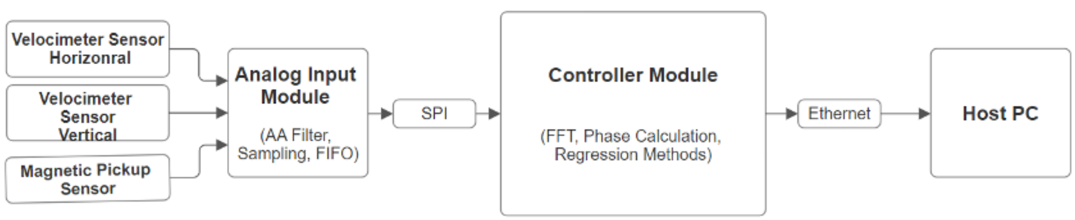

Figure 3.1. Block Diagram of Overall System Overview

3.1. Sensors

To make it clearer, the sensor types that are used in the system and their functions should be mentioned. A magnetic pick-up sensor for tracking the rotation of the main rotor is used. The Magnetic pick-up sensor produces a sine wave output whenever a change from non-magnetic material to magnetic material occurs. Since the vibration signals are periodic due to the rotation of the helicopter blades, it is very essential to track the period start time of the rotation of the blade. Helicopters can have more than two blades. Independent of the number of blades, one blade is chosen as the target blade and the target blade has a magnetic metal extension at the main rotor side of the target blade that can trigger the magnetic pick-up sensor that is mounted on the main rotor of the helicopter. Since the blades' rotational motion is 360^o, the front of the helicopter is accepted as 0^o. Whenever the target blade flies through the front of the helicopter magnetic pick-up sensor produces a sine wave-shaped signal. The voltage range of the output of the magnetic pick-up sensor is 12 Vpp, therefore a Zener diode is implemented for protection purposes at the input of the analog channels. The clamp voltage of the Zener diode is 2.5V. Therefore, period of vibration signals is determined. During these sinus peaks vibration signals are sampled and processed.

In helicopters, the main vibration source is the main rotor due to large and heavy rotating blades. The RPM value can change according to the helicopter type; however, in this study, the helicopter that is used rotates at 324 RPM. Large and heavy rotating blades create vibration on the aircraft both vertically and horizontally. To sense vibrations both x-axis and y-axis two velocimeter sensors are used. Velocimeters are mounted inside of the helicopter horizontally and vertically respectively. While a horizontally mounted velocimeter detects horizontal vibration, a vertically mounted velocimeter detects vertical vibration. These velocimeters need +12V and -12V supplies and produce very noisy sinusoidal vibration signals. Resolution of the velocimeters is 19 mV/IPS and can measure the vibration up to 100 IPS meaning that the maximum output signal range is 1.9Vpp. While the amplitude of the output of the velocimeter sensor defines the vibration magnitude, the phase of the signal with respect to magnetic pick-up sensor defines the vibration location. In the light of these information, sampling start of the velocimeter signals are triggered by magnetic pick-up signal.

IPS (inch per second) is a unit of measurement that is used for defining the velocity of a vibration. Since the output of the velocimeter sinusoidal, the conversion between the sinusoidal signal’s amplitude and IPS is defined in velocimeter datasheet as 1 IPS = 19mV. Therefore, vibration magnitude is given in IPS.

3.2. Analog Input Module

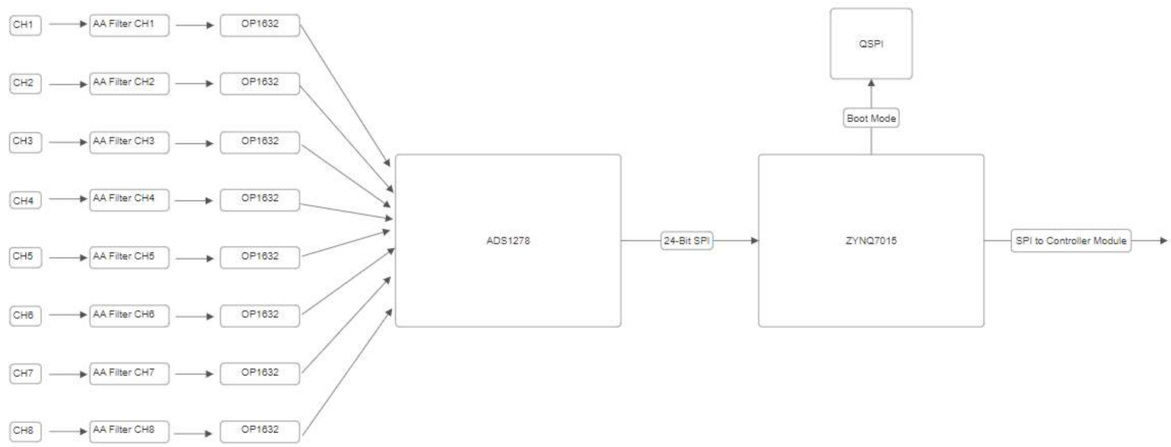

Figure 3.2. Analog Input Module Block Diagram

The specifications of the designed Analog input module can be summarized as follows;

- 8 simultaneous analog input channels
- Up to 144 kSPS data rate
- +/- 2.5V input range
- Low pass filter with cut off 10 kHz
- 0.298 uV resolution
- 15.6 uIPS vibration measurement resolution

Since the ADC has eight channels, analog input module also has eight input channels. The first channels is used for sampling magnetic pick-up sensor and the second and third channel is used for sampling the horizontal and vertical velocimeter sensors.

3.2.1. Signal conditioning and AA filter block

In order to design an anti-aliasing filter, we should know the frequency region that we are interested in. In our case, due to the rpm of both main and tail rotors, the maximum frequency that we would like to deal with is no more than 10kHz. (For this reason, in section 3.2.ADC

Block, Nyquist Frequency and ADC selection is given in detail). Of course, in different applications the frequency region of interest can vary due to the requirement of the system.

Analog filters can be used for different applications such as pre-amplification, equalization, tone control, tuning and preventing the aliasing for out of the frequency region of interest for digital signal processing applications. For the data acquisition systems general signal flow can be expressed as below figure;

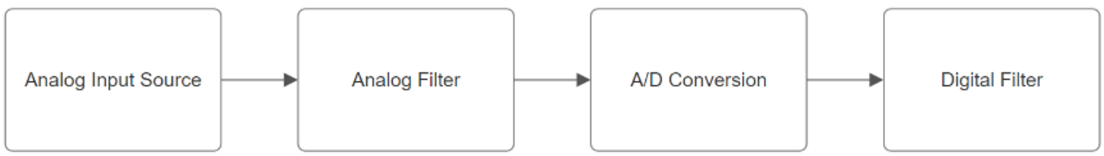

Figure 3.3. Data Flow Chart

Before proceeding to design the anti-aliasing filter, the filter type, that will be used, should be chosen. Therefore, filter types and their behaviors should be compared and examined. Electrical filters are the types of filters that allow to pass desired frequency regions and also block the undesired frequency regions. There are several ways to achieve this response electrically. First of all, the primitive ones are passive filters; which consists of R, L, C elements. On the other hand, active filters take advantage of operational amplifiers [9].

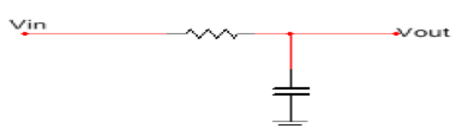

Figure 3.4. RC Low Pass Filter [9]

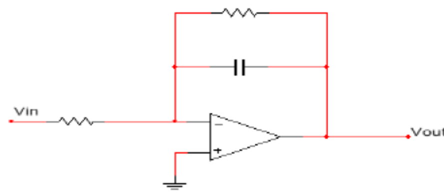

Figure 3.5. Simple Active Filter [9]

As one can see from above figures active filters do not use inductors instead of, they use operational amplifiers, which makes them cheaper and easy to fit in designs. Another advantage of the active filters, due to usage of operational amplifiers, their desired cut off frequencies and their roll offs are more precise than passive filters. In both passive and active filters, there are commonly four different types of filters that are low pass, high pass, band pass and band stop. After given brief explanation of passive and active filters, in depth explanation can be given relating active and passive filters [9].

3.2.1.1. Passive filters

Passive filters make use of resistive-capacitive (RC) and resistive-inductive (RL) circuitry. By using RC and RL circuitries in different manners, 4 types of, which are low pass, high pass, band pass and band stop, filters can be designed.

3.2.1.1.1 Low pass passive filter

Low pass filter is an electronic circuitry that allows to pass signals below certain frequency which is called as cut off frequency (f_c). The cut off frequency (f_c) can be calculated by using the below formula;

$$f_c = 1 / 2\pi RC \text{ for RC Filters} \quad (3.1)$$

$$f_c = 1 / (2\pi(L/R)) \text{ for RL Filters} \quad (3.2)$$

where R stands for resistance, C stands for capacitance and L stands for inductance in the above formulas. Circuitry representation can be seen below [9];

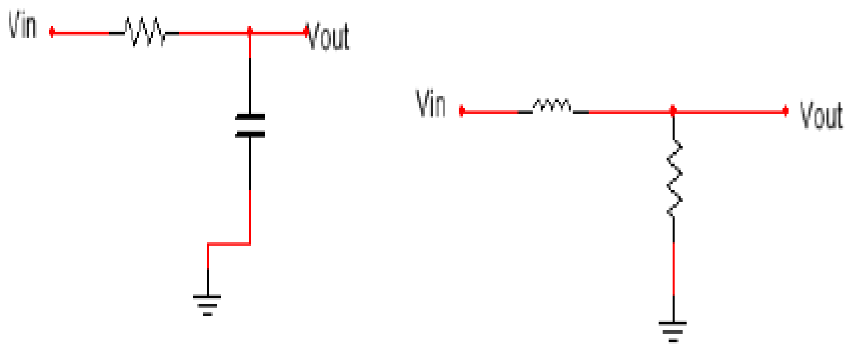

Figure 3.6. RC and RL Passive Filter [9]

3.2.1.1.2. High pass passive filter

High pass filter is an electronic circuitry that allows to pass signals above certain frequency which is called as cut off frequency (f_c). The cut off frequency (f_c) can be calculated by using the formulas Eq (1) and Eq (2). Circuitry representation can be seen below [9];

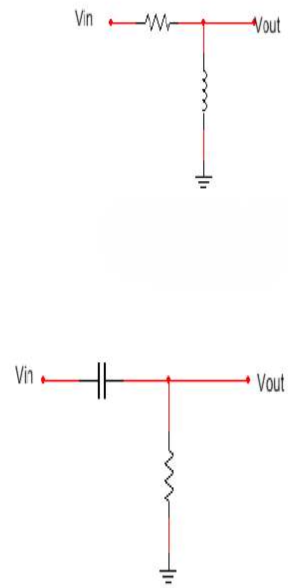

Figure 3.7. RC and RL High Pass Filter [9]

3.2.1.1.3. Band pass filter

Band pass filter is an electronic circuitry that allows to pass signals between two certain frequencies; f_{c1} and f_{c2}. Naturally, in band pass filters, there are two different cut off frequencies. f_{c1} represents the lower side of the frequency region and f_{c2} represents the upper side of the frequency region. Band pass filters can be considered as combination of both low pass and high pass filters. In order to calculate band pass region (ie. Band Width) below formula can be used;

$$BW = f_{c2} - f_{c1} \tag{3.3}$$

Where f_{c2} is upper cut off frequency and f_{c1} is lower cut off frequency. Circuitry representation can be seen below [9];

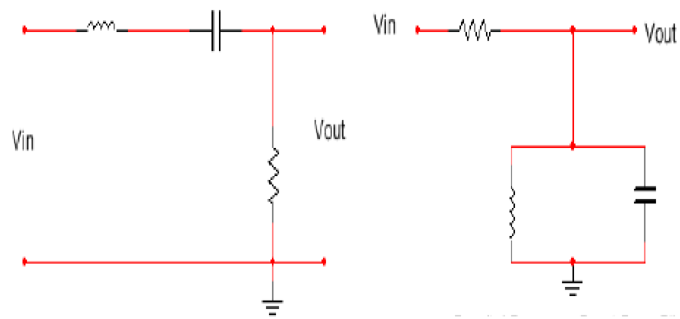

Figure 3.8. Series and Parallel Resonant Band Pass Filter [9]

3.2.1.1.4. Band stop filter

Band stop filter is an electronic circuitry that allows to block the signals between two certain frequencies; f_{c1} and f_{c2}. Band stop filter can be considered as exact opposite of the band pass filters. The circuitry representation can be seen below [9];

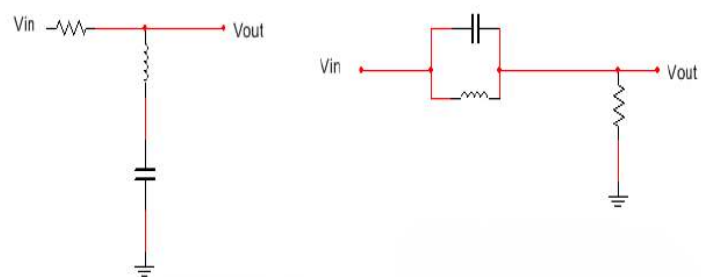

Figure 3.9. Series and Parallel Resonant Band Stop Filter [9]

3.2.1.2. Active filters

Like passive filters, active filters also have four different types which are low pass filter, high pass filter, band pass filter and band stop filter. Instead of inductors, active filters are consisting of resistances, capacitances and operational amplifiers. Unlike passive filters, active filters can increase the gain of the filtered signal thanks to operational amplifiers. An example circuitry of active filter is shown in Figure 4.10. [9]

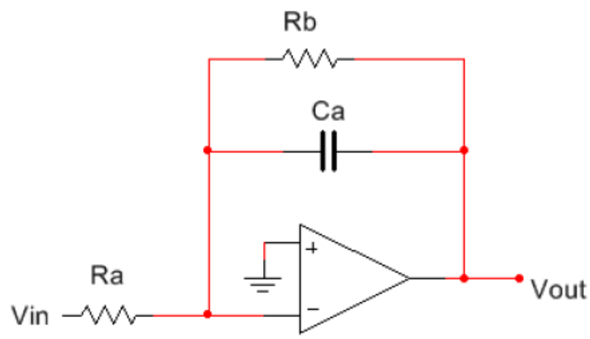

Figure 3.10. Active Filter Circuitry [9]

The relation between the input voltage and the output voltage can be expressed as below formula;

$$Vout = Vin \frac{-Rb}{Ra} \frac{1}{1+jw\mathrm{Rb}C} \tag{3.4}$$

Where R_a and R_b are resistive values, C is capacitance value, j is $\sqrt{-1}$ and w is frequency. In order to calculate the phase shift of the designed filter below formula can be used;

$$\emptyset(w) = \tan^{-1} \frac{w}{w0} \tag{3.5}$$

Where w_0 represents the center frequency and w represents the frequency. Furthermore, in order to calculate the gain of the active filters below formula can be used.

$$\text{Gain in decibels} = 20\log\frac{Vout}{Vin} \quad (3.6)$$

After summarizing passive and active filters, advantages and disadvantages should be mentioned. To begin with, passive filters have less amount of component which makes designs simple and easy. Since they are consisting of passive elements, they can become operative at high frequencies and voltages with less amount of noise. While these features make passive filters feasible to use, they have significant disadvantages relative to active filters, such as; passive filters contain inductors which are very large expensive circuit elements and passive filters have no capability to gain the filtered signal. Gaining the filtered signal can be very crucial to certain type of applications. Also, passive filters have very soft roll off after the cut off frequency with compared to active filters. Due to the advantages and the disadvantages of the active and passive filters, one can considerably choose the desired and most suited filter for the design.

After declaring the key features of the active and passive filters, more specialized filters should be given in detail. There are three different specialized filter types which are Chebyshev, Bessel and Butterworth, that are being used very commonly in this type applications. All of the filters that are mentioned before have their own advantages and disadvantages, and will be compared in detail.

3.2.1.2.1 Butterworth filter

Butterworth filter is a filter type which is well known and used very commonly in digital signal processing applications. It is designed by Stephen Butterworth, who is a British engineer, in 1930 [10]. The main advantage of Butterworth filters is that it has a very flat passband response which can be very useful for most applications. Besides it has flat bandpass response, Butterworth filters also have very steep stopband responses. It makes Butterworth filters very useful for filtering out the undesired signals and noises. Another important feature of Butterworth filters is simplicity with compared to other filter types because its transfer function is simple to analyze and design.

Butterworth filters are infinite impulse response (IIR) type of filters [11]. It provides flat amplitude response and gain in the passband region. While Butterworth filters can be implemented as both analog and digital, in this section analog implementation will be reviewed in detail. One can notice that, while frequency increases after cut off frequency Butterworth filters demonstrate monotonic decrease in amplitude response. At the infinite frequency amplitude attenuated close to zero [11]. This flat passband, sharp stopband response and simplicity of the analog design makes Butterworth filters advantageous to the other types of filters such as; Chebyshev and Bessel. The magnitude squared response of the Butterworth filters is given below;

$$H(jw) = \frac{1}{1+(\frac{w}{w_c})^{2N}} \text{ where N is the order} \tag{3.7}$$

For a fourth order two stages Butterworth low pass filter which has (-3db) 10 kHz cut off frequency and (-40db) 40 kHz stopband frequency design is made. In order to compare and understand the filter response simulation is conducted and given below [12].

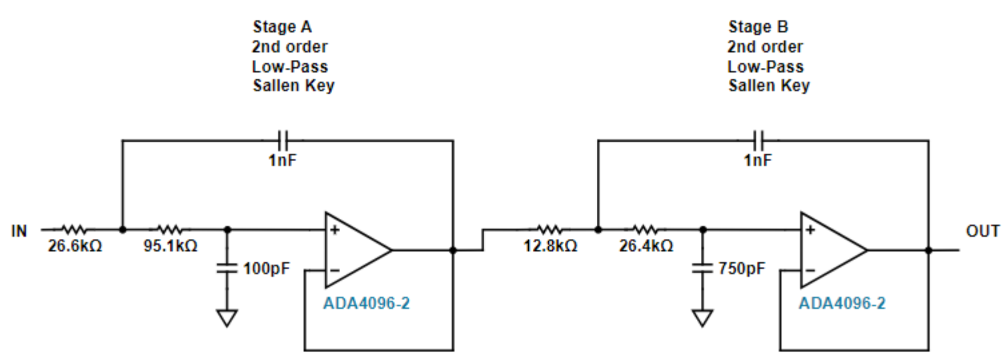

Figure 3.11. Fourth Order Two Stages Butterworth Low Pass Filter with 0 dB Gain [12]

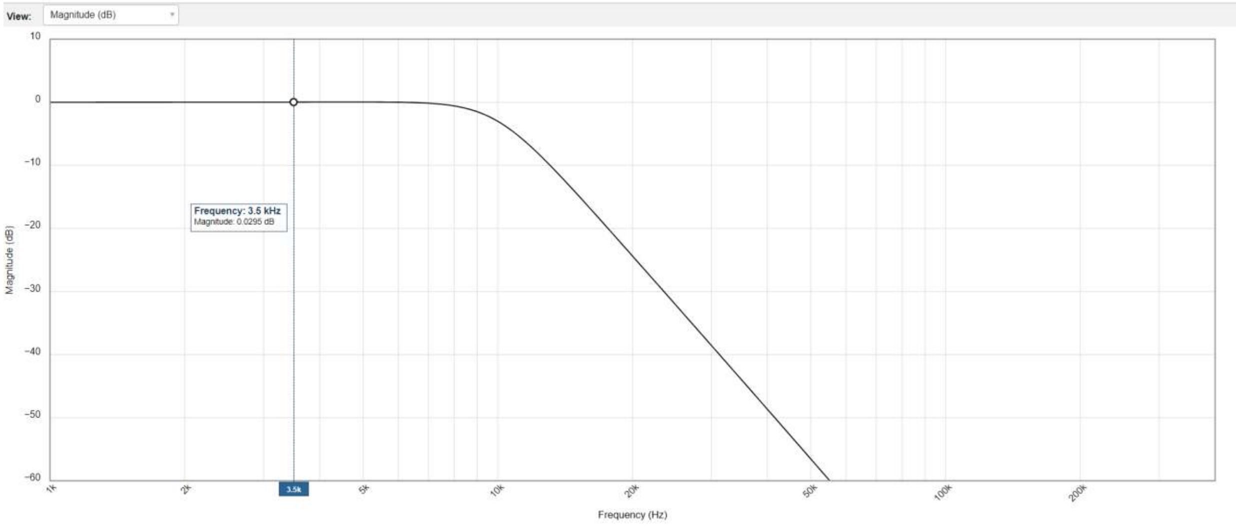

Figure 3.12. Magnitude Response of Fourth Order Two Stages Butterworth Low Pass Filter[12]

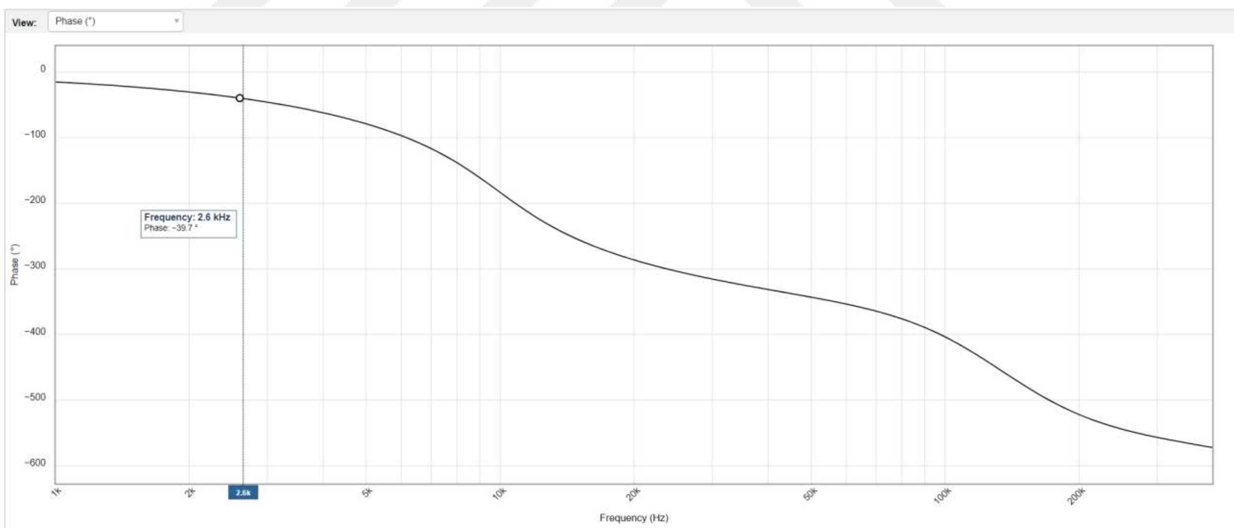

Figure 3.13. Phase Response of Fourth Order Two Stages Butterworth Low Pass Filter[12]

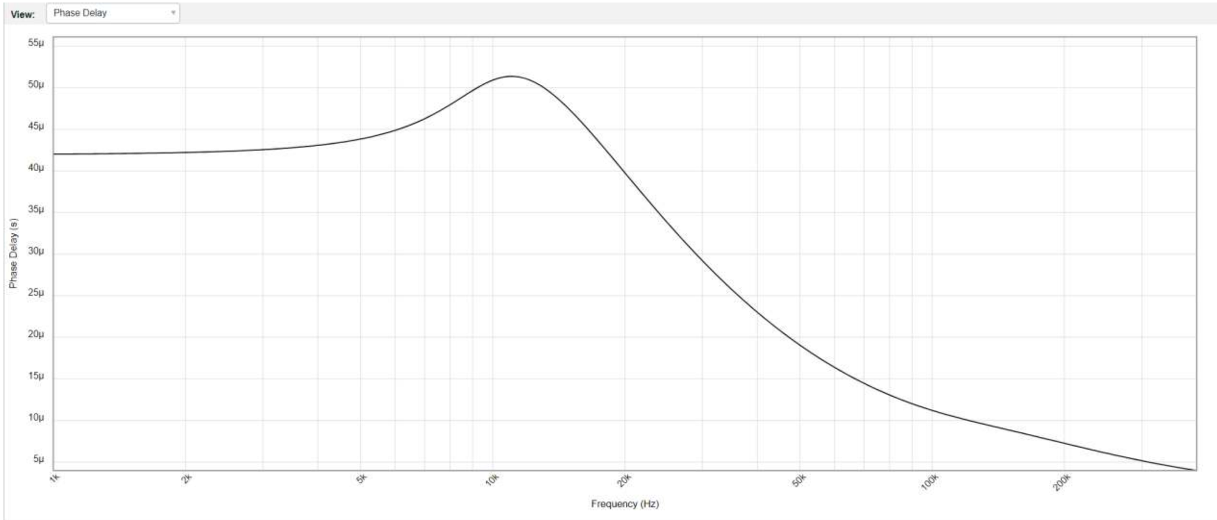

Figure 3.14. Phase Delay of Fourth Order Two Stages Butterworth Low Pass Filter[12]

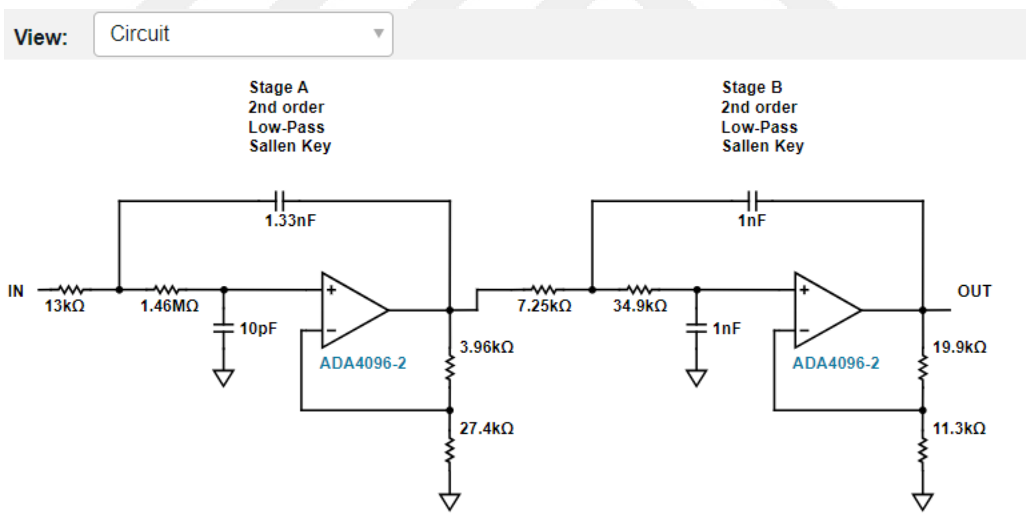

Figure 3.15. Fourth Order Two Stages Butterworth Low Pass Filter with 10 dB Gain[12]

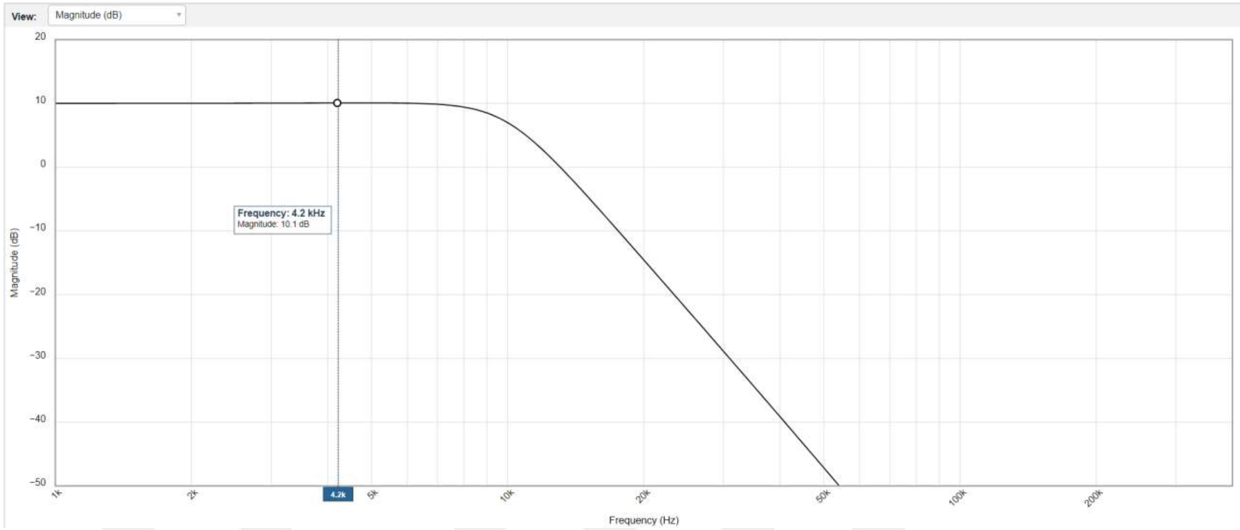

Figure 3.16. Magnitude Response of Fourth Order Two Stages Butterworth Low Pass Filter with 10 dB Gain[12]

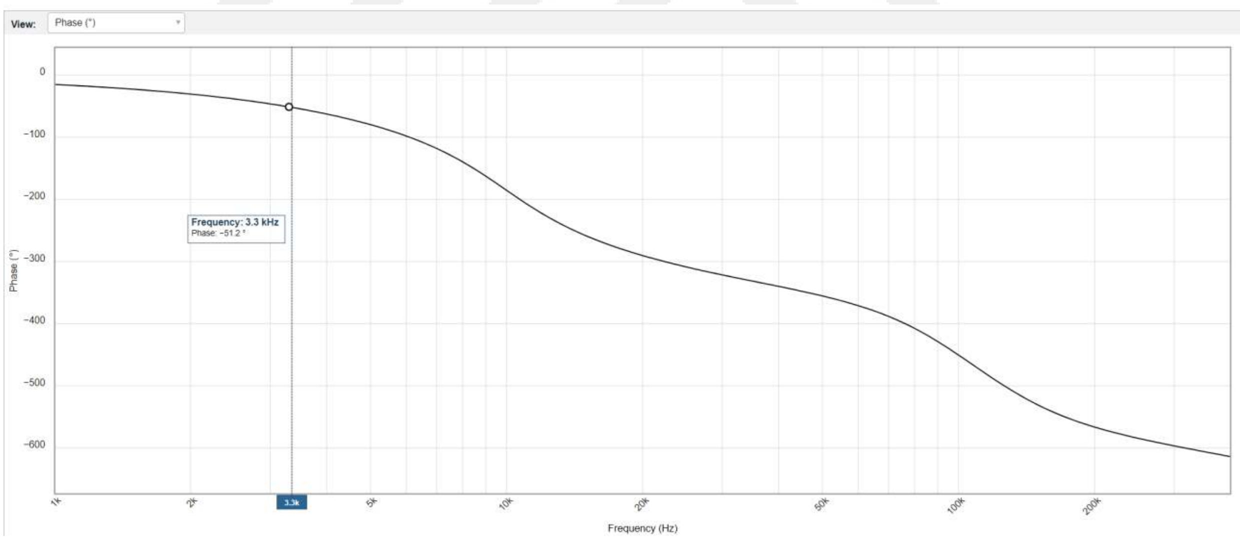

Figure 3.17. Phase Response of Fourth Order Two Stages Butterworth Low Pass Filter with 10 dB Gain[12]

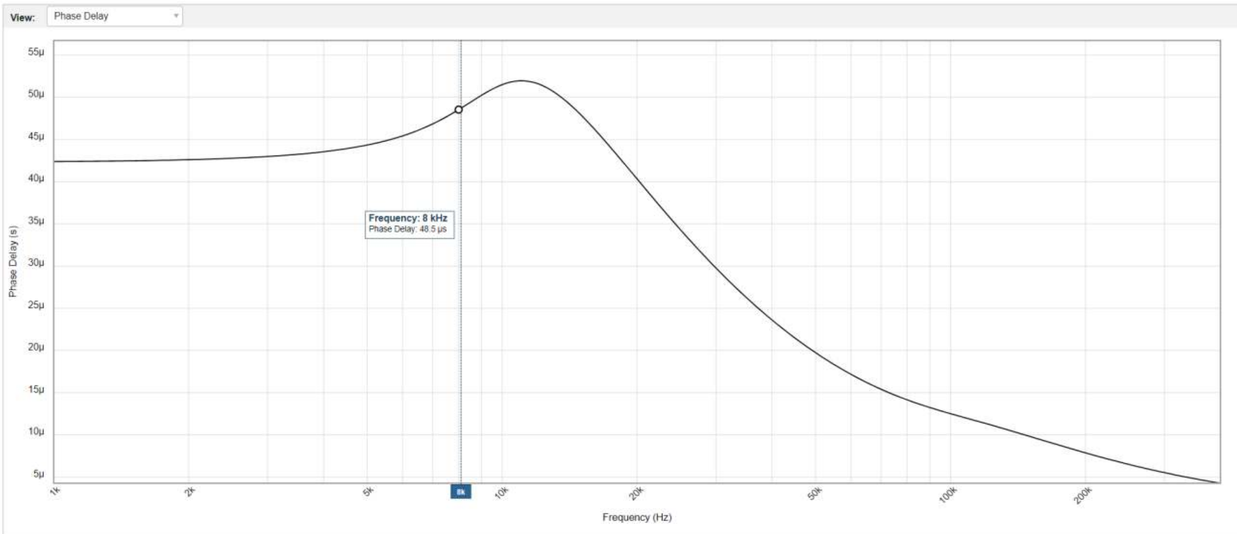

Figure 3.18. Phase Delay of Fourth Order Two Stages Butterworth Low Pass Filter with 10 dB Gain[12]

As it can be seen from simulation results, in the passband region Butterworth filter has very flat magnitude response. After adding 10db gain to the signal, passband flatness of both gain and magnitude response remains the same. This response is very convenient for applications that need steady gain in bandpass regions. Also, one may notice that adding gain to the active filter does not affect the phase response and phase delay of the filter.

3.2.1.2.2. Chebyshev filter

Chebyshev filter gets its name from well-known Russian mathematician Pafnuty Chebyshev, because filter’s mathematical model is derived from Chebyshev’s polynomial equations. This type of filter can be implemented both analog or digital, in this section analog implementation will be given in detail [13].

Chebyshev filters dissociate from Butterworth filters with their steeper roll offs in the stopband region and also more ripple in the passband region. There are two types of Chebyshev filters which are Type-I and Type-II (i.e. inverse Chebyshev). The square magnitude response formula of Type-I Chebyshev filter is given below;

$$|H(jw)|^2 = \frac{1}{1+ \epsilon^2 T_N^2(w/w_c)} \tag{3.7}$$

Where $T_N(w)$ is the N^{th} order Chebyshev polynomial which is given below;

$$T_N(w) = \begin{cases} \cos\left(N\cos^{-1}(w)\right) & |w| \leq 1 \\ \cosh\left(N\cosh^{-1}(w)\right) & |w| > 1 \end{cases} \tag{3.8}$$

Chebyshev filters minimize the error between ideal filters and real application filters by adding ripple to the passband region but in the stopband region steepness is increased.

In Type-II Chebyshev filters, passband is monotonic, the approximation error (i.e. error between ideal filters and real application) is minimized in the stopband region. Another difference from Type-I Chebyshev filters is that, no ripple occurs at the passband region, but steepness of the stopband region is not as sharp as Type-I Chebyshev filter. The square magnitude response formula of Type-II Chebyshev filter is given below;

$$|H(jw)|^2 = \frac{1}{1+\varepsilon^2\left[\frac{T_N(w_c/w_p)}{T_N(w_c/w)}\right]} = \frac{1}{1+\left[\frac{\delta^{-2}-1}{T_N(w_c/w)}\right]} \tag{3.9}$$

Where w_c is the cut off frequency of the filter [14].

For a third order two stages Chebyshev low pass filter which has (-3db) 10 kHz cut off frequency and (-40db) 40 kHz stopband frequency design is made. In order to compare and understand the filter response simulation is conducted and given below [12].

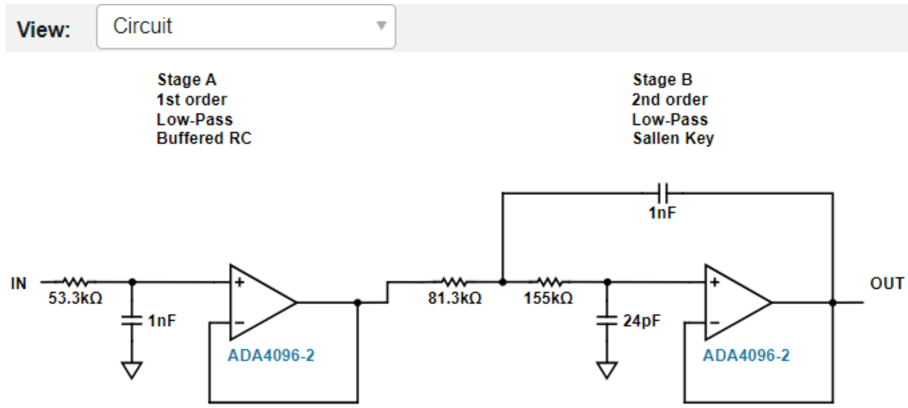

Figure 3.19. Third Order Two Stages Chebyshev Low Pass Filter[12]

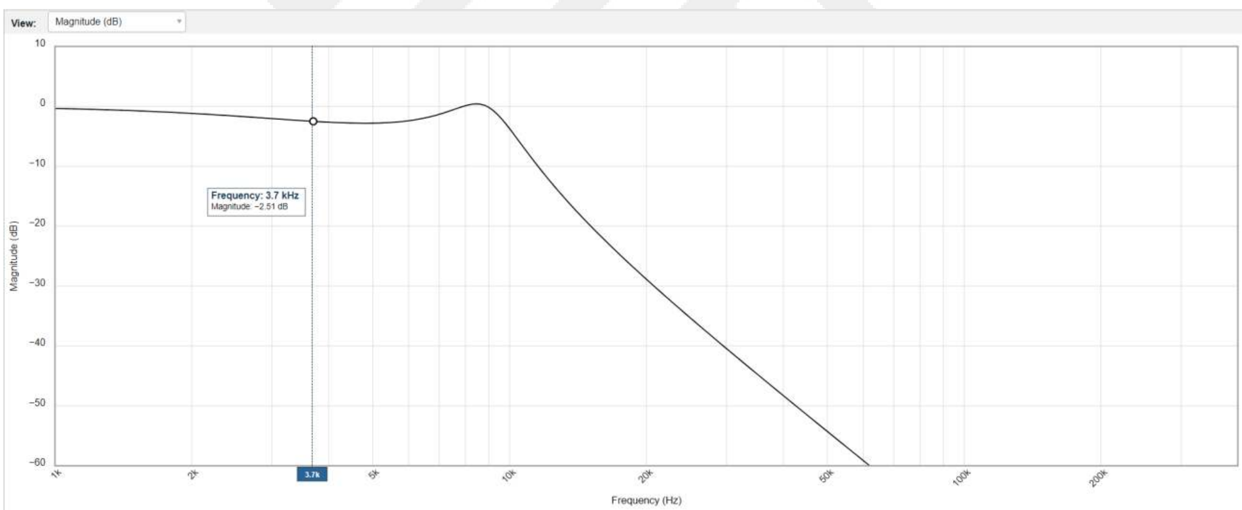

Figure 3.20. Magnitude Response of Third Order Two Stages Chebyshev Low Pass Filter[12]

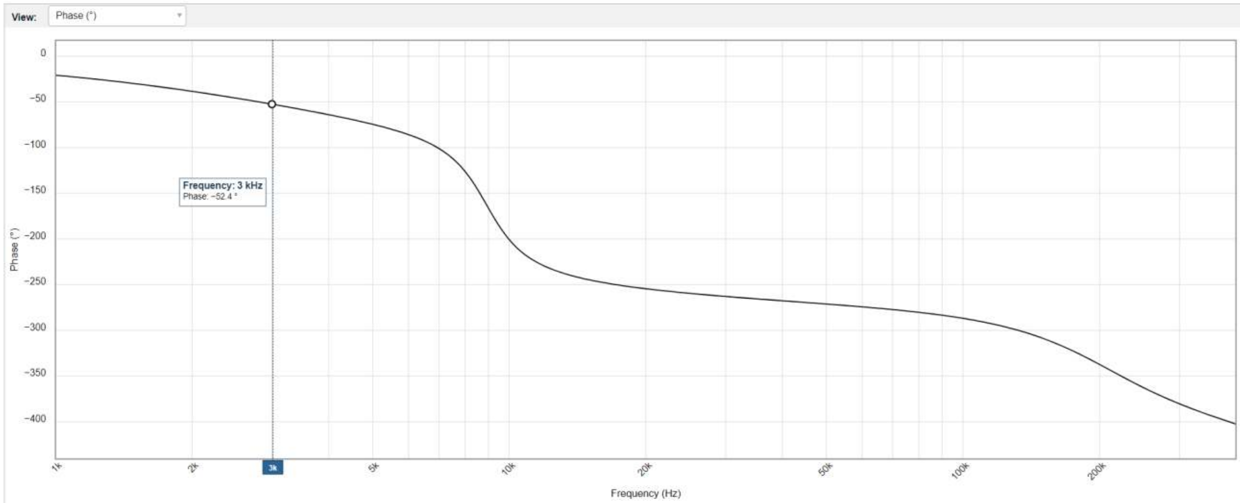

Figure 3.21. Phase Response of Third Order Two Stages Chebyshev Low Pass Filter[12]

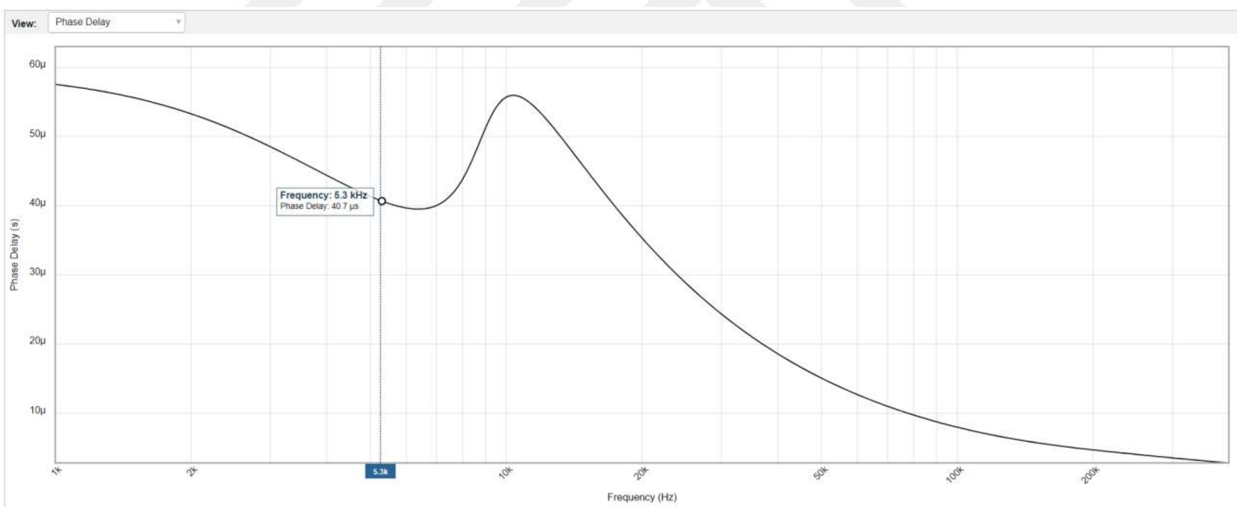

Figure 3.22. Phase Delay of Third Order Two Stages Chebyshev Low Pass Filter[12]

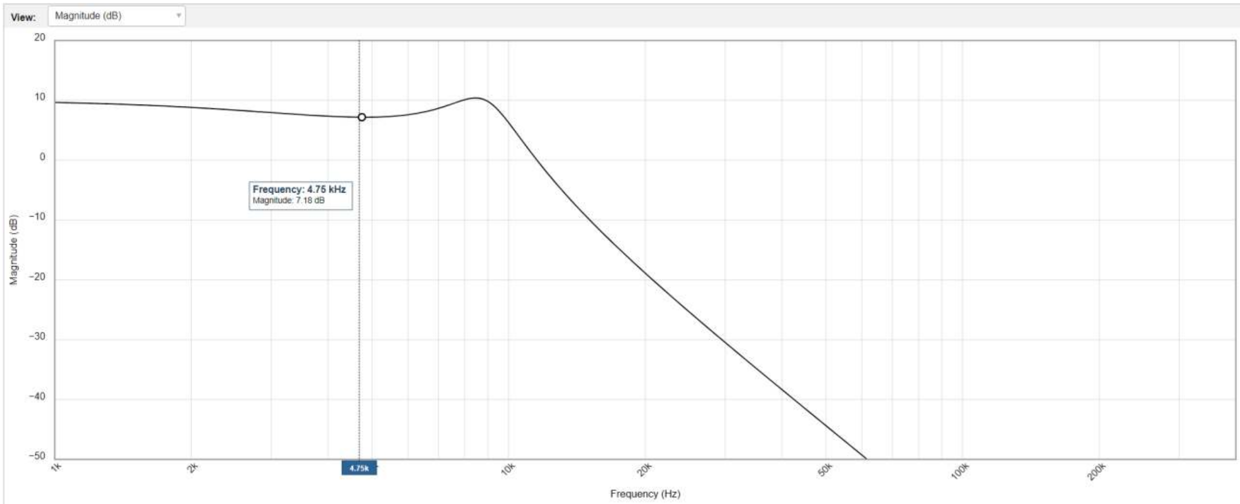

Figure 3.23. Magnitude Response of Third Order Two Stages Chebyshev Low Pass Filter with 10 dB Gain[12]

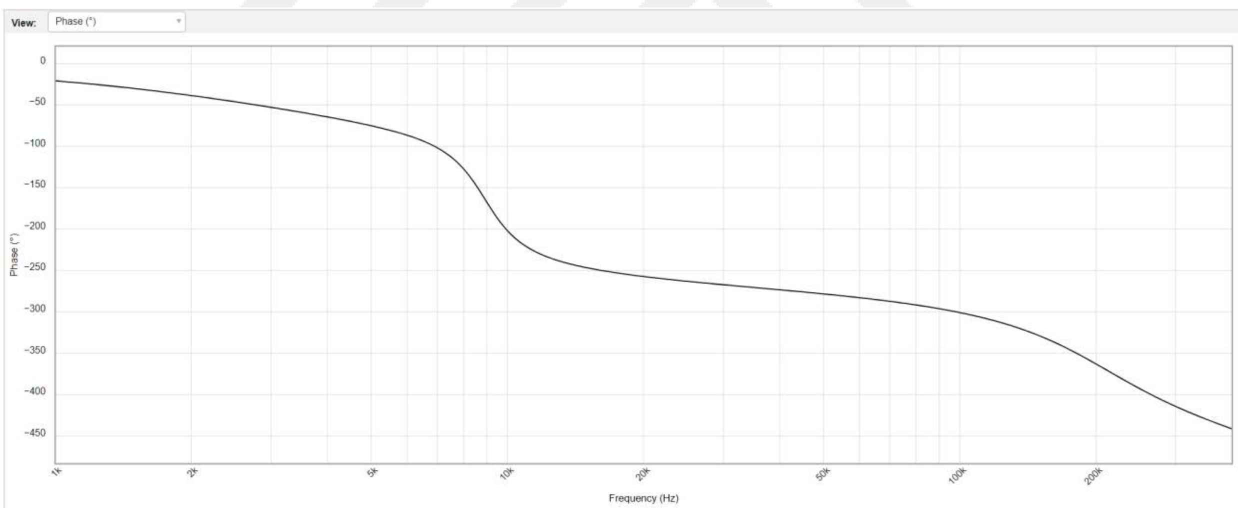

Figure 3.24. Phase Response of Third Order Two Stages Chebyshev Low Pass Filter with 10 dB Gain[12]

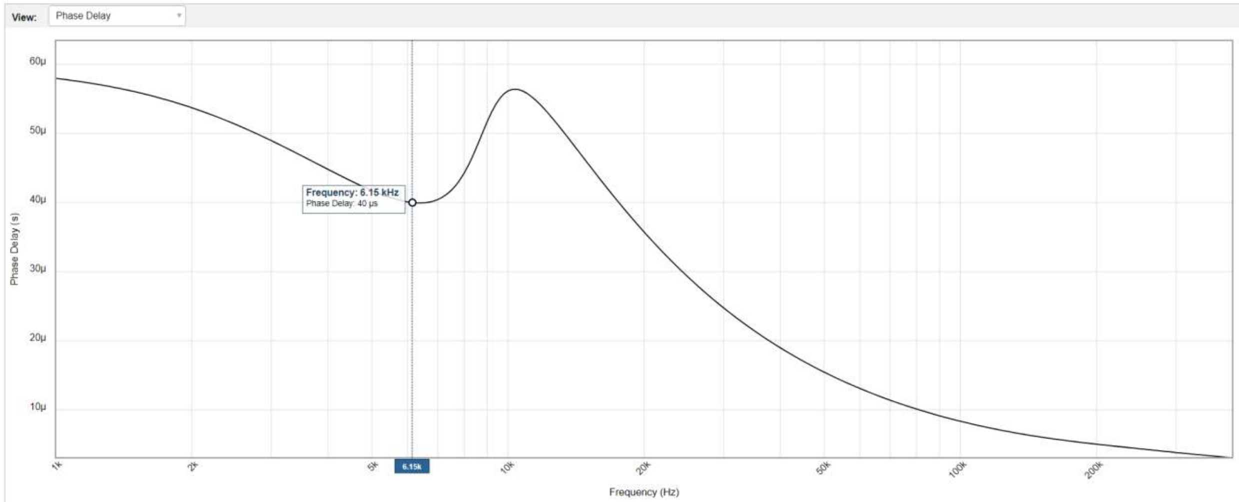

Figure 3.25. Phase Delay of Third Order Two Stages Chebyshev Low Pass Filter with 10 dB Gain[12]

As it can be seen from simulation results, the magnitude response of Chebyshev filter in the passband region has ripple and due to that ripple filtered signal has gain and attenuation through the passband region frequencies. However, one can notice that in the stop band region steepness of roll off is sharper than Butterworth filter. After adding 10db gain to the signal, passband ripple of both gain and magnitude response remains same. This response is very convenient for application that need for filtering the noise and undesired frequencies in the stopband region if the gain change in passband region is insignificant. Also, one may notice that adding gain to active filter does not affect the phase response and phase delay of the filter.

3.2.1.2.3. Bessel filter

Butterworth and Chebyshev filters are mainly focusing on the magnitude response of the filter and the signal. Filters' behavior on passband and stopband region was the main comparison. However, the phase characteristics of those filters are non-linear, meaning the delay of the filter is changing with changing frequency. In applications that need constant or linear phase delay Butterworth and Chebyshev filters are not preferred. When the linear or constant phase delay is needed Bessel filters are good option to use in designs. All pole transfer function of Bessel Filters is given below;

$$H(s) = \frac{b_0}{s^N B(s)} \tag{3.10}$$

Where B(s) is Bessel polynomial and is given below;

$$b_i = \frac{(2N-i)!}{2^{N-1} i!(N-i)!} \tag{3.11}$$

The magnitude response of Bessel filter is given below;

$$|H(jw)|^2 = \frac{2b_0^2}{\pi w^{2N+1}[J_{-v}^2(w)+J_v^2(w)]} \tag{3.12}$$

Where v = N+1/2 and $J_v(w)$ is given below;

$$J_v(w) = w^v \sum_{i=0}^{\infty} \frac{(-1)^i w^{2i}}{2^{2i+v} i!\Gamma(v+i+1)} \tag{3.13}$$

where Γ(.) is the gamma function.

For a sixth order three stages Bessel low pass filter which has (-3db) 10 kHz cut off frequency and (-40db) 40 kHz stopband frequency design is made. In order to compare and understand the filter response simulation is conducted and given below.

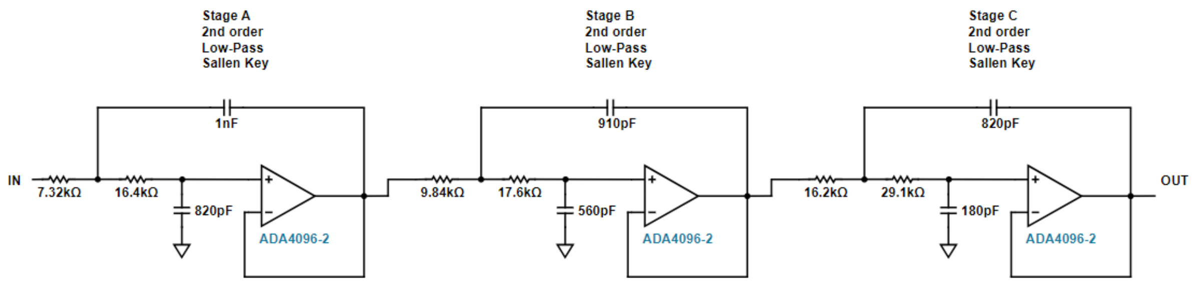

Figure 3.26. Sixth Order Three Stages Bessel Low Pass Filter with 0 dB Gain[12]

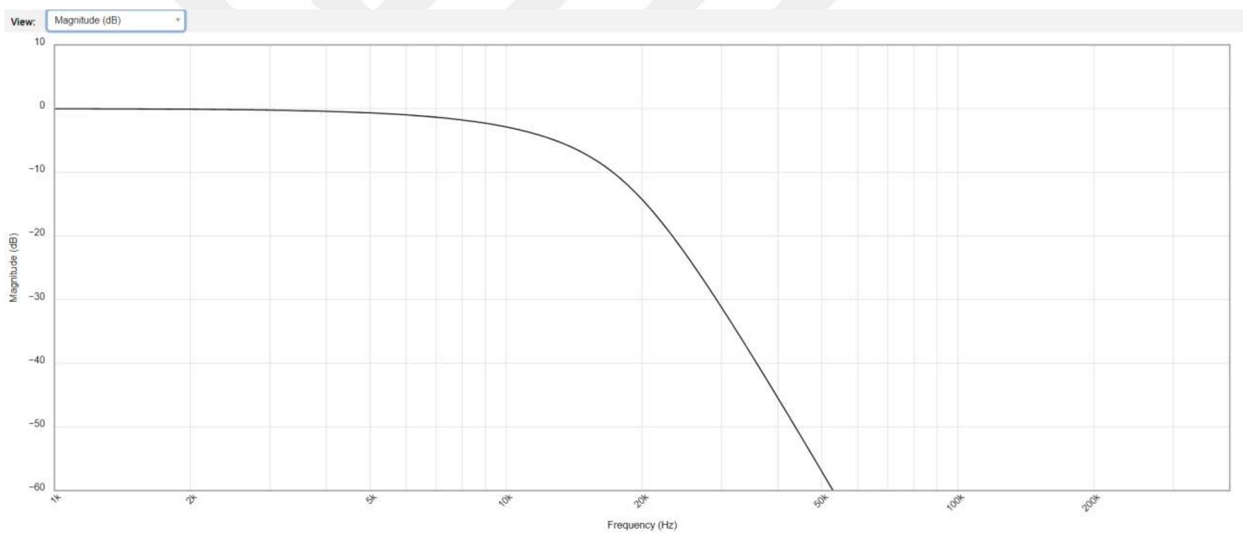

Figure 3.27. Magnitude Response of Sixth Order Three Stages Bessel Low Pass Filter with 0 dB Gain[12]

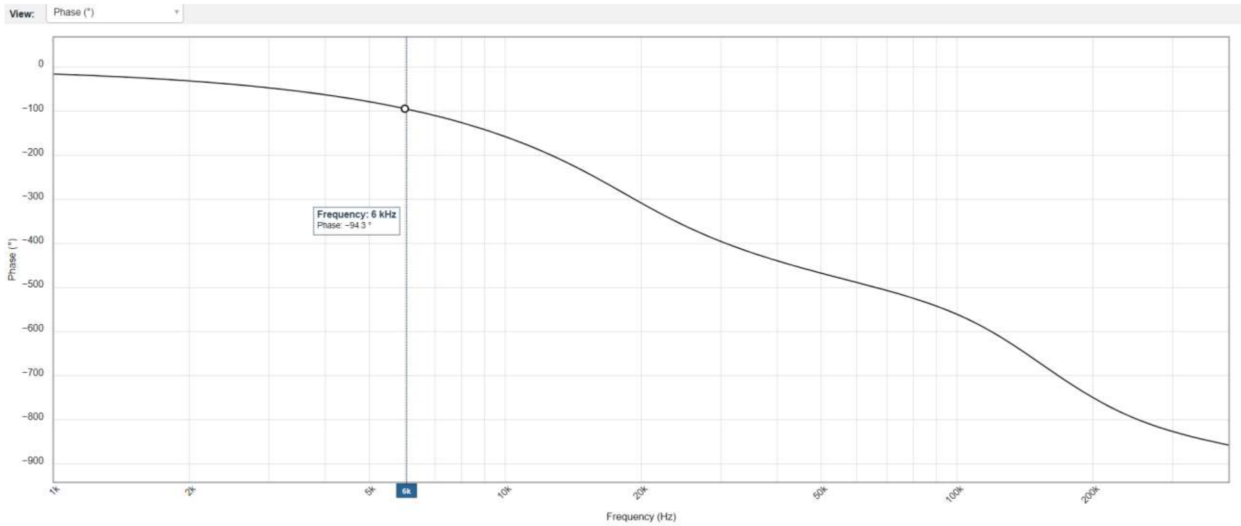

Figure 3.28. Phase Response of Sixth Order Three Stages Bessel Low Pass Filter with 0 dB Gain[12]

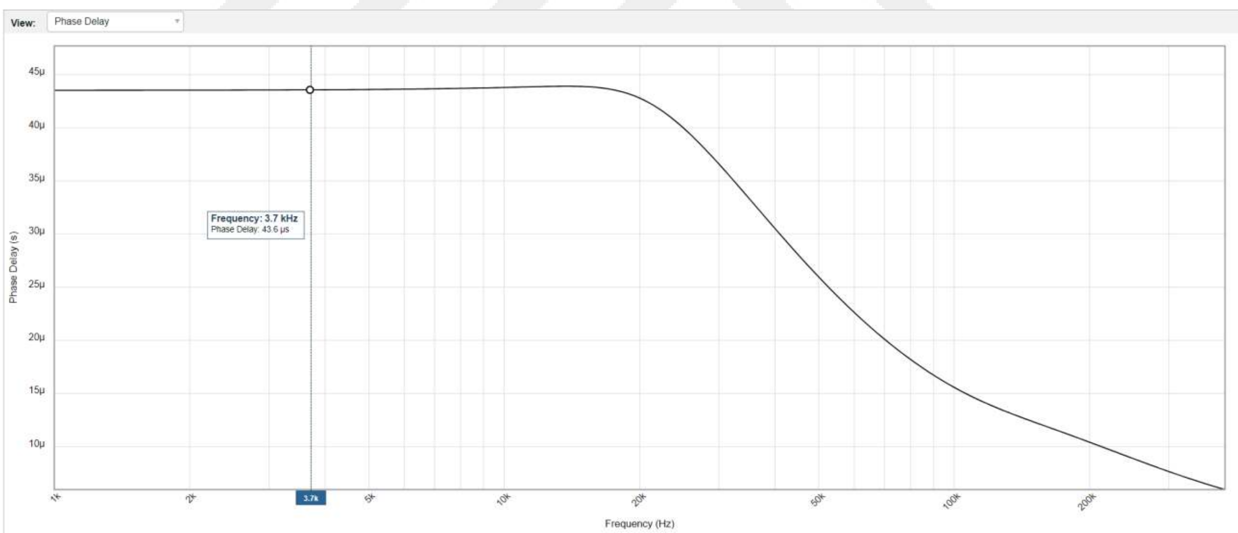

Figure 3.29. Phase Delay of Sixth Order Three Stages Bessel Low Pass Filter with 0 dB Gain[12]

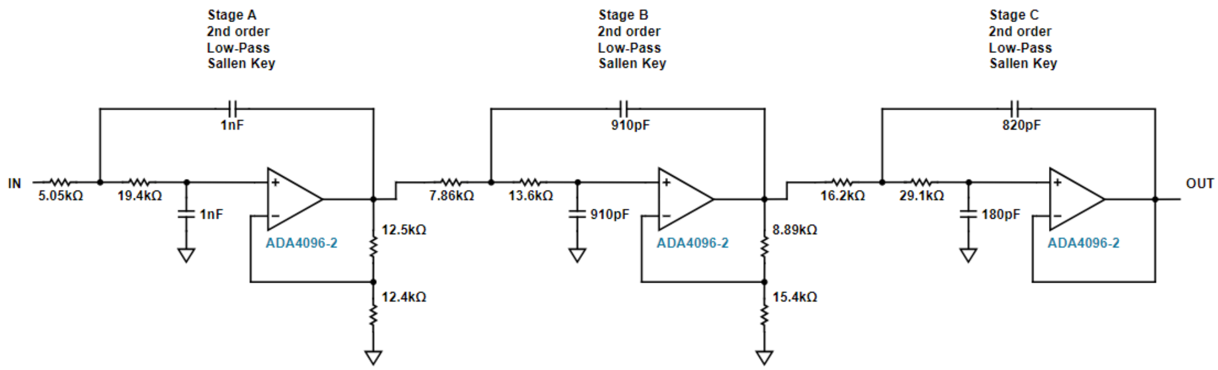

Figure 3.30. Sixth Order Three Stages Bessel Low Pass Filter with 10 dB Gain[12]

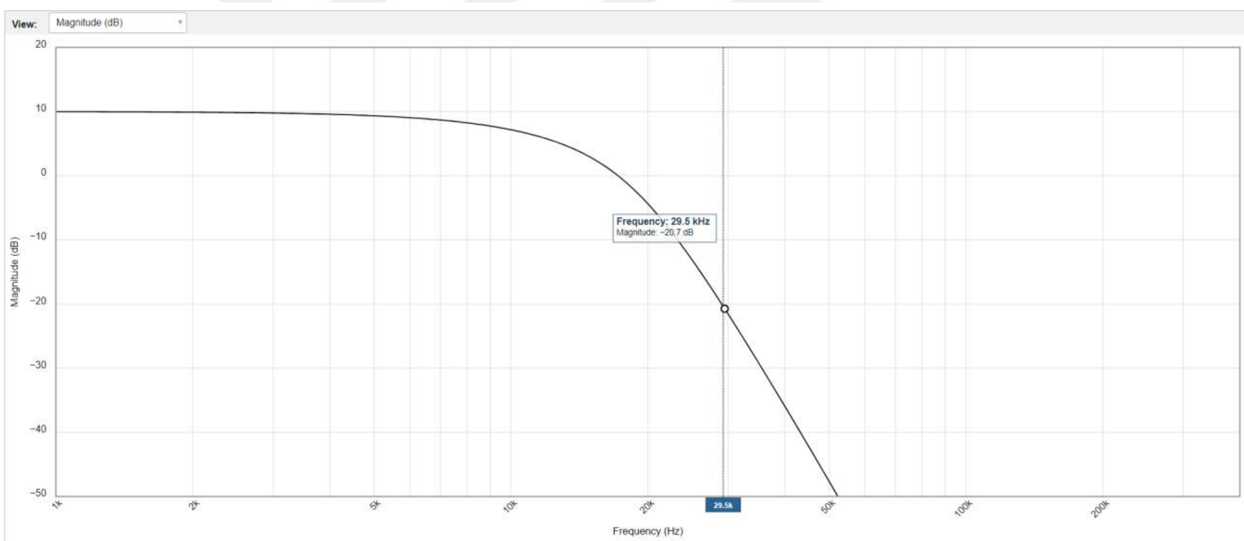

Figure 3.31. Magnitude Response of Sixth Order Three Stages Bessel Low Pass Filter with 10 dB Gain[12]

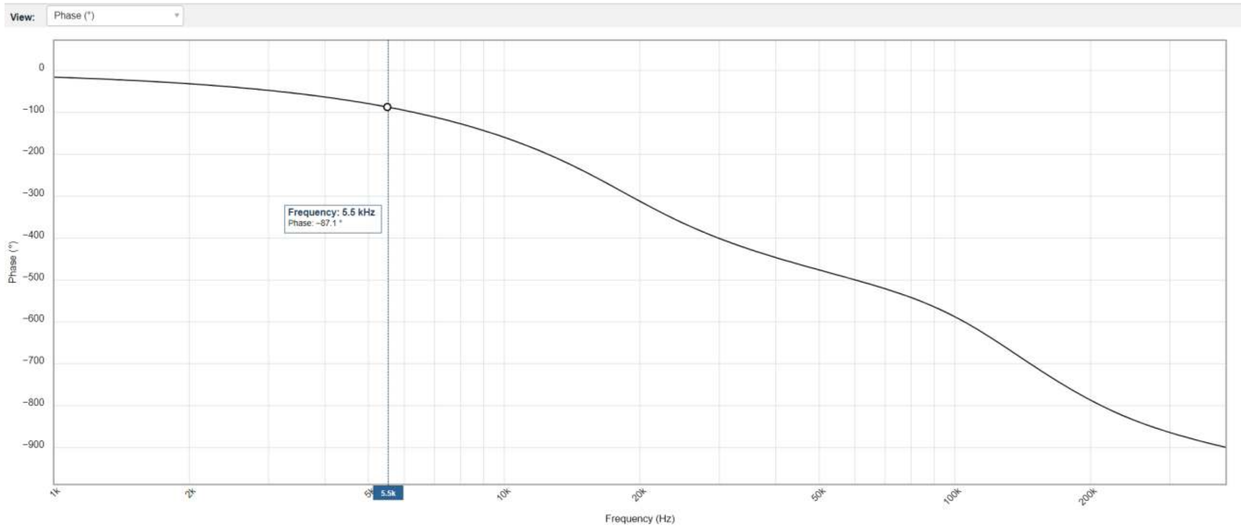

Figure 3.32. Phase Response of Sixth Order Three Stages Bessel Low Pass Filter with 10 dB Gain[12]

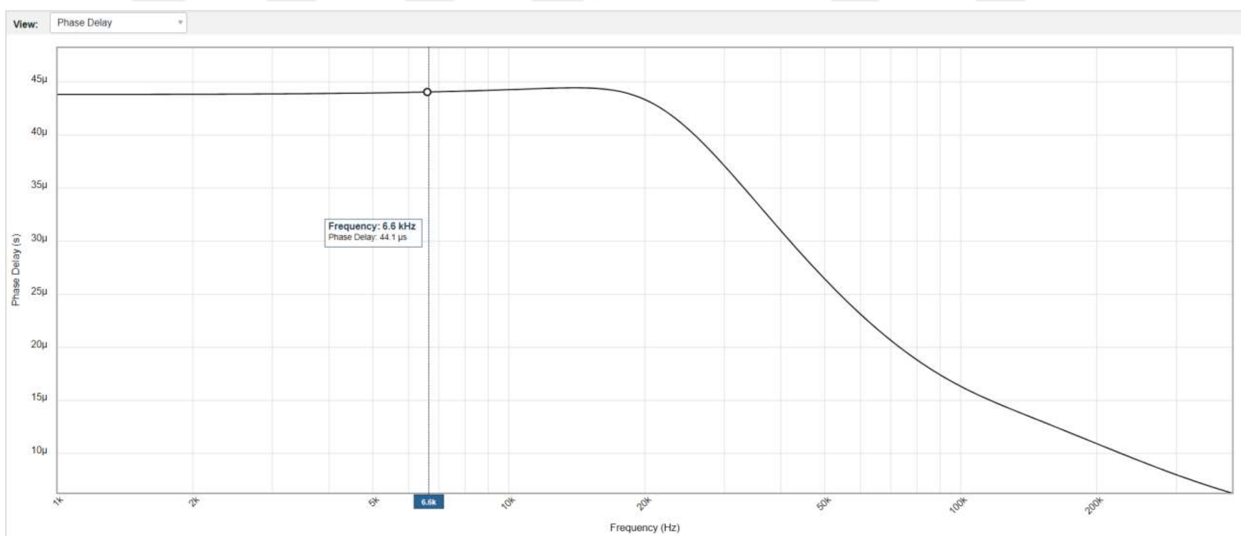

Figure 3.33. Phase Delay of Sixth Order Three Stages Bessel Low Pass Filter with 10 dB Gain[12]

As it can be seen from simulation results; while phase delay is very linear with compared to Butterworth and Chebyshev, magnitude response of Bessel filter is poorer. Another difference of Bessel filter is that Bessel filters require higher amount of filter orders with compared to other filters which is a disadvantage in terms of both design complexity and cost. However, for applications that requires constant phase delay Bessel filters become very advantageous [14].

In the light of the previous filter approximations, Butterworth filter is best suit for data acquisition system that is designed. Since the vibration magnitude detection is done by using velocimeter signal’s amplitude, flat bandpass response of filters is chosen for simplicity of the both design and calculations.

3.2.1.3. Sampling and aliasing

Another concept for digital signal processing and data acquisition devices that should also be mentioned is that sampling and aliasing. As one should know that analog sensors produce analog signals which are continuous waveforms that can be consisted of DC signal, signal with a certain frequency or signal composed of different frequencies. In order to process these sensors’ outputs signals should be transformed to digital domain from analog domain. This transformation is done mostly by the ADCs (Analog to Digital Converters), and the theory behind the ADCs’ is sampling theory.

Under definite conditions, any continuous-time signal can be represented by its equally time spaced samples in discrete form. Moreover, represented discrete-time signal can be completely recoverable to its continuous-time signal. This concept is known as Sampling Theorem. Sampling theorem has significant role in the relation between the continuous-time signals and discrete-time signals [15].

Although there are several methods to get the discrete-time signal representation of continuous-time signal, the most known and used is periodic sampling. According to the periodic sampling, obtained discrete samples x[n] can be represented as below formula [16];

$$X[n] = x_c(nT) \quad -\infty < n < \infty \tag{3.14}$$

where T is the sampling period and $f_s = 1/T$ is sampling frequency.

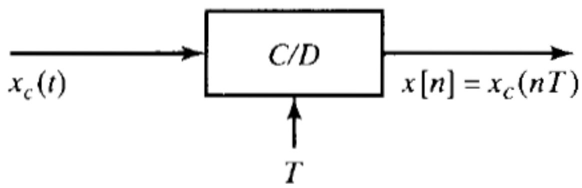

Figure 3.34. Ideal Continuous to Discrete Time Converter C/D[12]

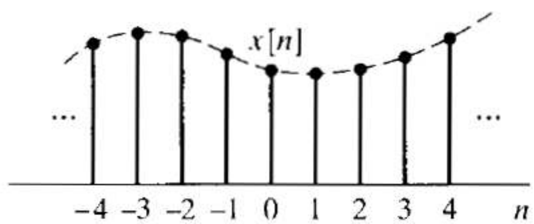

Figure 3.35. Sampled Discrete x[n] of x(t) [12]

In order to obtain frequency domain relationship between continuous time signal and discrete time signal of ideal C/D converter in other words relationship between the input and the output of the C/D converter can be described as below;

$$s(t) = \sum_{n=-\infty}^{\infty} \delta(t - nT) \tag{3.15}$$

Where $\delta(t)$ is the dirac delta function (Unit impulse). Modulating s(t) with $x_c(t)$ below formula is reached;

$$x_s(t) = x_c(t)s(t) \tag{3.16}$$

$$x_s(t) = x_c(t) \sum_{n=-\infty}^{\infty} \delta(t - nT) \tag{3.17}$$

$x_s(t)$ can be represented by using the shifting property of the dirac function which is given below;

$$x_s(t) = \sum_{n=-\infty}^{\infty} x_c(nT)\, \delta(t - nT) \tag{3.18}$$

Fourier transform of $x_s(t)$ can be considered as convolution of the Fourier transforms $X_c(j\Omega)$ and $S(j\Omega)$. Following equations represent the Fourier transforms $X_c(j\Omega)$ and $S(j\Omega)$;

$$S(j\Omega) = \frac{2\pi}{T} \sum_{k=-\infty}^{\infty} \delta(\Omega - k\Omega_s) \tag{3.19}$$

Where $\Omega_s = 2\,\pi/T$

$$X_s(j\Omega) = \frac{1}{2\pi} X_c(j\Omega) * S(j\Omega) \tag{3.20}$$

Where * is the convolution operation. Then $X_s(j\Omega)$ becomes as follows;

$$X_s(j\Omega) = \frac{1}{T} \sum_{k=-\infty}^{\infty} X_c(j(\Omega - k\Omega_s)) \tag{3.21}$$

Fourier transforms of the input and output of the impulse train modulator is obtained by the previous formula. From the formula one can easily see that periodically recurring copies of the Fourier transform of $x_c(t)$ constructs the Fourier transforms of $x_s(t)$. By shifting and combining the copies of $X_c(j\Omega)$ with multiple values of f_s (sampling frequency) the periodic Fourier transform of the impulse train can be produced.

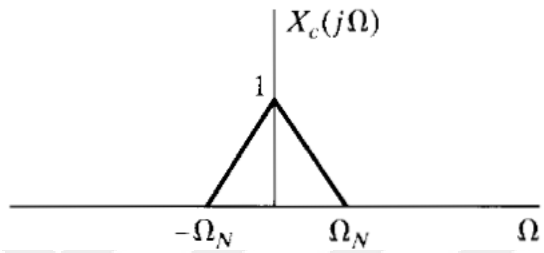

Figure 3.36. A Original Signal's Spectrum [12]

Above figure depicts the Fourier transform of the signal that has a highest nonzero frequency component at Ω_N. Below figure depicts sampling function $S(j\Omega)$. In figure C one can see that it is the convolution of the $X_c(j\Omega)$ with $S(j\Omega)$. Moreover, figure C shows the relation of not overlapping of replicas of $X_c(j\Omega)$ when $\Omega_s > 2\Omega_N$

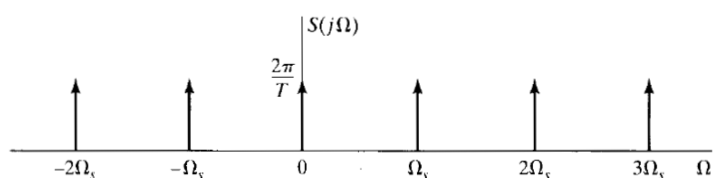

Figure 3.37. B Spectrum of Impulse Train (Sampling Function) [12]

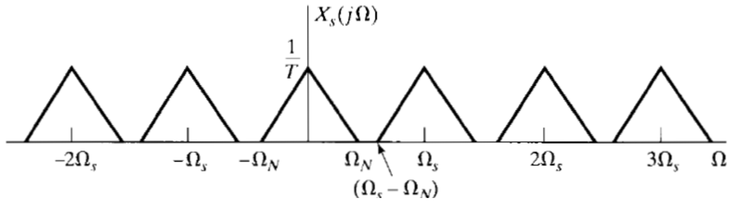

Figure 3.38. C Sampled Signal's Spectrum with Ωs > 2ΩN [12]

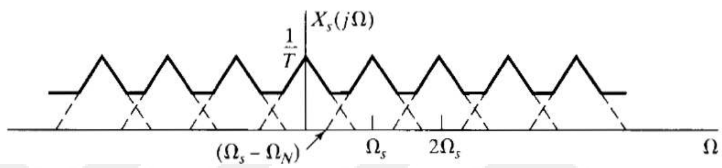

Figure 3.39. D Sampled Signal's Spectrum with Ωs< 2ΩN [12]

Figure D depicts that when $\Omega_s < 2\Omega_N$, replicas of Xc(jΩ) overlaps. In other words, signal become not recoverable. When this case occurs in the condition of $\Omega_s < 2\Omega_N$, which is sampling with lower than two times of Nyquist Frequency, the reconstruction of the output signal to the original input signal becomes distorted. This distortion phenomena is known as Aliasing [16]. Since the frequency range requirement for the system is up to 10 kHz and the ADC's sampling rate is up to 144 kSPS, the design meets the Nyquist sampling theorem needs. Also, AA filter is designed for not to occur any aliasing.

3.2.1.4. Designed filter

After the bandpass region is determined as 10 kHz, designing an anti-aliasing filter can be considered. Before getting the design stage, it is also known that helicopters and other aviation crafts are very noisy environments in terms of both electrically and mechanically. That is why we would like to design anti-aliasing filter's roll of very sharp. That is why Butterworth low pass filter with 10kHz Cut off, stop band at 20kHz with a -60dB gain is designed. The reason of the selection of the Butterworth filter topology is flat bandpass response. Since the magnitude estimation is crucial for the vibration magnitude of the system, gain change in bandpass region is not wanted. Therefore, 0db gain with a flat bandpass response Butterworth filter is designed as follows. In order to achieve filter characteristics 10^{th} order 5 stage Butterworth low pass filter have been used. The circuitry is given below;

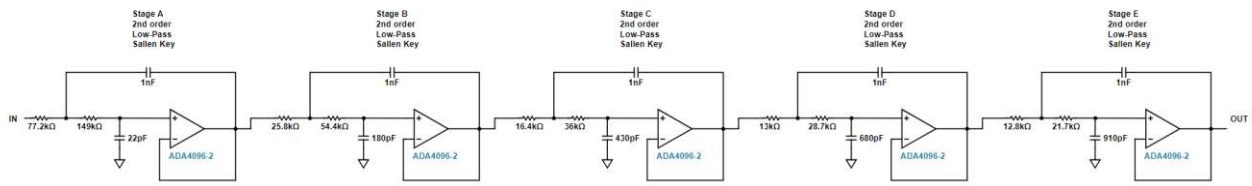

Figure 3.40. Designed 10th Order 5 Stage Butterworth Low Pass Filter with 10kHz Cut off, stop band at 20kHz with a -60dB gain [12]

The magnitude response of designed Butterworth filter is given below [12];

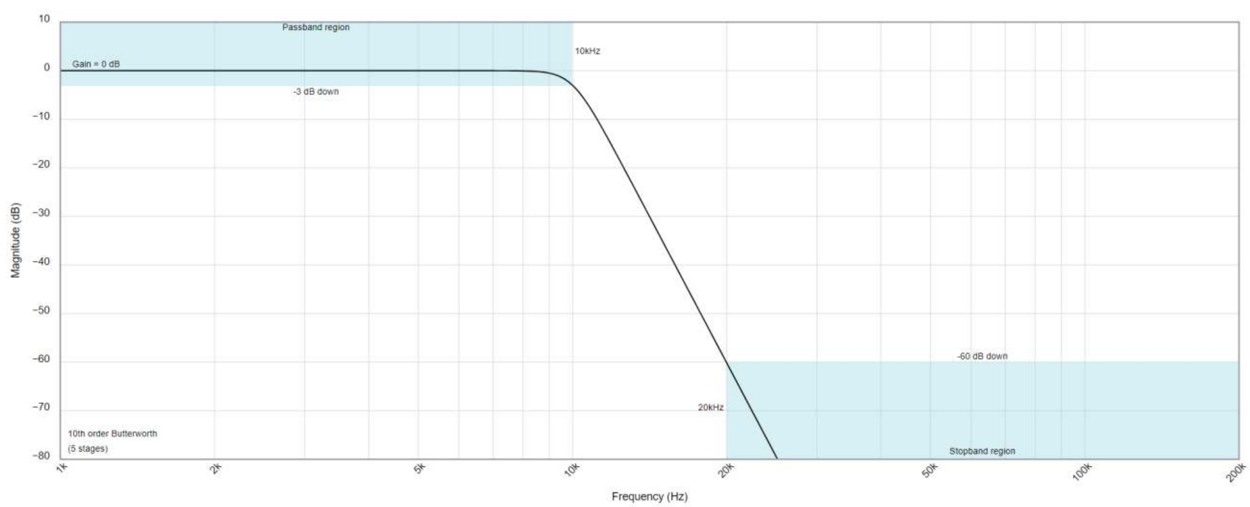

Figure 3.41. Magnitude Response of Designed Butterworth Filter [12]

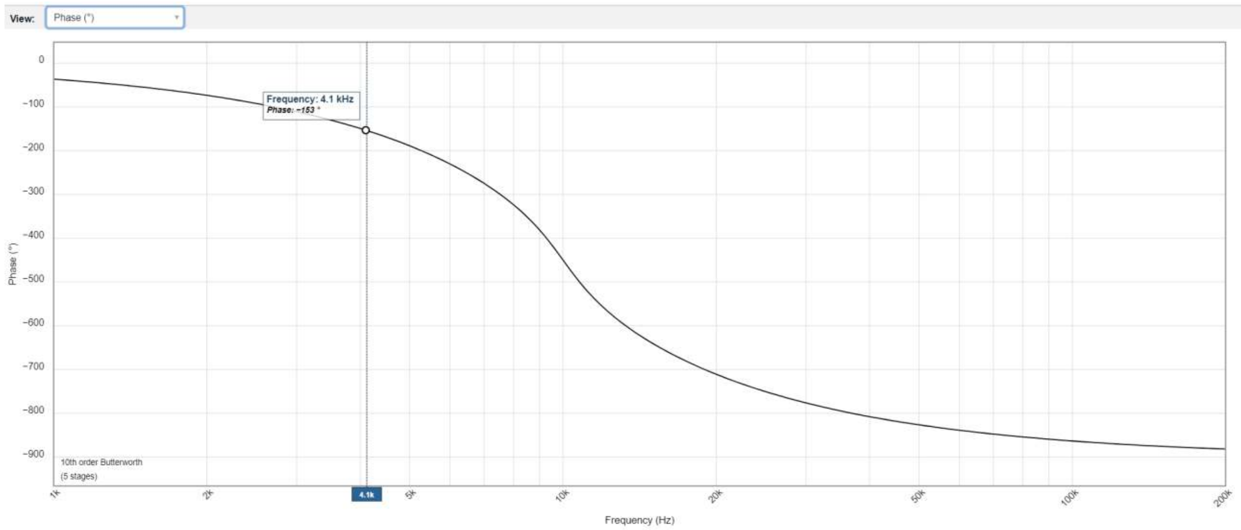

Figure 3.42. Phase Response of Designed Butterworth Filter [12]

3.2.2. ADC Block

Before getting to the specifications of the selected ADC, different ADC architectures and their advantages and disadvantages also, areas of usage should be reviewed in detail. Because selecting the proper ADC for the desired application has huge impact on the design. The ADCs are used in various applications and industries but the common areas can be categorized in four such as; data acquisition applications, industrial precision measurement, audio and voice applications and high-speed applications (mostly sampling rate > 5 MSPS). Regarding those four areas, three types of ADC architecture can meet the needs for the appropriate design and the ADC types are Sigma-Delta (∑-Δ), SAR (successive-approximation) and Pipelined ADCs.

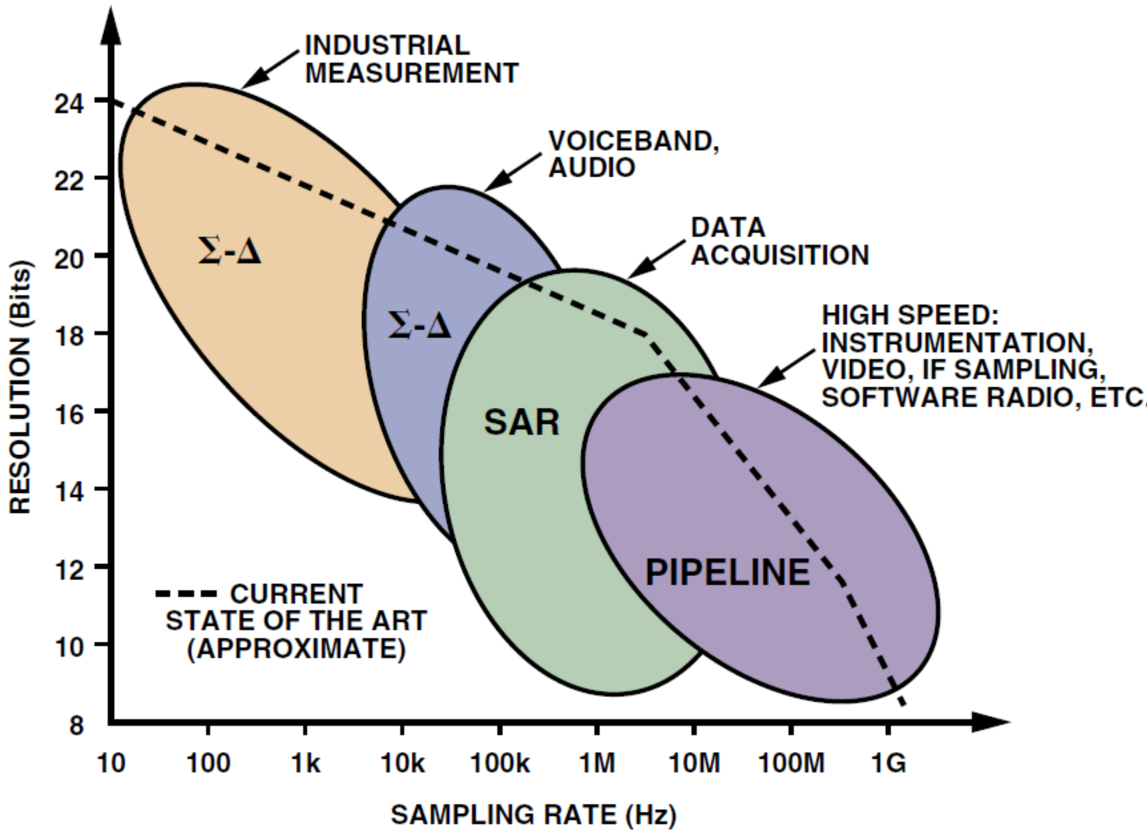

Figure 3.43. ADC Architectures, Resolution, Sample Rates and Applications [17]

In the above figure, it is illustrated that ADC types that is used in different areas and their related sampling rates according to the resolution needed [17].

3.2.2.1. Successive approximation (SAR) ADCs

In the field of ADC usage, SAR ADCs are extremely common. Especially when multiple channels are needed in complex designs. The first SAR ADC was introduced in 1954, which was designed by using vacuum-tube technology, by Bernard Gordon with 11-bit resolution and 50-kSPS sampling rate that dissipates 500 watts of energy. With evolving technology, current SAR ADCs can be found for 8-bit to 18-bit and up to several MSPS sampling rates. Luckily, their power consumptions are much less than 500 watts.

As one can know, ADCs are devices that convert analog signals to digital signals. Therefore, while they take analog inputs from various analog outputs, digital data are fed through their outputs. When low sampling frequencies are considered, the ADCs digital outputs are usually SPI, I2C or parallel outputs.

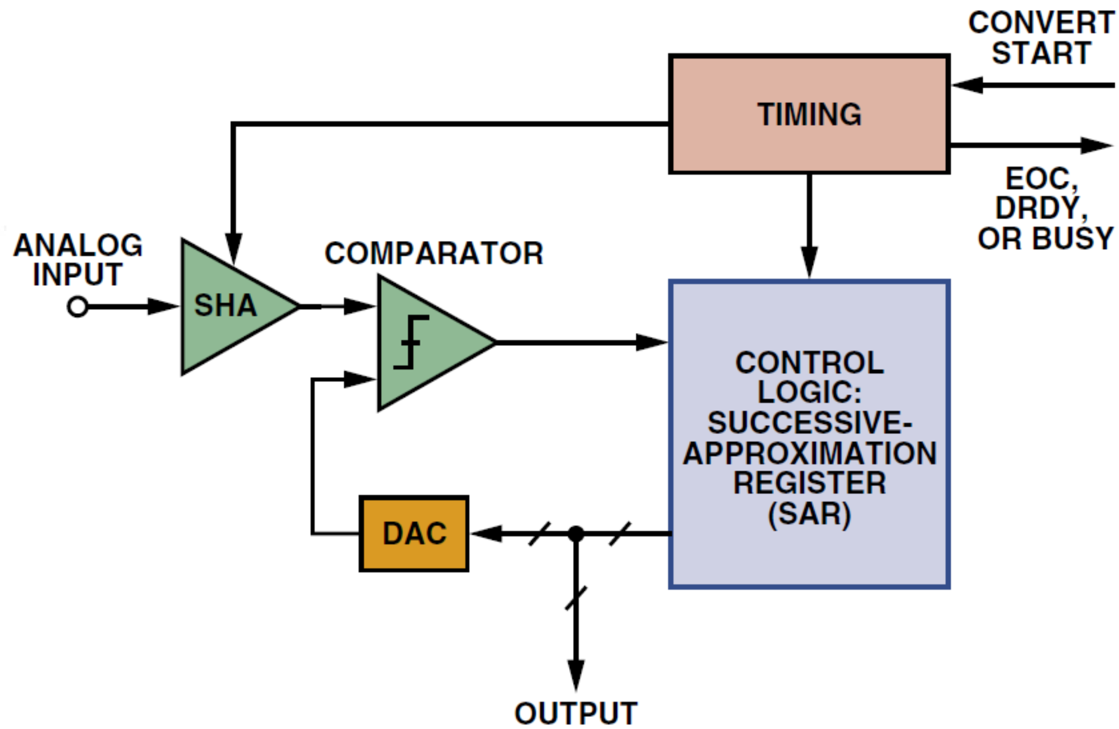

Figure 3.44. Basic Successive Approximation (SAR) ADC Block Diagram [17]

In the above figure [17], SHA refers to Sample and Hold, DAC refers to Digital to Analog Converter. As can be seen from the above figure, SAR ADCs have sample and hold circuitry at the input of their designs in order to keep the signal level steady while conversion continues. Conversion is started by setting the threshold value of the comparator by using DAC. Then, determining whether the output of the SHA circuitry is greater or less than the threshold which is set by DAC output is done by comparator. Afterward, successive approximation registers to restore the result in digital form which is 0 or 1 (The first conversion is referred to as the most significant bit (MSB)). After the first bit of conversion is performed, the DAC output's scale is changed to ¼ or ¾ based on the MSB value, and comparator output which is the second bit of the conversion is stored in the SAR registers. Subsequently, conversion is continued until all bits are converted and stored in the registers.

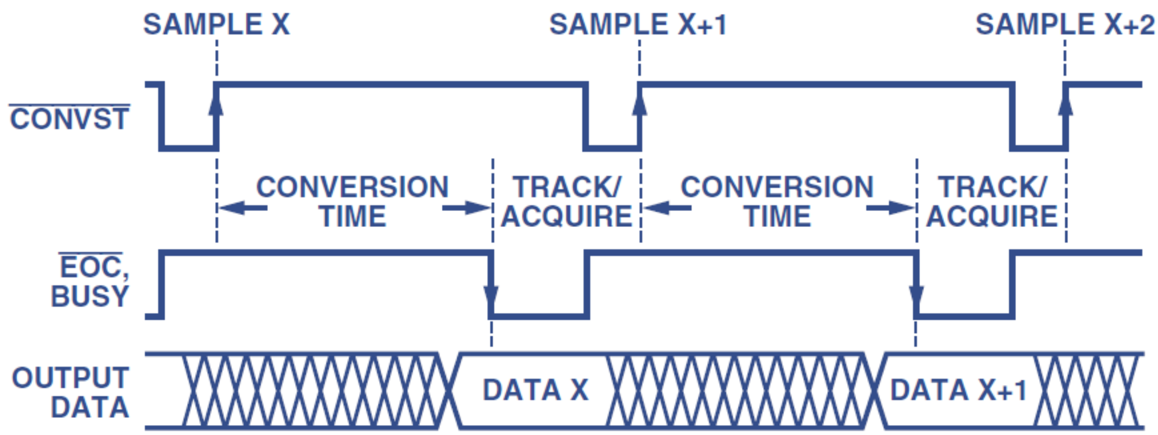

Figure 3.45. Typical Timing Diagram of the SAR ADC [17]

Above figure represents the typical timing diagram for SAR ADCs. Where CONVST is conversion start and EOC is end of cycle. As it can be seen from the figure data sample is ready at the end of the conversion cycle meaning that there is no delay or latency that makes SAR ADCs convenient to use in designs. Most of the current SAR ADCs uses high speed clock to control their internal operations. This clock can be internal (i.e. embedded in the SAR ADC IC) or external.

Successive-approximation ADCs' algorithm depends on the mathematical problem of discovering the unknown weight of an object with minimum iterations. This makes SAR ADCs algorithm go back to the fifteenth century. This mathematical problem's solution has been defined by Tartaglia in 1556. He used the binary series as weight resolutions meaning that; using1 kg, 2kg, 4kg, 8kg, 16kg, 32kg etc. weights one can approach to the unknown weight. In order to make this solution clear, let's assume that unknown weight is 45 kg and the following figure explains how the determining of unknown weight and also principle of successive-approximation ADC algorithm works.

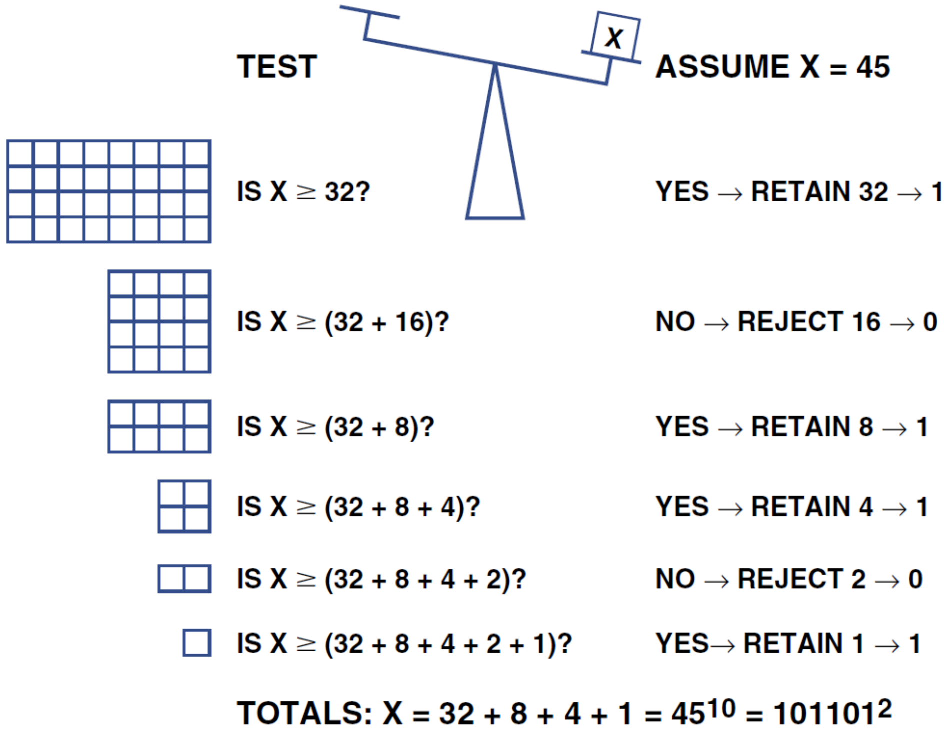

Figure 3.46. Algorithm of Successive Approximation ADC Explained with Binary Weighing [17]

Since the threshold value that is generated for comparator is synthesized by internal DAC, the SAR ADC's accuracy, linearity and performance are relying on the DAC's characteristics. While early SAR ADCs were designed by using DACs with laser trimmed thin film resistors, modern SAR ADCs are using the switched-capacitor DACs in CMOS-based SAR ADCs. The reason behind the change is that high-accuracy photolithography can provide the accuracy and the linearity which is essential for SAR ADCs' performance. Modern SAR ADC block diagram is given below [17];

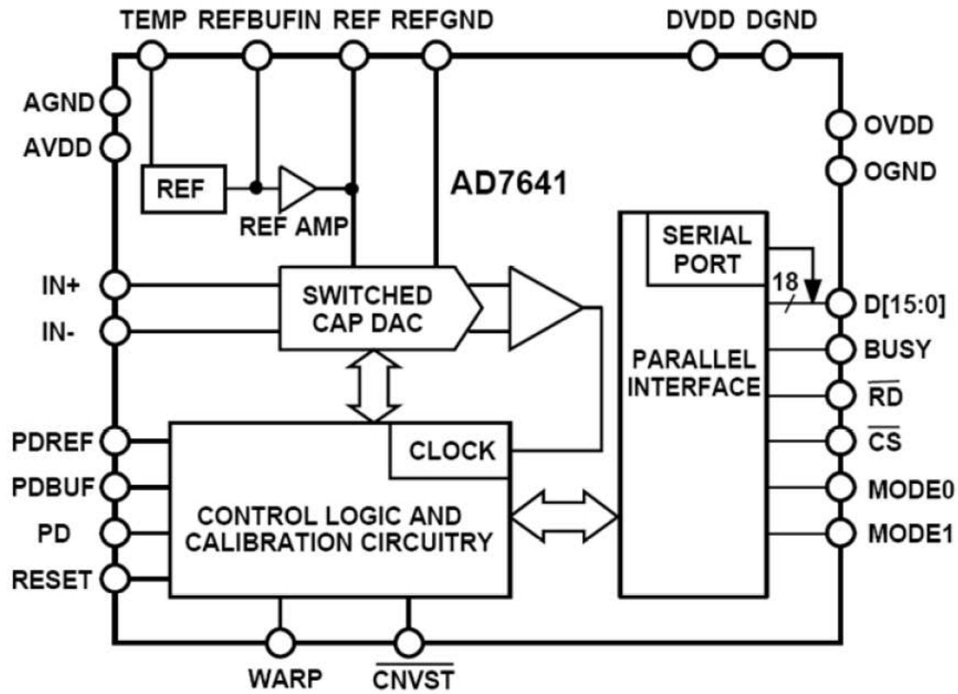

Figure 3.47. Modern SAR ADC Block Diagram [17]

3.2.2.2. Sigma-delta (∑-∆) ADCs

Sigma-delta ADCs are preferred in audio, vibration and high-resolution (16-24 bit) precision measurement applications. Due to its architecture sigma-delta ADCs have high precision and resolution and can be found up to 1MSPS sample rate.

The discovery of sigma-delta ADCs is established in Bell Labs in 1950s. Starting with experimental approach in digital transmission systems by using the technique of delta modulation and differential PCM (pulse-code modulation). Then, the concept of sigma-delta architecture is comprehended during the 1960s. Unfortunately, IC design of sigma-delta ADCs was not very common until the 1980s because sigma-delta architecture is containing digital filter due to its architecture.

There are four different concepts that are used in sigma-delta architecture which are:

- Oversampling
- Noise-Shaping
- Digital Filtering
- Decimation

Below figure represents the benefits of fundamental concepts that is used in sigma-delta ADC architecture [17].

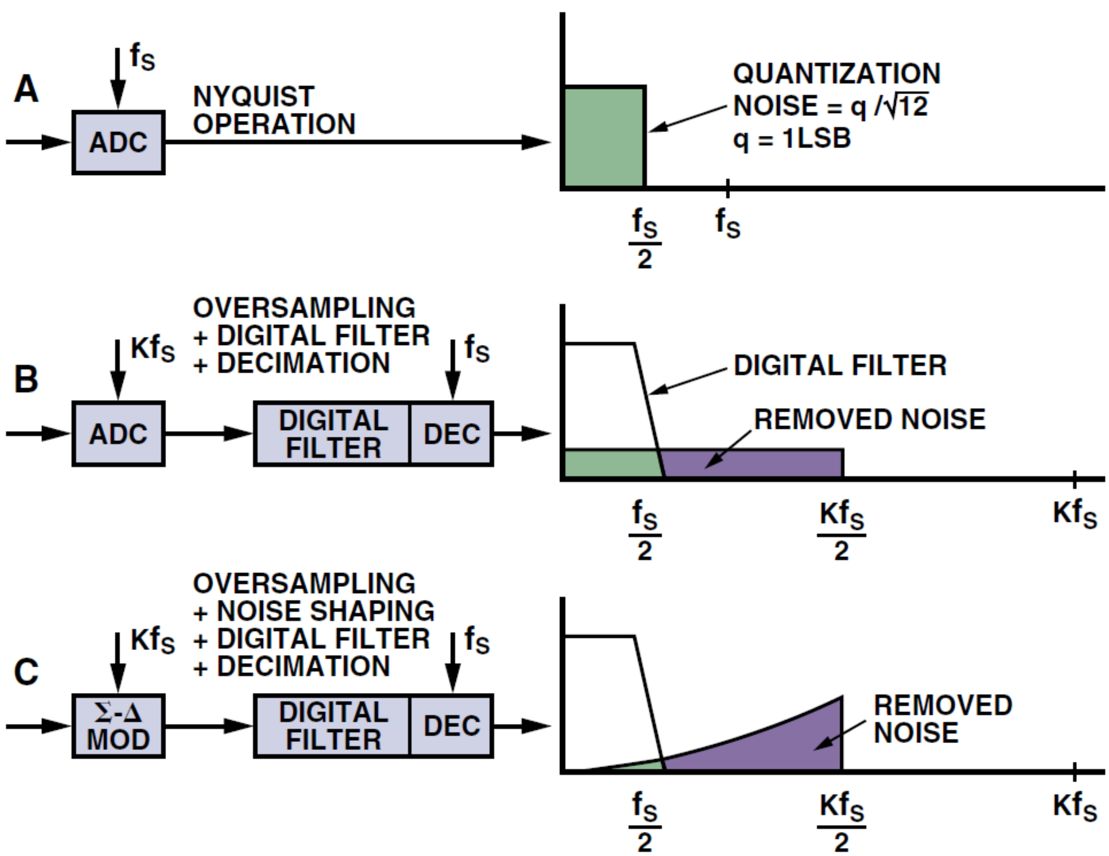

Figure 3.48. Effects of the Four Different Concepts That is Taken Advantage of by the Sigma-Delta ADCs [17]

In the figure A represents noise spectrum of the simple Nyquist theorem which is sampling rate of the ADC is two times higher than the input signal's bandwidth. In other words, bandwidth of input signal is from dc to $f_s/2$ where f_s is sampling frequency. Bandwidth contains the quantization noise uniformly between dc and Nyquist frequency. B represents the increased sampling rate with a constant K while the input signal bandwidth is unchanged. This process is defined as oversampling and K is defined as oversampling ratio. Occurrence of the quantization noise outside of the bandwidth is cleared with digital filter. Afterwards, output data rate which is increased by the oversampling constant K should be reduced to its Nyquist frequency ($f_s/2$). Decreasing the sampling rate is known as decimation and the whole process is represented in the figure C. This whole process consisting of fundamental concepts of sigma-delta ADC (oversampling, noise shaping, digital filtering and decimation, increases the performance of ADC's by increasing the SNR level in the bandwidth of the signal. By multiplying K with two, SNR value increases 3dB within the bandwidth. The block diagram of the basic sigma-delta ADC is shown below.

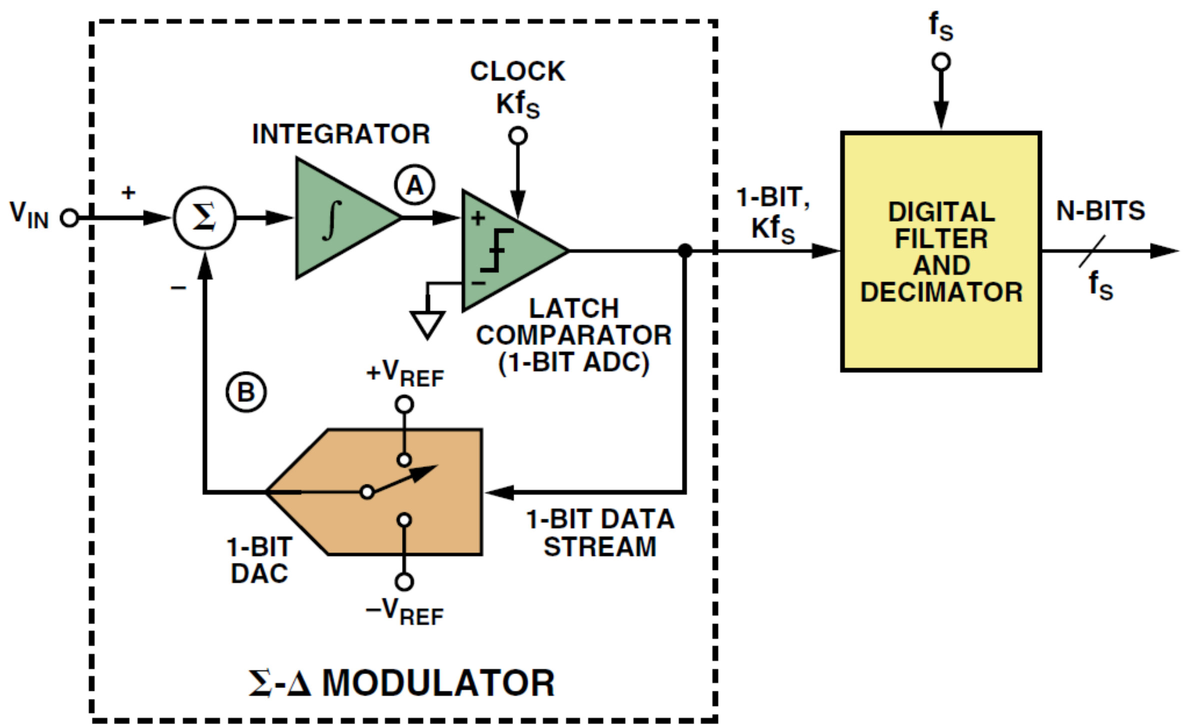

Figure 3.49. First Order Sigma-Delta ADC [17]

The main components of first order sigma-delta modulator are 1-bir ADC (comparator) and 1-bit DAC. As one can guess, the output of the modulator is 1-bit. Modulator behaves like low pass filter for the input signal and for the quantization noise modulator behaves like high pass filter. By doing so, modulator can achieve the one of the fundamental concepts of sigma-delta architecture which is noise shaping.

While the first order sigma-delta modulator is linear and monotonic, noise shaping performance, of course, is not adequate for the most applications. In order to increase the noise shaping performance of the sigma-delta modulator, used number of integrators should be increased. All individual integrators can be considered as poles of the filters. Increasing the numbers of integrators increases the sharpness of the filter. The relationship between the integrator number and the noise characteristics is given below [17].

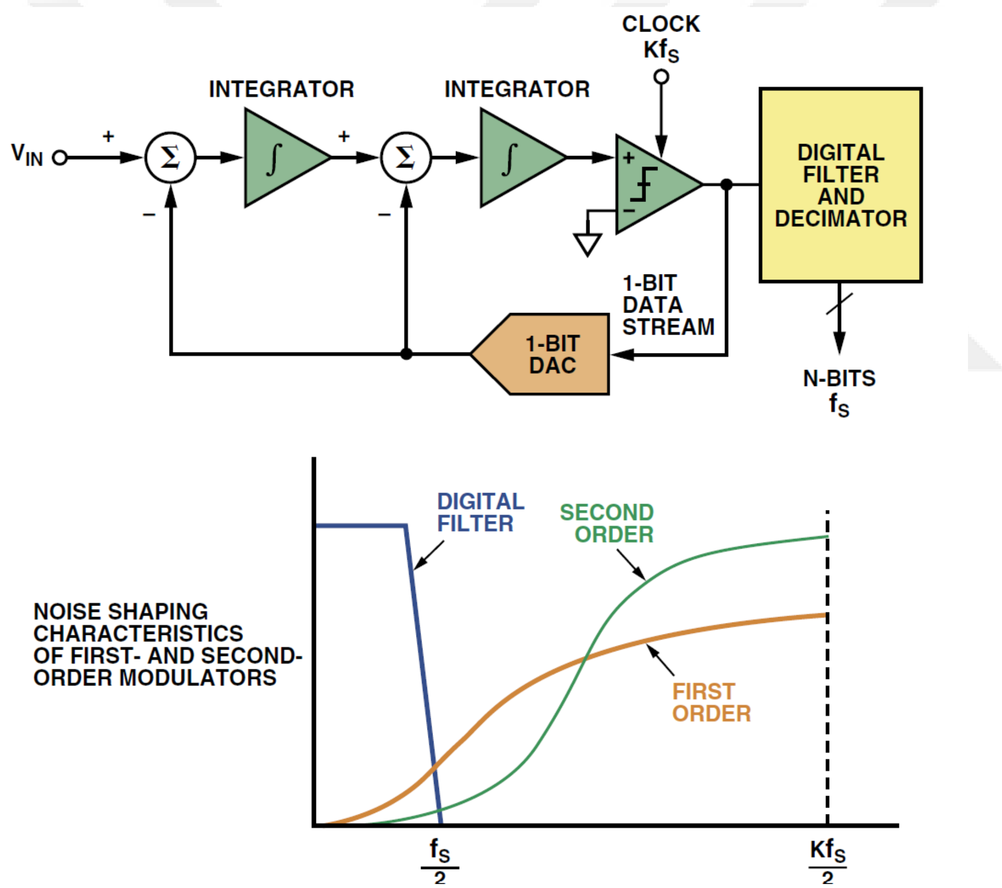

Figure 3.50. Second Order Sigma-Delta Modulator and Comparison of Noise Characteristics [17]

3.2.2.3. Pipelined ADCs

Applications that are required more than 5 MSPS sampling rate can be considered as high-speed applications. Therefore, as it can be seen from, at higher sampling rates pipelined ADCs are becoming good choice for designs. The pipelined ADCs can be tracked back to 1950s with a close relation of subrange architecture. The block diagram of 6-bit subrange ADC is shown below;

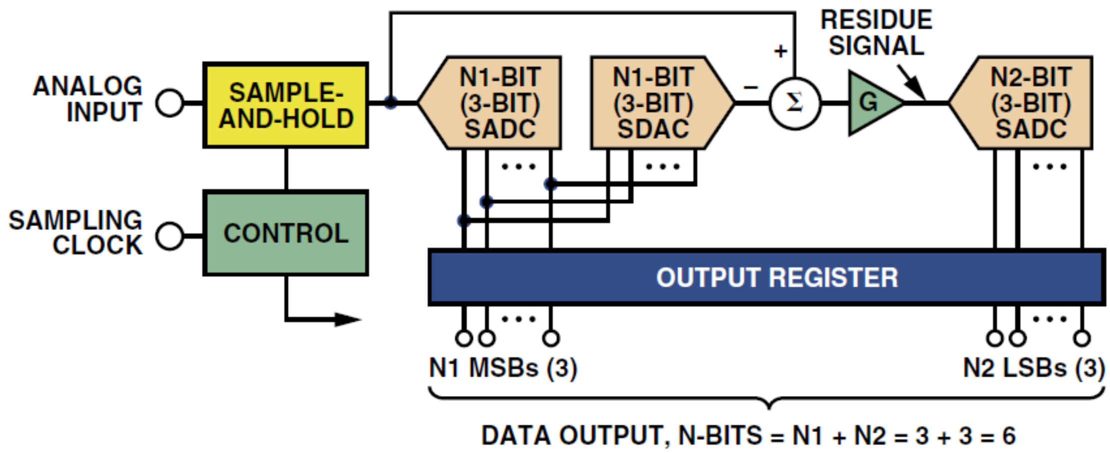

Figure 3.51. 6-bit Subranging ADC Block Diagram [17]

In the above figure [17], the first 3-bit sub-ADC samples the signal coming from the sample and hold circuitry. Then, the digitized signal is transformed back to an analog signal with a help of 3-bit sub-DAC shown in the figure. Afterwards, by removing the sub-DAC output from the sample and hold circuitry output, signal goes through gain block. After the amplification this residue signal, another 3-bit sub-ADC is used to sample the residue signal. The signal, which is given below figure, can be considered as very common when the ramp signal with low frequency is applied to ADC. Since the missing codes are not wanted, residue signal amplitude should be in the range of the second stage ADC, which is represented in the ideal ADC case. This dictates that both of the N1 bit sub-ADC's and the sub-DAC's accuracy should exceed the N1+N2 = 6-bit. Otherwise, the resulting missing code situation can appear by the effect of non-linear N1 sub-ADC or mismatch at the gain stage of the architecture. The representation of the ADC output when the mentioned conditions are occurred is given below.

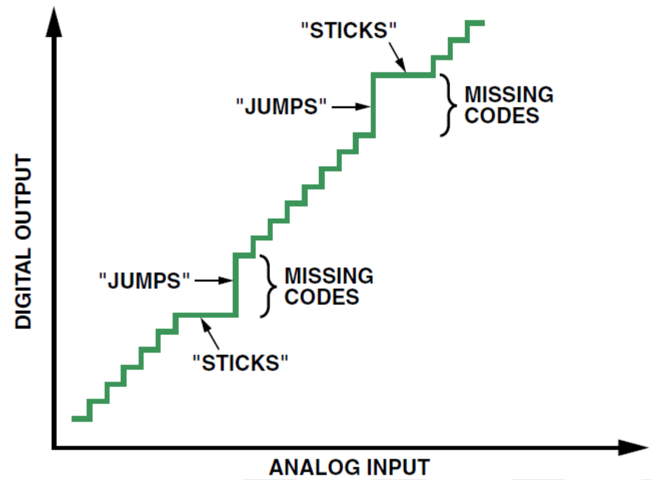

Figure 3.52. Missing Codes Caused by Non-Linear N1 sub-ADC or Mismatch at the Gain Stage of the Architecture [17]

Previously mentioned 6-bit architecture is practical up to 8-bits, meaning that N1 = 4 bit and N2 = 4 bit. This 8-bit limitation can be overcome with error correction addition. After a decade, in 1960s, to acquire better resolution with the subranging architecture the bit size of the second stage sub-ADC is increased by 1-bit. Increased bit size in the second stage ADC allows that residue signal is not exceeding the ADC's range. Nonetheless, need for N1 + N2 bit accuracy for sub-DAC remains the same. Below figure represents the basic block diagram of the 6-bit subranging ADC with error correction.

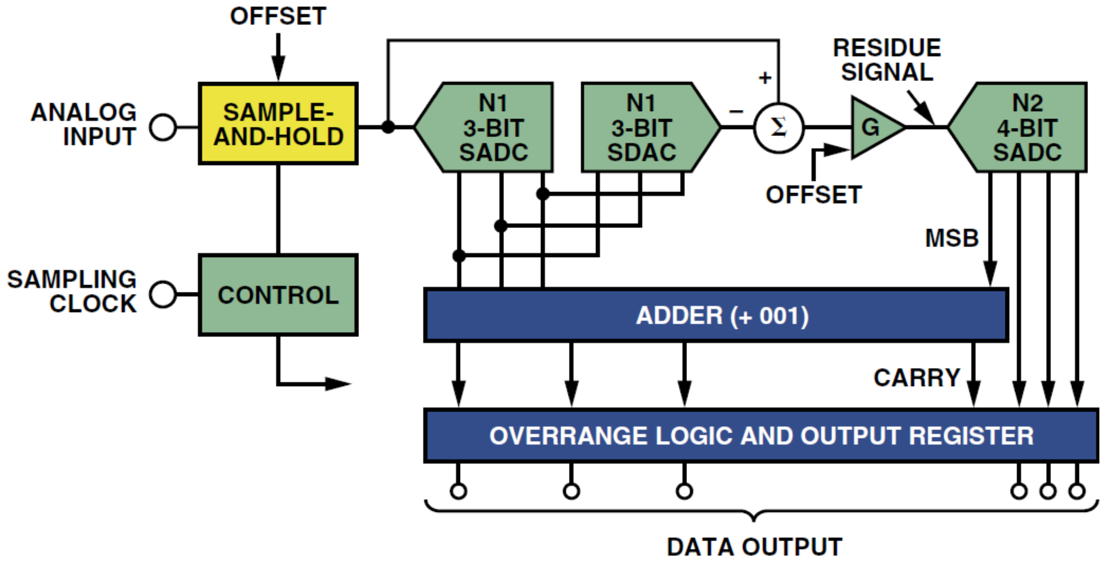

Figure 3.53. Basic Block Diagram of the 6-bit Subranging ADC with Error Correction [17]

As one can see, the second stage sub-ADC bit size is increased to 4-bit. Also, it is seen in the figure that additional logic is implemented for the case that the residue signal falls beyond the ADC range. With this logic, simply an adder, the second ADC chooses whether the MSB should be incremented by 001 or not. This adder is being used as DC offset and of course, the value of 001 can vary.

One should know that error correction subranging ADCs does not have pipeline delay. Because, while the following processes, that is given below, occur, the sample and hold circuitry's input waits at hold mode.

- N1 sub-ADC decision making
- Reproducing N1 sub-ADC output by subtracting the SHA output from sub-DAC's output.
- Amplification
- Digitization with N2 sub-ADC
- Error correction logic
- Writing to output registers

When the higher speed of the subranging ADCs occurred, the pipelined ADC architecture was being used. The following figure shows the block diagram of the pipelined architecture.

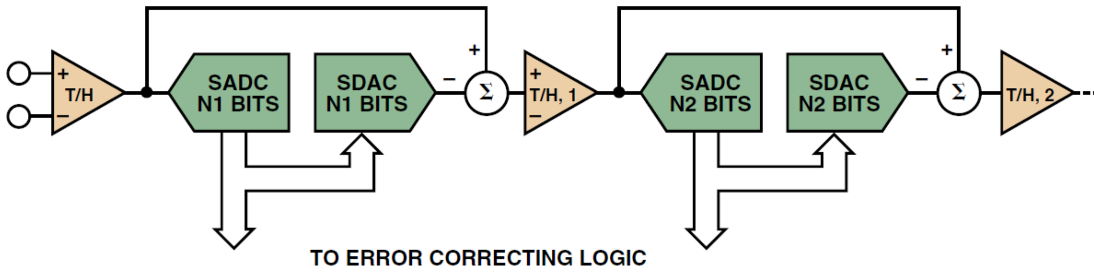

Figure 3.54. Block Diagram of Pipelined Architecture with Error Correction Logic [17]

The pipelined ADC architecture contains digitally corrected subranging architecture meaning that the first stage handles the data for half a cycle of the conversion time and passes through the residue signal to the next stage to be handled in the remaining half cycle of the conversion time. The T/H circuitry, meaning that Track and Hold, between the stages, has a duty as an analog delay line. It begins to hold a signal when the first stage ADC completes its conversion. By doing so, other sub-ADCs, sub-DACs, and amplifiers in the pipeline gain more time to settle. Therefore, higher speed rates are achieved by the pipelined architecture compared to the non-pipelined architecture [17].

To sum up, one should know that even though pipelined ADCs are subranging, subranging ADCs do not have to be pipelined. The pipelined ADCs can be found sampling rates up to 10 MSPS. They have good SNR and spurious-free dynamic range. It is very feasible to use the pipelined ADCs in SDR (software defined radio) applications. Following figure represents the timing relationship of classical pipelined ADC.

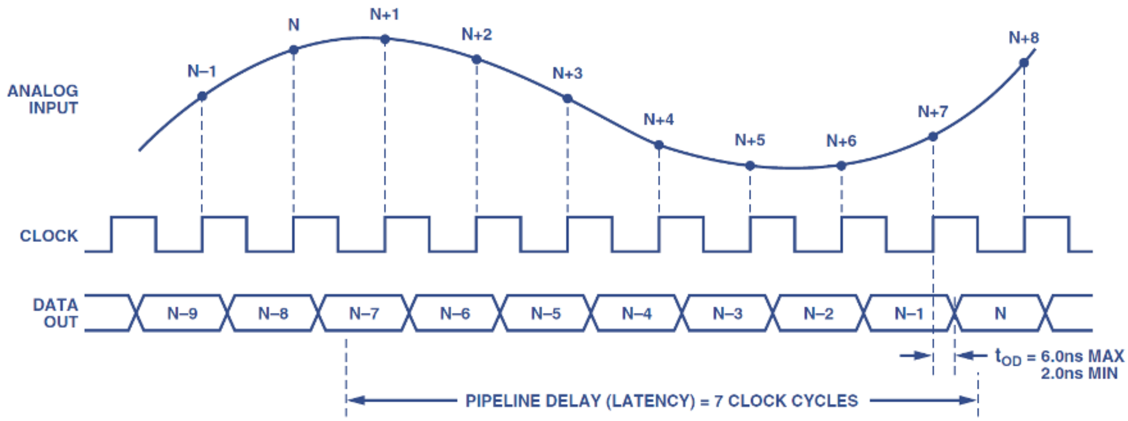

Figure 3.55. Timing of a pipelined ADC with 65 MSPS Sampling Rate[17]

So far, successive approximation, sigma-delta and pipelined architectures have been summarized. Successive approximation (SAR) ADCs are good choice for data acquisition applications. They are easy to use and can be found for up to 3MSPS sampling rate and up to 18-bit. For more precise industrial measurement applications sigma delta ($\sum$-Δ) ADCs are perfect fit due to their up to 24-bit resolutions. This makes sigma delta ADCs good choice for sensor-conditioning. In most designs, thanks to 24-bit resolution, there is no need for external signal conditioning block and sensors can be directly connected to ADC input channels. This allows to simplify the designs. For higher sampling rate (between 5 MSPS and 100 MSPS) pipelined ADCs are better choice due to their pipelined architecture and their SFDR and SNR values.

3.2.2.4. ADS1278

All things considered, in our application sigma-delta type ADC is preferred. Since the output of the velocimeter sensor is in the range of millivolts, the data acquisition system needs higher resolution and, of course, one may can know, aircrafts are very noisy environments for both electronically and mechanically. Due to defining these design constraints and the determination of desired region of frequency, ADC with a manufacturing part number ADS1278 is chosen. ADS1278 is an excellent choice for our design due to several reasons. Such as; It has simultaneous sampling capability up to 8 channels, 144kSPS data rate which is more than enough for the Nyquist frequency, very high signal to noise ratio (111dB), SPI data interface, differential analog input that is resilient to common mode noise.

Due to the analog input ranges of the ADS1278, input signal range of the system is -2.5V to +2.5V and the resolution of ADS1278 is 0.298 uV meaning that has very high resolution for the study. Another approach is that designed system can measure the vibration with a resolution as low as 15.6 uIPS. Since the velocimeter output is single ended and the inputs of ADS1278 are differential ended, single ended to differential ended converter op-amp is used. For this purpose, OPA1632 differential amplifier is used. The reason for selection of OPA1632 is that it has very wide supply range (+/- 15V) and it is recommended in ADS1278 datasheet for compatible input type.

For the voltage reference (VREFP) of the ADS1278, voltage reference IC REF5025 is used. Privileges of the voltage reference ICs can be summarized as follows;

- Very low output noise
- Very high precision output voltage accuracy
- Very low drift

Since ADC's performance is depending upon the its voltage reference, it is wise to use low noise and high precision voltage reference ICs.

Due its stable passband response ADS1278 is configured for high resolution mode in this design. The response is given below [18].

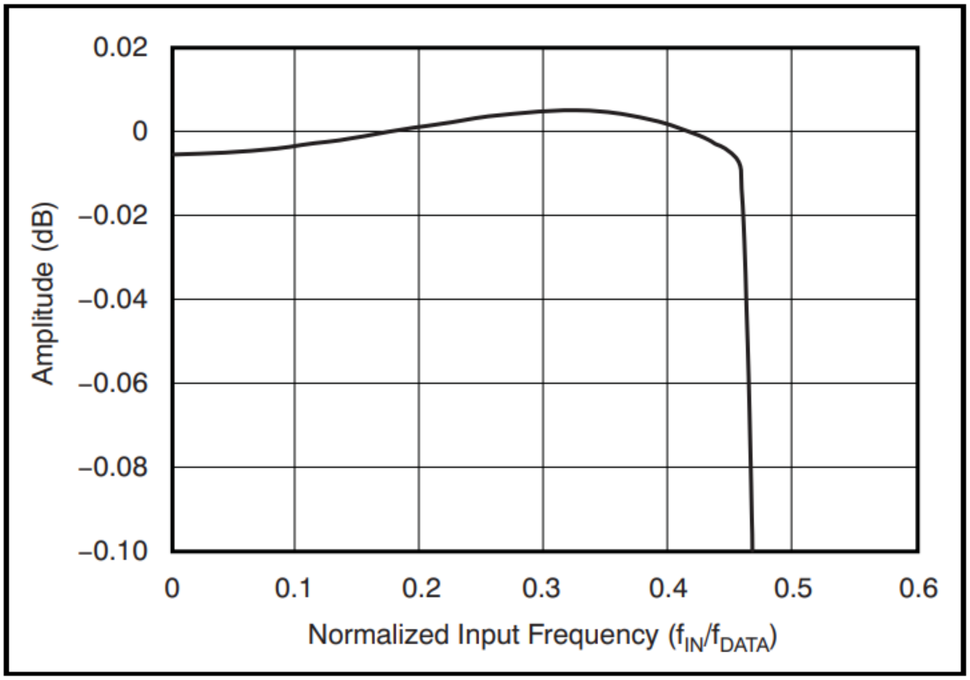

Figure 3.56. Passband Response of ADS1278 [18]

In order to configure ADS1278 for high resolution mode, MODE[1:0] pins are set to '01', clock frequency is set to 27MHz and sample rate of the ADS1278 is set to 52.734 KSPS. For the digital output of the ADS1278, FORMAT[2:0] pins are set to '001' for SPI interface and fixed TDM data output mode meaning that, at the first DOUT1 pin of ADS1278, sampled data are fed through in channels order (i.e. CH1, CH2, CH3 etc.). The representing figure is shown below.

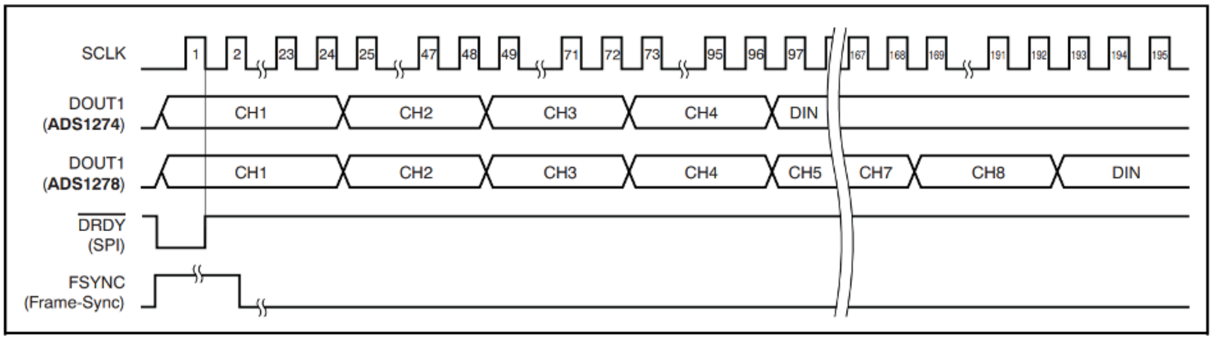

Figure 3.57. TDM Mode All Channels Enabled [18]

3.2.3. FPGA block

FPGA (Field Programmable Gate Array) is type of integrated circuit that can be repeatedly programmable after the manufacturing. They are consisted of grid of interconnected programmable logic elements. Also, FPGAs can be considered as blank circuitry that can be programmed into anything via VHDL or Verilog languages. This unique structure helps the designers to implement various designs. Another benefit of the FPGAs is that they don’t have to work as sequential, meaning that they can operate the processes parallelly. This feature also has huge impact on complex designs. For these reasons, in many applications FPGAs are preferred, especially in digital signal processing applications.

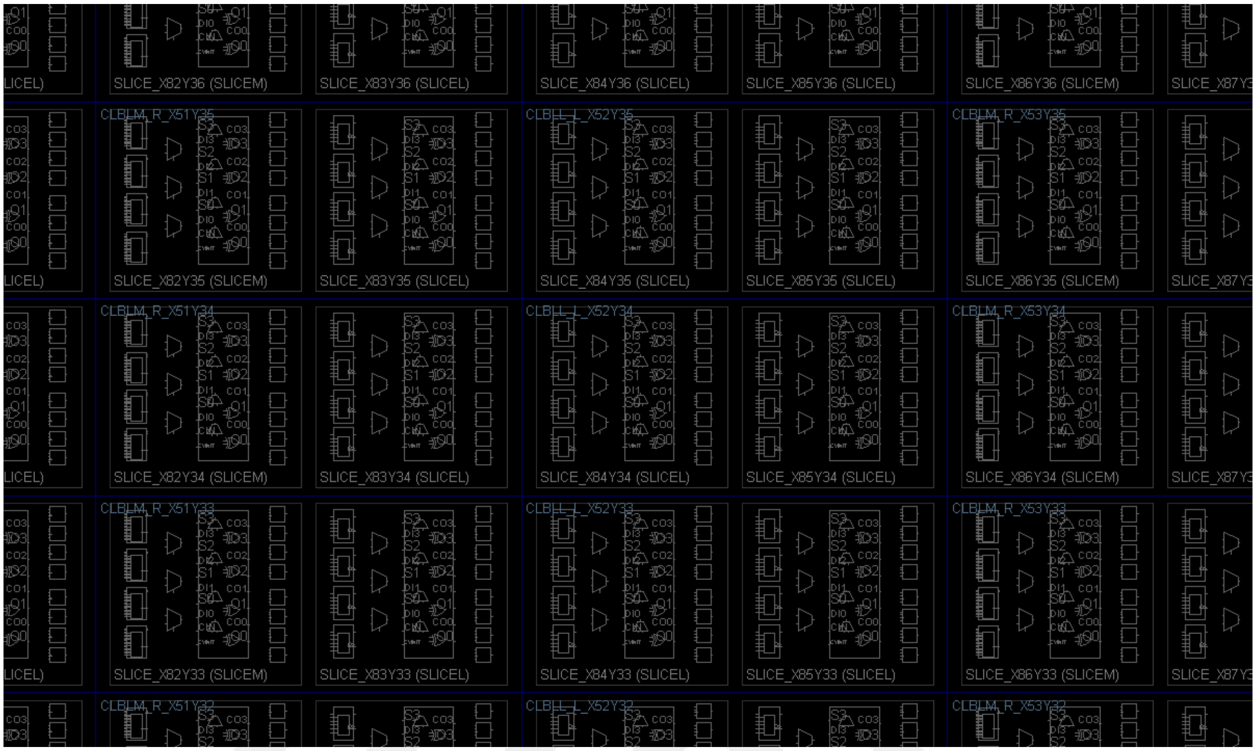

Figure 3.58. Internal Structure of the FPGA

In this design, FPGA of Zynq 7015 family has been used to collect sampled data from ADC. Unlike the FPGAs, selected Zynq-7015 is in the SoC (system on Chip) family. SoCs are consisted of two parts which are PL (Programmable Logic) and PS (Processing System). PL side is an FPGA part and working principle is identical with FPGAs. PS side can be considered as ARM Based MCU (Micro Controller Unit) and working principle is same as MCUs. In order to program PS side C language can be used. Main properties of Zynq-7015 both PL and PS are listed below;

PS SIDE:

- 2.5 DMIPS/MHz per CPU
- CPU frequency: Up to 1 GHz
- Coherent multiprocessor support
- ARMv7-A architecture
- Single and double precision Vector Floating Point Unit (VFPU)

- Three watchdog timers
- One global timer
- Two triple-timer counters
- On-chip boot ROM
- 256 KB on-chip RAM (OCM)
- 16-bit or 32-bit interfaces to DDR3, DDR3L, DDR2, or LPDDR2 memories
- 8-bit SRAM data bus with up to 64 MB support
- Parallel NOR flash support
- ONFI1.0 NAND flash support (1-bit ECC)
- 1-bit SPI, 2-bit SPI, 4-bit SPI (quad-SPI), or two quad-SPI (8-bit) serial NOR flash
- Two 10/100/1000 tri-speed Ethernet MAC peripherals with IEEE Std 802.3 and IEEE Std 1588 revision 2.0 support
- Two USB 2.0 OTG peripherals
- Two full CAN 2.0B compliant CAN bus interfaces
- Two SD/SDIO 2.0/MMC3.31 compliant controllers
- Two full-duplex SPI ports with three peripheral chip selects
- Two high-speed UARTs (up to 1 Mb/s)
- Two master and slave I2C interfaces
- Up to 54 flexible multiplexed I/O (MIO) [19]

PL SIDE:

- Look-Up tables
- Flip-Flops
- Cascadeable Adders
- 36 Kb Block RAM
- 18x25 signed multiply
- 48-bit added/accumulator
- 25-bit pre-adder
- Supports LVCMOS, LVDS, SSTL
- 1.2V to 3.3V Voltage Level

- JTAG boundary scan
- PCI Express up to Gen2 x8 lanes
- Up to 16 12.5 Gbit/s receiver and transmitters
- Two 12-bit ADC [19]

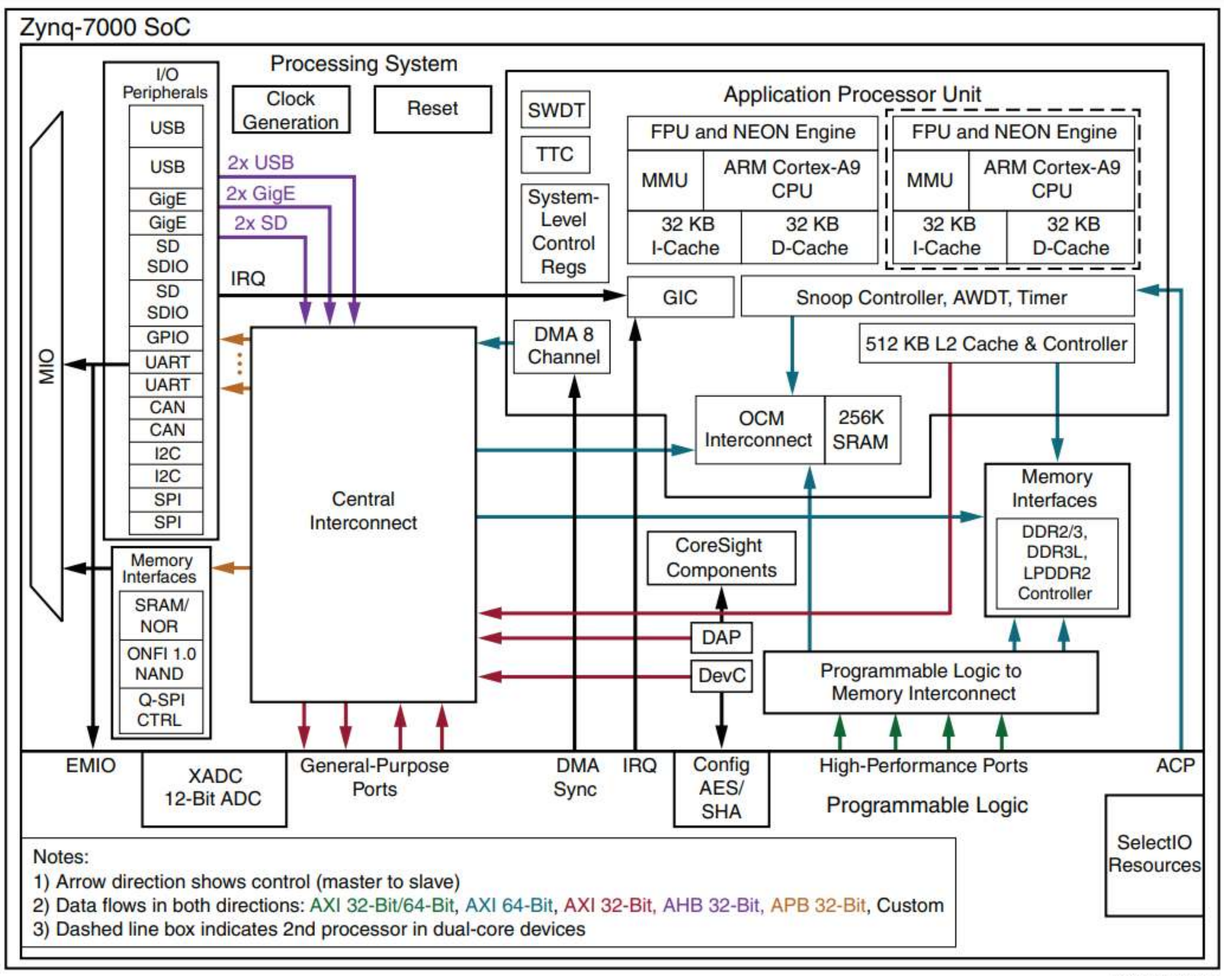

Figure 3.59. ZYNQ 7000 Architecture [19]

Since the ADS1278 has SPI interface, SPI communication module is designed in VHDL for configuration the ADS1278 and also data collection. In order to boot the FPGA and keep the relevant data for the algorithm also QSPI and EEPROM IC is included in the design. Also, for the communication between the Analog Input Module and Controller Module AXI Quad SPI IP is used.

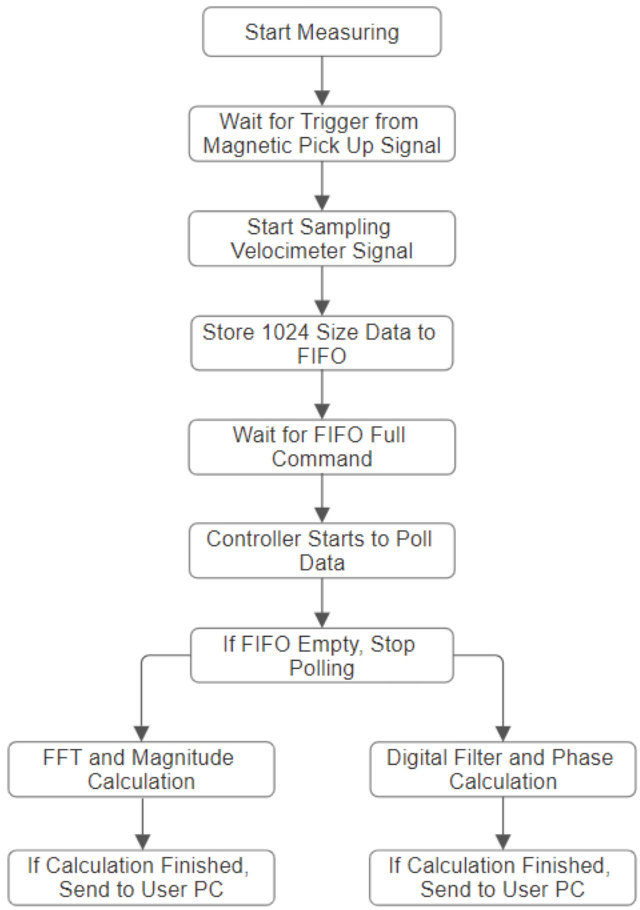

Figure 3.60. Pseudo Code of Measuring and Analysis Process

3.3. CONTROLLER MODULE

3.3.1. Communication interfaces and module features

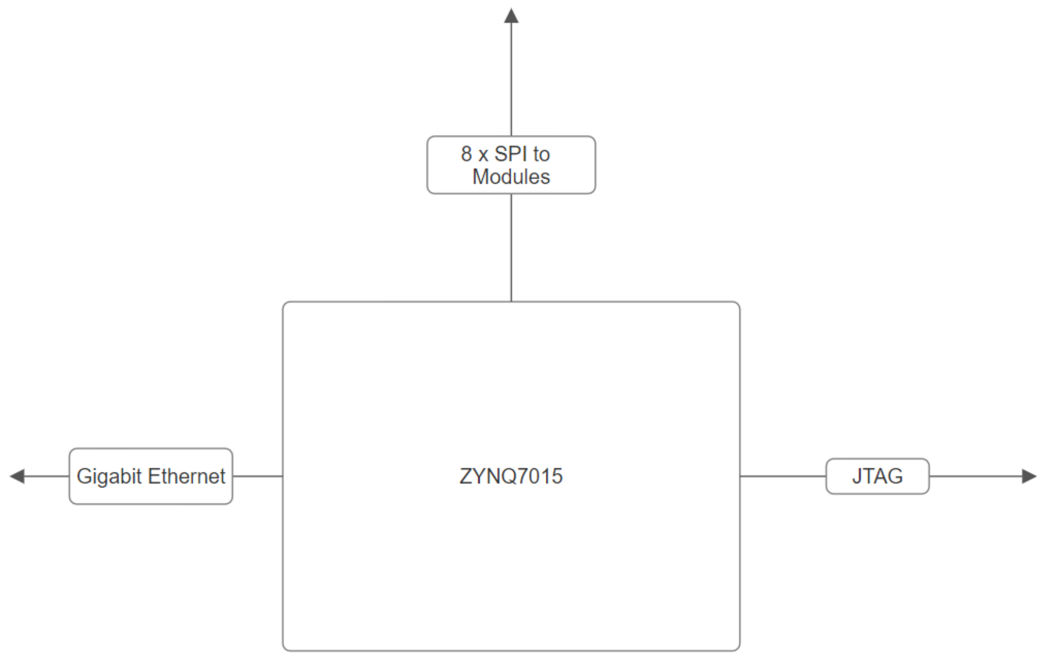

Figure 3.61. Block Diagram of Communication Interfaces

3.3.1.1. Gigabit ethernet

In this design, Gigabit ethernet communication interface is implemented in order to link the designed DAQ device to user PC. As one can know, ethernet interface is very common and available in many current computers. Moreover, since the gigabit ethernet is backward compatible meaning that it can work as 100-base or 10-base, gigabit ethernet selection is efficient for this design.

For the physical layer Marvell 88E1512 PHY with RGMII interface has been chosen. In RGMII interface there are 4 data lanes and also there are one control and clock lanes for each transmit and receive side. 88E1512 integrated circuit converts RGMII interface to ethernet interface. In gigabit ethernet interface, there are four differential lanes (MDI[0], MDI[1], MDI[2], MDI[4]) these data lanes can be routed to RJ45 ethernet connector or different high speed connectors in order to connect ethernet data lines together. During the design phase, hardware designer should take attention for matching the lengths of receiver and transceiver traces of RGMII signals individually and for the MDI signals also should be matched. Length matching issue is very crucial for high-speed interfaces because travelling time or delay time for each data lanes should be equal. If the mismatch occurs between the lanes, then communication interface cannot be established due to design failure. The overall block diagram of the ethernet is given below;

Figure 3.62. Block Diagram of Ethernet Interface

After clarifying the hardware side of ethernet protocol, the IwIP is used for embedded side. The IwIP is TCP/IP ethernet protocol implementation that can be found in Vitis IDE (Integrated Development Environment) which is development tool that AMD provides for PS side implementations. Usage efficiency and availability of the IwIP is considered, many embedded designers are using IWIP for ethernet application implementations.

In this design, example codes of lwIP echo server application had been used for constructing overall system ethernet communication. The controller module is getting data of analog modules, then processing with DSP operations and algorithms after that sends the output of the processed sensor data to host pc through ethernet interface. The embedded design of the system is conducted by colleague of mine. The overall data flow representation is given below.

3.3.1.2. Serial peripheral interface (SPI)

SPI is a type of synchronous serial communication system that works as master slave architecture. Usually, it is used in wired communication in short distance and it is easy to implement in embedded systems. It is compound of four different signals which are

- SCLK (Serial clock signal responsible for synchronization
- CS (Chip select signal responsible for starting the communication)
- MISO (Master in slave out data signal)
- MOSI (Master out slave in data signal)

In order to start the communication, master should pull the CS pin to low, then during the each cycle of the SCLK signal data transmission between the master and slave occurs in the MOSI and MISO signals, meaning that it is a full duplex communication. At the end of the data transmission master ends clock signal and pull high the CS pin to high.

As mentioned before, controller module is communicating with other modules through SPI protocol and AXI Quad SPI IP is used for this purpose. Therefore, eight different SPI interface is implemented considering future expansion of the system. However, this design supports up to three modules for now.

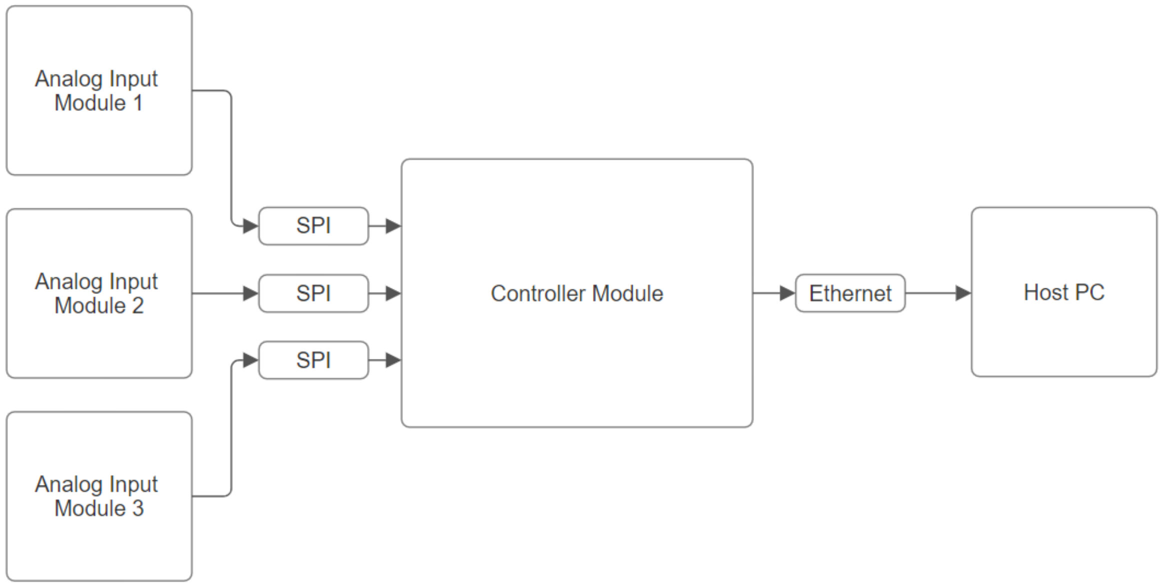

Figure 3.63. Communication Data Flow Chart Between the Modules and Host PC

3.3.1.3. JTAG interface

In addition to ethernet interface, JTAG (Joint Test Application Group) interface implementation is a must for FPGAs. Because, every connection and programming are done through JTAG interface. In this design, analog input modules' FPGAs can be programmed through controller module because JTAG chain structure is designed that way for user's convenience.

3.4. Power Module

3.4.1. Power requirements of system

Before designing the power module of the FTI system, power requirements of the entire system are listed. Then, the power design had been conducted and implemented. Power requirement of the system can be summarized as follows;

- 1500V isolation voltage
- 1000 Mohm isolation resistance
- -40/+85 ^{o}C working temperature
- +15V +/- 100mVp-p ripple, 0.5A output
- -15V +/- 100mVp-p ripple, 0.5A output
- +12V +/- 100mVp-p ripple, 0.5A output
- -12V +/- 100mVp-p ripple, 0.5A output
- +5V +/- 75mVp-p ripple, 4A output
- Overvoltage protection
- Overcurrent protection
- 18 – 40 VDC input voltage range

3.4.2. Designed power module specifications

In order to meet the criteria's, Traco power TEN20WIN series of DC/DC converters are used and implemented in the power module of the system. TEN20WIN has various types of output voltage levels and appropriate for ruggedized military designs. A number of crucial features of the DC/DC converter are listed below [8];

- 18 – 75 VDC input voltage range
- 3.3 VDC, 5VDC, 12VDC, 15VDC, -5VDC, -12VDC, -15VDC output
- Efficiency between 85-89%
- 5VDC 4A output capacity
- +15V 667mA capacity
- -15V 667mA capacity
- +12V 883mA capacity
- -12V 883mA capacity
- -40 to +85 ^{o}C operating temperature
- MIL-STD 810F compliance
- 27g weight

Although I have contributed to system design and requirement definition of the power module, PCB design of the module was conducted by colleague of mine. After doing several simulations and calculations, PCB is designed and produced according to requirements of the system.

3.5. Implementation Of Digital Design, Software and Algorithms on FPGA

3.5.1. Signal processing algorithms

3.5.1.1. Fast Fourier transform (FFT)

Before getting into the signal processing algorithm, FFT (Fast Fourier Transform), which is a well-known method for signal analysis, should be reviewed. FFT can be described as computing DFT (Discrete Fourier Transform) in a faster way or computationally easy way. As one can know, DFT is converting equally spaced time domain sample series into frequency domain series. For this reason, DFT is known as frequency domain representation of time domain signals. In order to represent the signal in the frequency domain or apply the DFT on signal, signal should be periodic. In order to compute the DFT of a periodic signal below formula can be used;

$$X(k) = \sum_{n=0}^{N-1} x(n) W_N^{kn} \qquad k=0,\ 1,\ \ldots\ ,\ N-1 \tag{3.22}$$

Where X(k) is frequency domain of input signal series, x(n) is time domain of the input signal series and W_N is given below [20];

$$W_N = e^{-j2\pi/N} = \cos\left(\frac{2\pi}{N}\right) - \mathrm{j}\sin\left(\frac{2\pi}{N}\right) \tag{3.23}$$

Combining the two equations then we get;

$$X(k) = \sum_{n=0}^{N-1} x(n) e^{-j2\pi \frac{k}{N} n} \tag{3.24}$$

In order to compute the DFT of a N sized series of x(n) requires N^2 computations. However, with FFT these computations reduce significantly to the $NLog_2(N)$. For example, size of a N=1024 sample of x(n) series needs 1024^2 = 1.048.576 computations for DFT but in FFT it requires $1024\log_2 2^{10}$ = 10.240 computations. FFT algorithms are basically DFT algorithms but FFT has a computational convenience in terms of programming.

3.5.1.2. Digital filter design and implementation

After determining the vibration magnitude, the phase of the vibration signal should be determined. Since the output of the velocimeter signal is noisy, calculating the phase is challenging. In order to eliminate this problem digital filter should be applied to signal for eliminating the noise from vibration signal. For designing digital filter, the MATLAB tool Filter Designer is used. Because it is very efficient for designing filter with different parameters and also for simulating the designed filter with MATLAB environment.

With Filter Designer tool, FIR equiripple lowpass filter is designed with cutoff frequency at 0.08 normalized frequency and stopband normalized frequency is 0.12. Gain ripple in passband region is set 0.01 dB and stopband attenuation gain is set to -100 dB for better performance. As a result of these parameters, 236th order lowpass FIR filter is implemented in the phase detection algorithm. The magnitude response of the FIR filter is shown below. As one can see from the figure the filter has very flat passband response and filter's roll off is very sharp due to adjusted filter parameters.

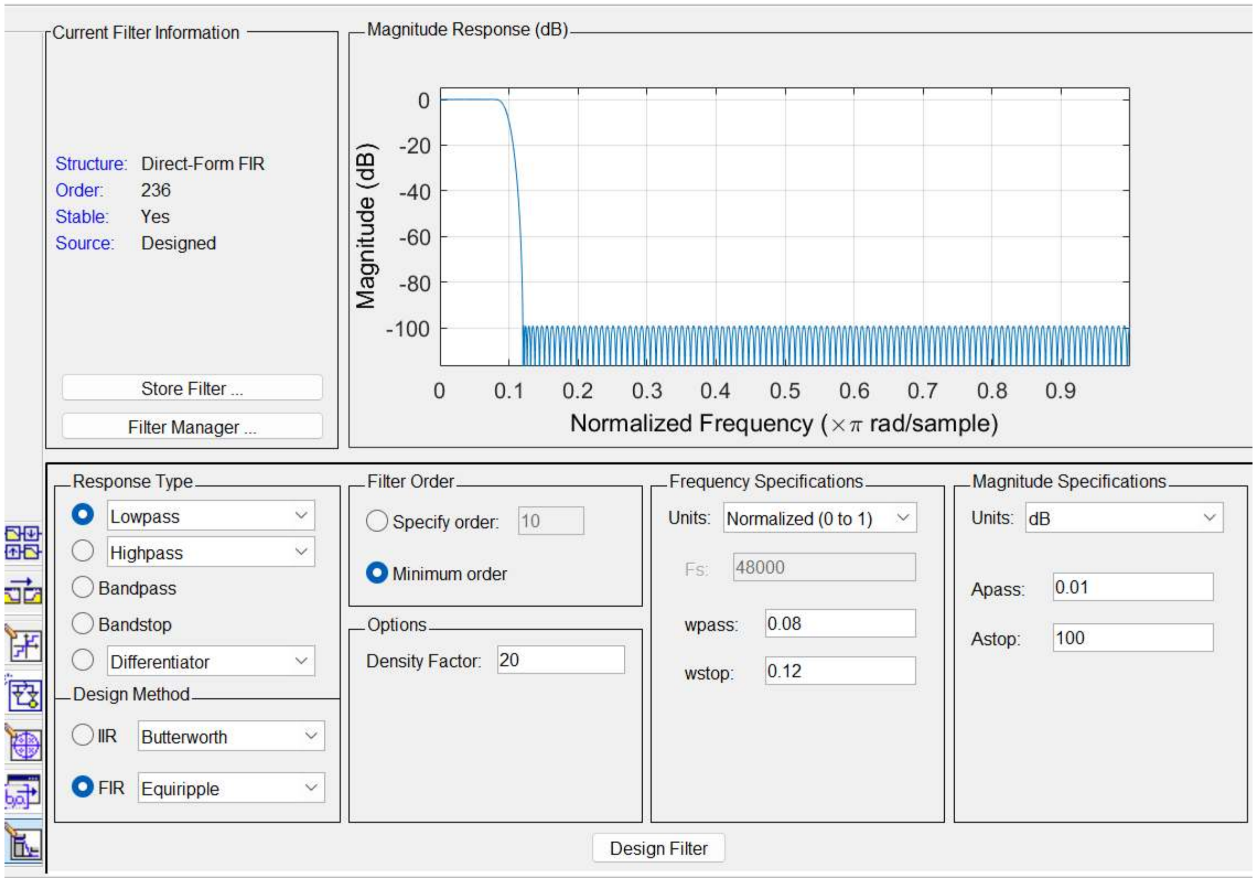

Figure 3.64. Magnitude Response of Digital Lowpass Filter

Conversion between the frequency and the normalized frequency can be done through the following formula;

$$\text{Normalized Frequency (in rad/sample)} = (f \times 2\pi) / \text{Sampling Frequency} \qquad (3.25)$$

In this design decimation is set to 30 for sampling the velocimeter output, resulting in sampling frequency to 1757 SPS (i.e. 52734/30 = 1757). After calculating the frequency using the new sampling frequency approximately filter has a cutoff frequency at 22 Hz and stopband frequency at 33 Hz. Since the interested signal is at 15 Hz this filter works very efficient for this application. Designed filter’s group delay (in samples) is shown below.

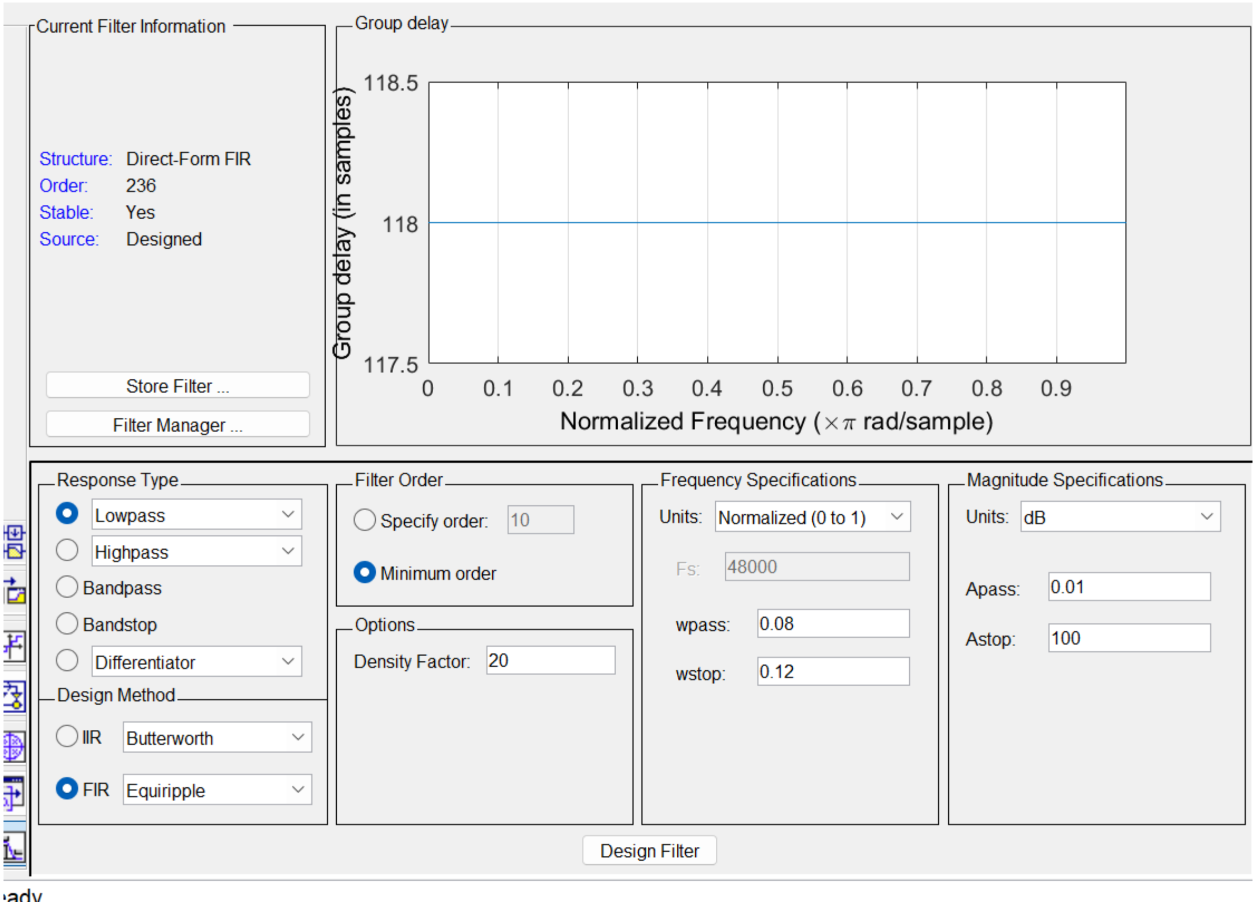

Figure 3.65. Group Delay of Digital Lowpass Filter

3.5.2. Regression methods

In this part of the thesis, another approach for estimating the vibration levels due to sampled vibration signals is described. Alternate to signal processing algorithms regression model-based approach had been implemented in MATLAB. In order to do so, lots measurements are taken from both constant vibration generator lab device and also from the helicopter. Afterwards, these measurements are used to train the regression models for estimating the vibration level and phase more accurate. The algorithms that predicts the vibration magnitude and phase better are Support Vector Machine (SVM), Decision Trees, Gaussian Process Regression and Ensemble Learning. Then, these models were compared according to evaluation metrics. The evaluation metrics that are used in this study are Mean Square Error (MSE), Root Mean Square Error (RMSE) and Mean Absolute Error (MAE).

3.5.2.1. Support vector machine (SVM)

Support Vector Machine is a machine learning algorithm and can be defined as set of related supervised learning methods. This algorithm is usually used for regression and classification. The advantages of SVM can be considered as training the algorithm is convenient because no local optimal. Also, SVM can be scaled for high dimensional data. SVM algorithms require good kernel function so this can be considered as disadvantage [23].

3.5.2.2. Decision trees

Decision tree learning is a machine learning algorithm that is in the type of supervised learning. In order to predict the outcome regression decision trees can be used as predictive models. Decision trees are used very commonly in machine learning application in order to predict the target value by using set of input data. the key feature of decision trees is a recursive segmentation of a target data field based on the values of related input fields or indicators to form divisions, along with related descendant data segments (referred to as leaves or nodes), that include progressively comparable intra-leaf objective values and gradually varying inter-leaf at specific level of the tree [24].

3.5.2.3. Gaussian process regression

Gaussian process is known as stochastic process in both probability and statistics theory meaning that variables that are collected or sampled randomly are indexed by time or space. In order to inference the best possible output from a given data set, Gaussian process regression model can be used as efficient algorithm. Gaussian process regression can be defined as non-parametric Bayesian approach meaning that by using a theoretically limitless number of parameters and allowing the data to determine the amount of complexity through the use of Bayesian inference, it may capture a wide range of links between inputs and outputs [25].

3.5.2.4. Ensemble learning

Ensemble learning method depends on using multiple learning algorithms in order to give better predictions. In simulation bagged trees approach was revealed as better performance. Bagging method can be considered as first ensemble learning method and it is reviewed as one of the simplest methods of ensemble learning methods. The technique employs bootstrapping or sampling with replacement method in order to use several versions of a training set. A distinct model is trained using each of these data sets. Aim is to produce a single output; the model outputs are aggregated by voting (for classification) or averaging (for regression) [26].

3.5.2.5. Mean square error (MSE)

Mean square error can be described as signals similarities or discrepancy/variations. Therefore, commonly one signal is assumed as original signal and the other assumed as distorted or noisy signal. Then the MSE of the signals can be define as follows;

$$MSE(x, y) = \frac{1}{N}\sum_{i=1}^{N}(x_i - y_i)^2 \tag{3.26}$$

Where x and y are two finite discrete signals with a sample size of N.

Generally, e_i is defined as error signal and equals to the subtraction of x and y signals.

$$e_i = x_i - y_i \tag{3.27}$$

Then, formula of the MSE becomes as follows [21];

$$MSE(x, y) = \frac{1}{N}\sum_{i=1}^{N}(e_i)^2 \tag{3.28}$$

3.5.2.6. Root mean square error (RMSE)

The idea behind the root mean square error is that it is the quadratic mean of error signal (i.e. e_i). By this methodology, accuracy of the model can be measured. The following formula express the RMSE,

$$RMSE = \sqrt{\frac{1}{N}\sum_{i=1}^{N}(x_i - y_i)^2} \ = \sqrt{\frac{1}{N}\sum_{i=1}^{N}(e_i)^2} \tag{3.29}$$

Where x and y are two finite discrete signals with a sample size of N and e_i is defined as error signal and equals to the subtraction of x and y signals [22].

$$e_i = x_i - y_i \tag{3.30}$$

3.5.2.7. Mean absolute error (MAE)

Similar to MSE and RMSE mean absolute error can be described as sum of absolute errors divided by sample size N. It is an alternative to MSE and RMSE and the formula for MAE is given below;

$$MAE(x, y) = \frac{1}{N}\sum_{i=1}^{N}|x_i - y_i| = \frac{1}{N}\sum_{i=1}^{N}|e_i| \tag{3.31}$$

Where x and y are two finite discrete signals with a sample size of N and e_i is defined as error signal and equals to the subtraction of x and y signals.

$$e_i = x_i - y_i \tag{3.32}$$

These defined evaluation metrics are used to compare the machine learning algorithms. Successful algorithms which are observed in “Regression Learner” MATLAB Module are; Support Vector Machine (SVM), Tree, Gaussian Process Regression, Ensemble and Kernel.

3.5.3. Programmable logic side

In this design PL side is used in the FPGA of analog input module. All of the configurations of ADS1278 are set by FPGA PL side and also for the communication, SPI protocol is used in PL side. SPI protocol is not written from scratch, an open-source SPI communication protocol is implemented in PL side in VHDL but in order to make compatible with ADS1278 SPI protocol and designed system communication requirements, a top module is written for SPI protocol in VHDL. This module basically getting commands from controller module’s SPI protocol from PS side and configuring the ICs on analog input module. Also, top module is managing the sampling start and stop commands. As mentioned before, 1024 size of data set are used for signal processing. Whenever start sampling command is raised by controller, top module of SPI protocol is managing the getting 1024 set of data and after that it raises a flag that sampling done and data is sent through the FIFO.

Between the top module of analog input module and controller module SPI, 24bit 1024 sized FIFO is used. Because ADS1278 is 24-bit ADC and every sampled data has a size of 24-bit. While sampling, written top module was getting data from ADS1278 and placing them in FIFO. After 1024 data is sampled by ADS1278 and placed in FIFO, it is ready for pulling by controller module and waiting for the command. Controls of commands and queries like data pull, FIFO empty, FIFO full, clear the FIFO or start sampling are given to controller module. Because eventually command chain is starting from host pc and according to those commands configuration and data collection is done by top module of analog input module and sampled data is sent back to controller module.

3.5.4. Processing Subsystem Side

In this design, PS side of the FPGAs is used in both analog input module and controller module. Since the AXI Quad SPI IP is implemented for the communication between the modules, both analog input module and controller module have AXI Quad SPI IP control on PS sides.

The algorithm for vibration signal measurement that is described in 3.5.1 Signal processing algorithms is implemented PS side of FPGA in controller module. Since the algorithm were developed in MATLAB environment, MATLAB coder module was used in order to convert MATLAB codes to C codes that can be compiled and run in ZYNQ 7015 PS side. Developing an algorithm in C environment is very challenging, in order to decrease the design duration due to easiness of debugging and simulations algorithm was developed in MATLAB environment than codes are converted into C language with the help of the MATLAB Coder tool.

After implementing the algorithm in PS side, ethernet IwIP echo server application is implemented in PS side. With the gigabit ethernet protocol commands and data between the host PC and DAQ system’s controller module is transferred. This embedded design part of the system is done by colleague of mine who works in the embedded design department. However, data structures, ICD (Interface Control Document) and command tree structures were decided together.

3.5.5. Experimental setup

3.5.5.1. Lab device studies

In this design, FFT is used for determining magnitude of the vibration level. In order to test the algorithm a device that can produce constant vibration is used. This device produces a vibration at 0.4 IPS (+/- 0.04 IPS), 275^o (+/- 15^o), and also velocimeter and magnetic pick-up can be mountable on the device in order to get vibration signal and the device rotating at 15 Hz meaning that vibration signal is expected at 15 Hz. Device is designed by Chadwik Helmuth but later company is acquired by Honeywell. The mounting positions of the sensors are given in Figure 4.67. Representative image of the device is given below;

Figure 3.66. Constant Vibration Generator

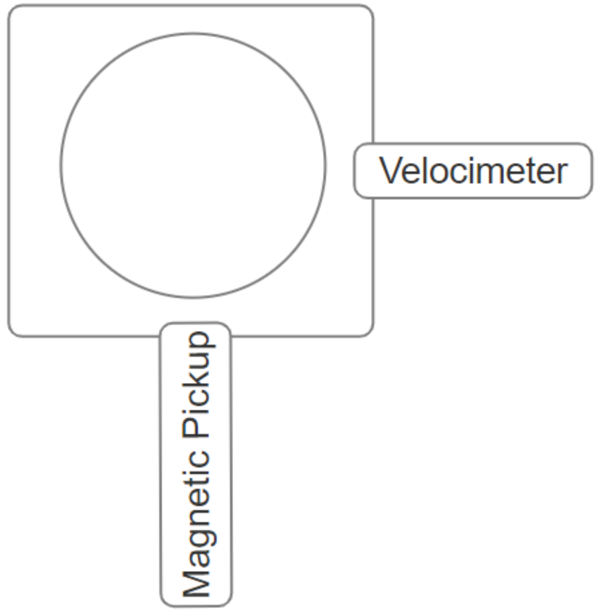

Figure 3.67. Top View Constant Vibration Generator

For FFT calculations size of 1024 (N=1024) time series samples are used. Since the ADC's sample rate is 52.734 kSPS and the used lab device is generating vibration signal at 15Hz, 52.734 kSPS is unnecessary. Therefore, decimation technique is used for simplify the calculations. After the decimation 1024-point FFT is performed in MATLAB. The plotted raw data of the vibration signal of test device is given below;

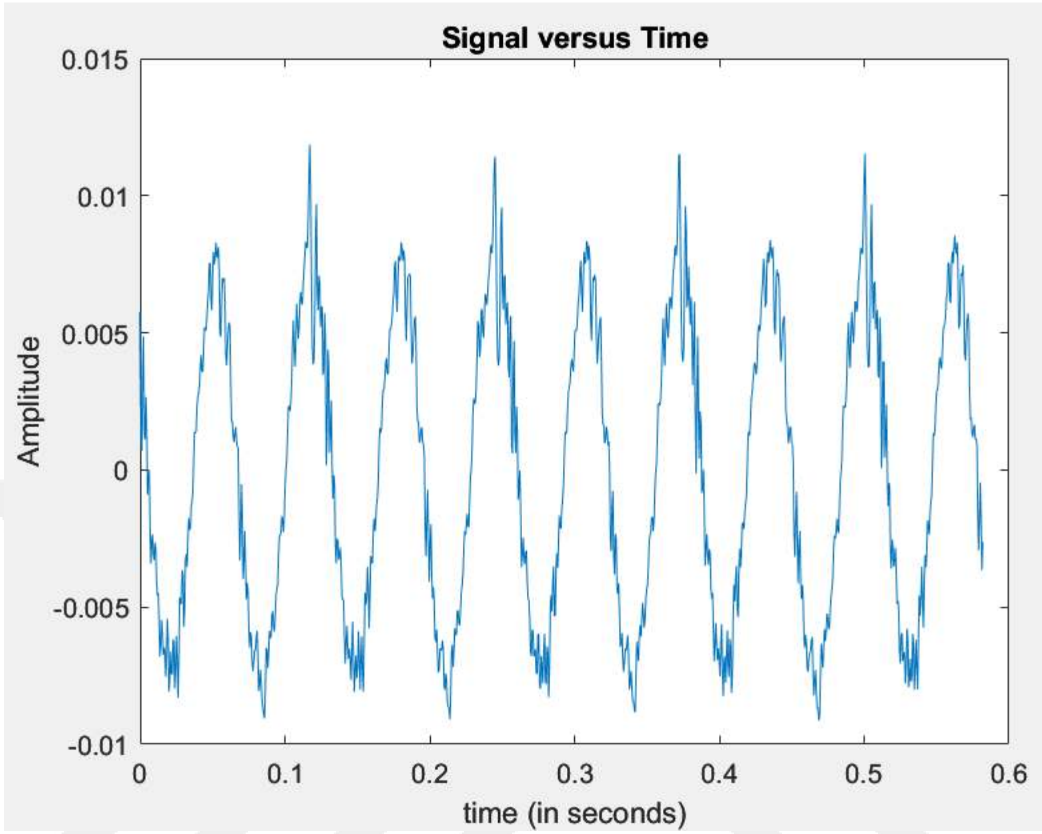

Figure 3.68. Raw Data of the Vibration Signal

After taking FFT of the raw data, vibration signal in frequency domain can be seen as follows;

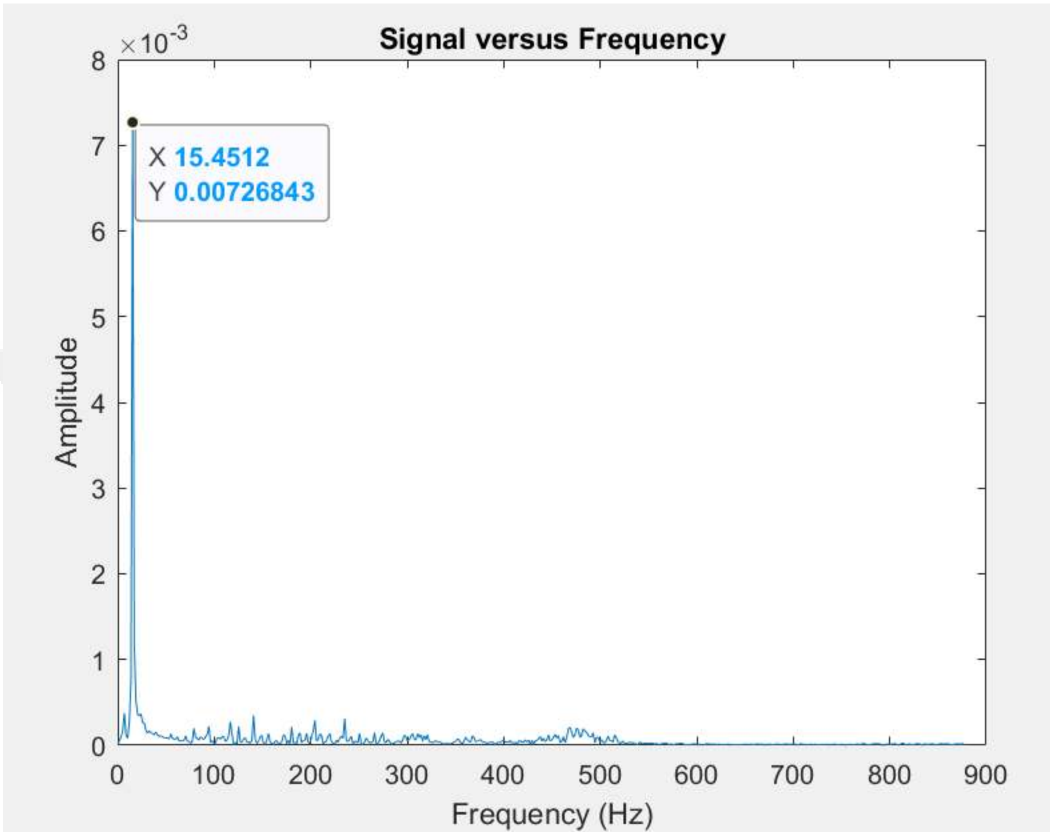

Figure 3.69. Vibration Signal in Frequency Domain

As mentioned before, after taking FFT of the signal, peak is detected at 15 Hz as expected with a magnitude of 7.26843 mV. Since 19 mV is equal to 1 IPS then 7.26843 mV / 19 mv = 0.3825 IPS. This also shows that both the measurement and the calculation of the vibration level consistent because these studies are done due to constant vibration producer device.

After applying the lowpass filter to the raw velocimeter signal, filtered signal is given below figure. As one can see, filtered vibration signal is almost pure sinusoid, after removing the noisy components of the signal.

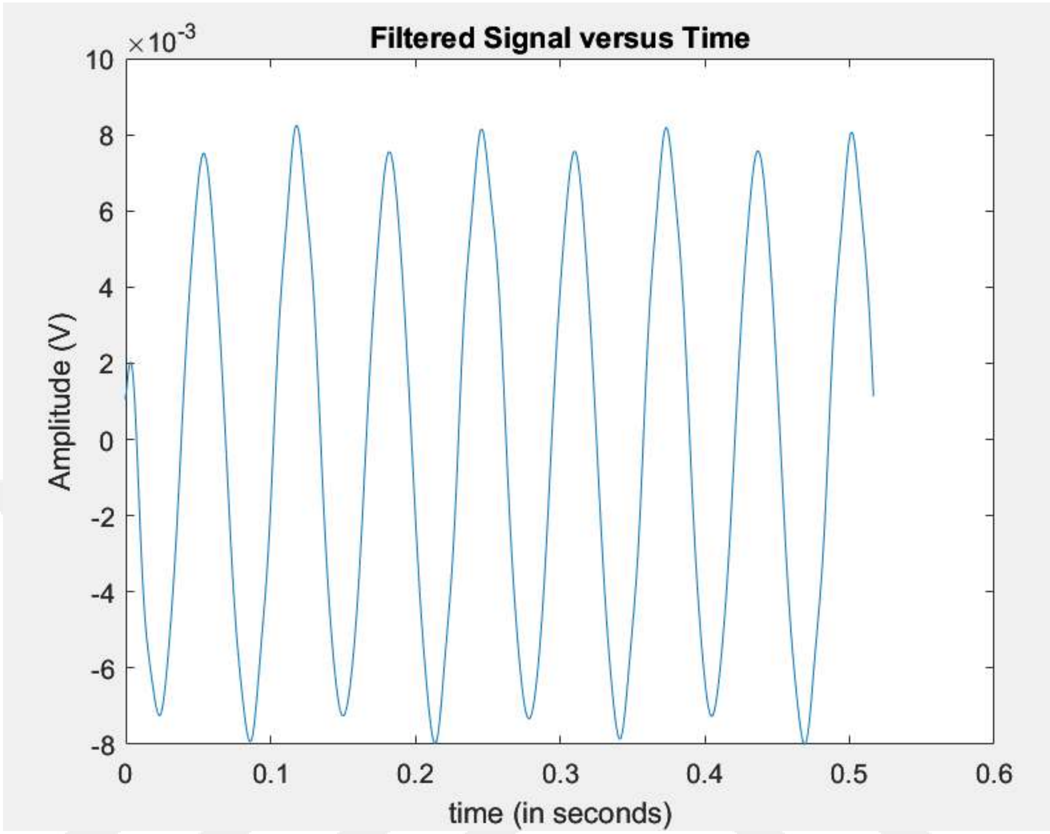

Figure 3.70. Filtered Signal

After getting the filtered data, phase of the vibration signal can be calculated. Group delay of digital low pass filter, group delay of ADC because sigma-delta ADC also have embedded digital filter in it and also phase response of anti-aliasing analog filter are taking into account, the phase of the vibration signal with respect to magnetic pick-up sensor can be calculated.

When calculating the phase of vibration signal, time domain filtered signal sampled with respect to peak value of the magnetic pick-up sensor is used. Due to this triggered sampling technique, converting first peak of vibration signal's time value to phase in terms of degrees, one can get the phase of the vibration signal.

3.5.5.2. Helicopter studies

After verifying the algorithm with laboratory set up, measurements on helicopter had been made. Of course, the digital filter had gone through few modifications with respect to change of the vibration frequency. However, as it can be seen from the below figure, raw velocimeter data on helicopter is noisier than the laboratory set up as expected due to noisy nature of aircraft both mechanically and electronically.

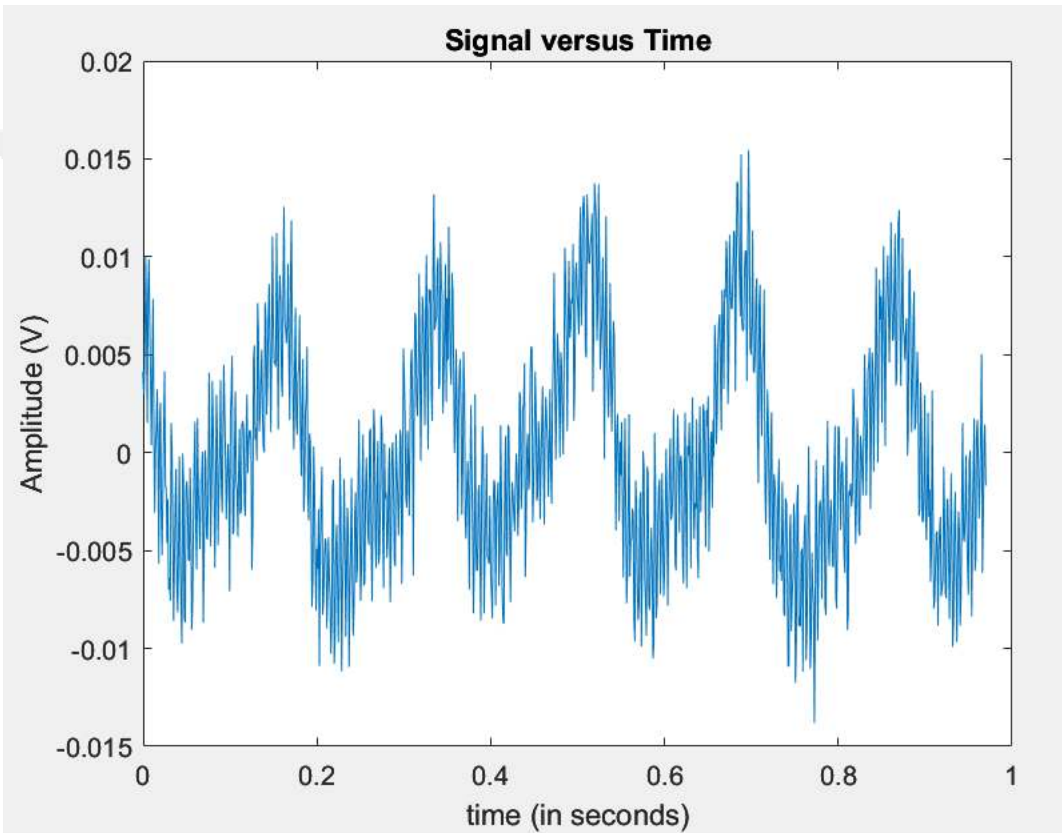

Figure 3.71. Velocimeter Raw Data Taken from Helicopter

Since the subject aircraft for the study has a constant 324 RPM main rotor blade rotation speed meaning that 5.4 Hz frequency, the filter characteristics have been changed according to the application. For the causation of the noisy environment, bandpass filter with very sharped and narrowed bandwidth had been designed with cutoff frequencies at 5.2 Hz and 6 Hz. Moreover, band-stop frequencies of the filter had been set to 3 and 10 respectively. The magnitude response of the designed filter is shown below.

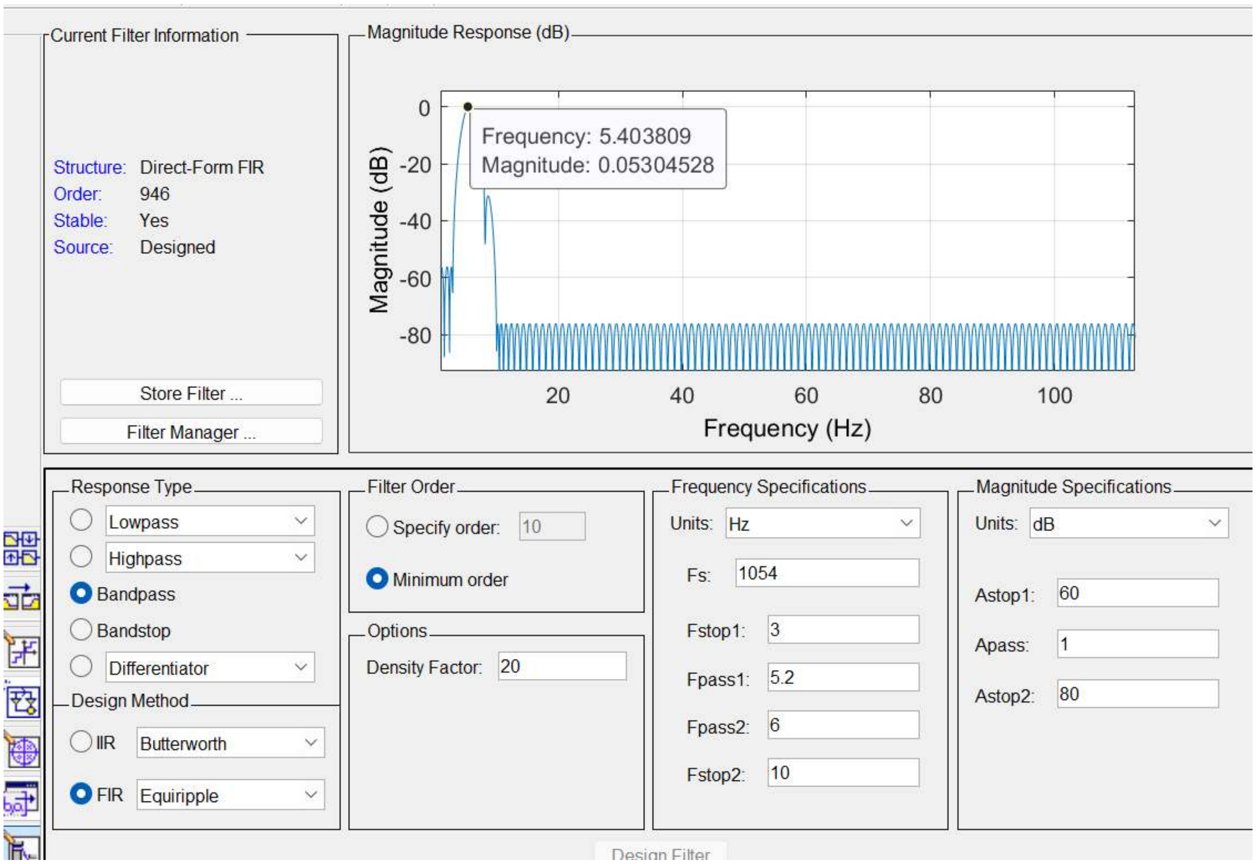

Figure 3.72. Designed Digital Bandpass Filter for Helicopter

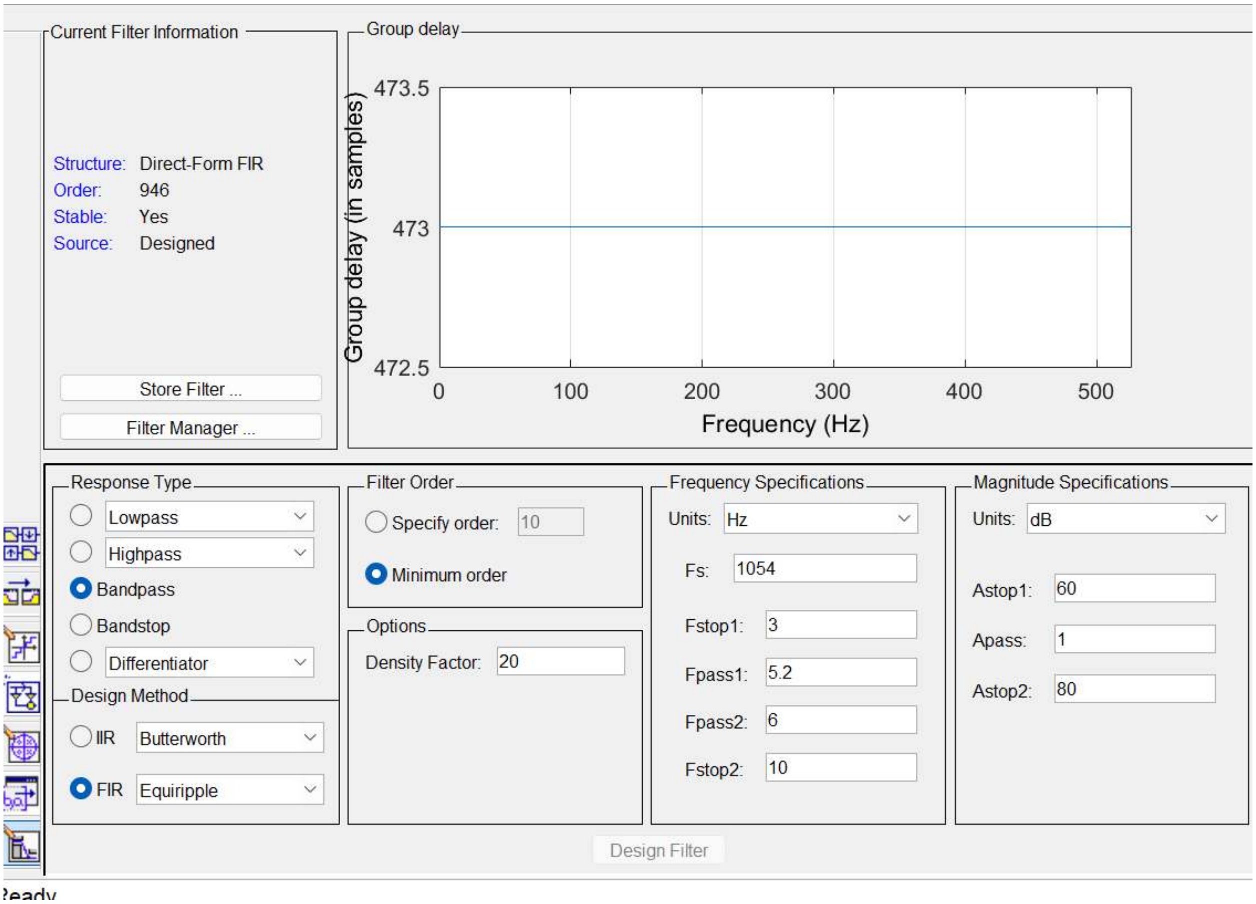

Figure 3.73. Group Delay of Digital Filter for Helicopter

As the sharpness increases and the bandwidth decreases, the order of the filter is increasing as expected. Due to these specifications group delay is increases. After applying the new filter for the raw data of the velocimeter which is taken from the aircraft, the filtered signal becomes as follows.

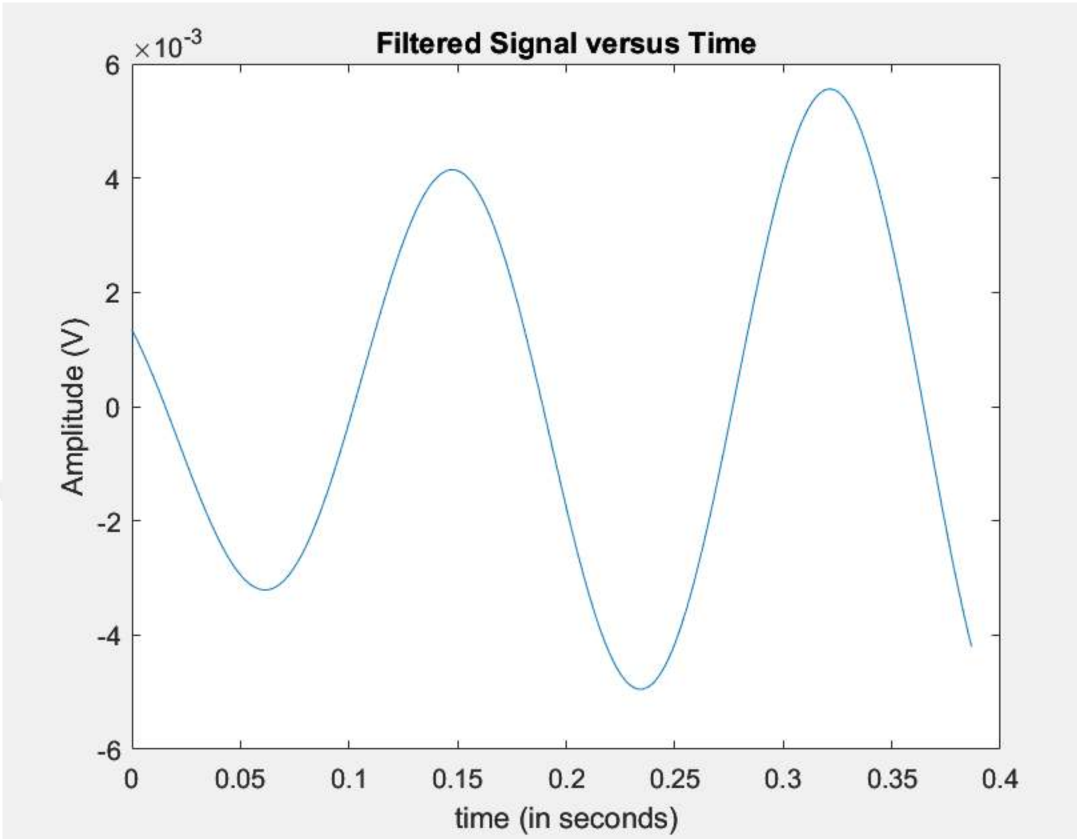

Figure 3.74. Filtered Vibration Signal of Helicopter

The vibration magnitude of aircraft is identical with the laboratory study, taking FFT of the signal shows a peak at the 324 RPM or 5.4 Hz. Result of the FFT calculation of aircraft velocimeter can be seen below. As a result, vibration magnitude is measured as approximately 0.2 IPS.

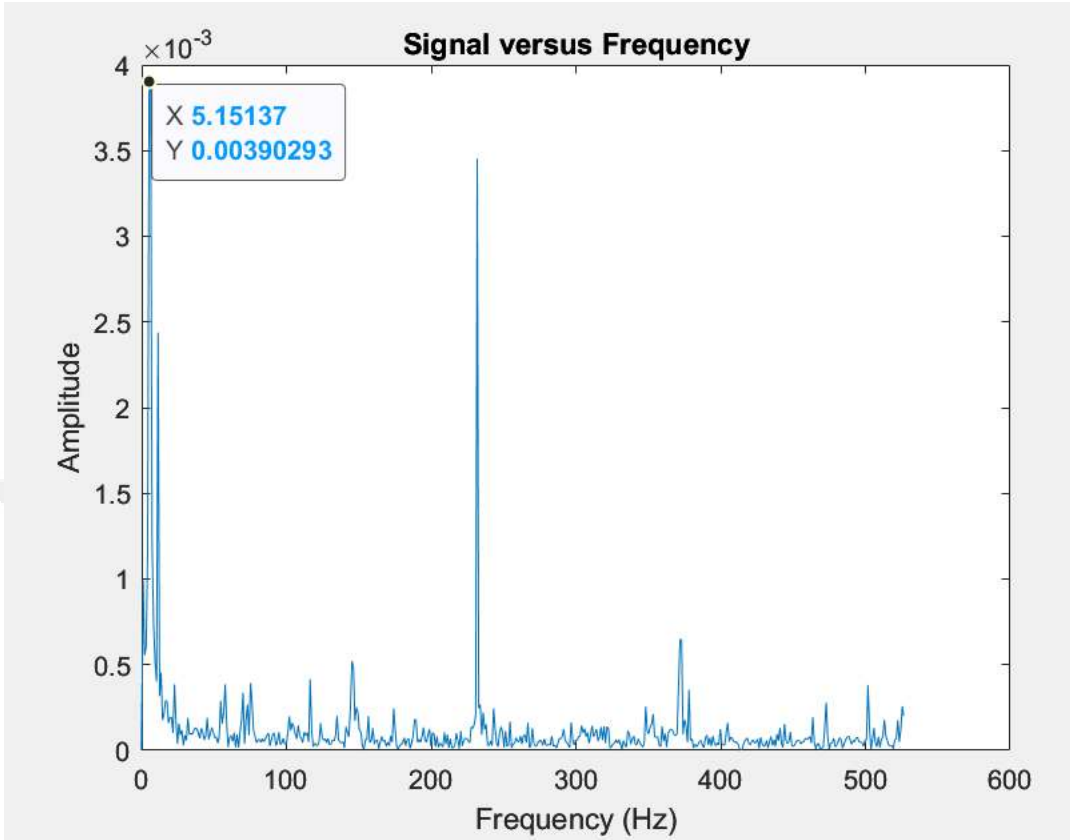

Figure 3.75. FFT Plot of Aircraft Measurement

Of course, both in laboratory environment and in aircraft lots of measurements are taken. Comparison of these measurements and methods will be reviewed Discussion and Result topic.

4. DISCUSSION AND RESULTS

4.1. Result of Signal Processing Algorithms

4.1.1. Case 1: Result of lab device studies

Within the scope of this thesis, an FTI system is designed for vibration signal measurement on helicopters. Then a signal processing algorithm is developed and implemented designed FPGA-based FTI system. The developed algorithm is verified by using constant vibration generator lab device. As it is mentioned before, the vibration generator lab device was producing constant 0,4 IPS (+/- 0.04 IPS) vibration at 275^o (+/- 15^o) phase angle. The measurements taken for verification from lab device is given below.

Table 4.1. Result of Vibration Signal of Lab Device

Number	Vibration Magnitude (in IPS)	Vibration Phase (in Degree)	Number	Vibration Magnitude (in IPS)	Vibration Phase (in Degree)
1	0.3896	278,09	28	0.3882	278,63
2	0.4038	278,22	29	0.3881	278,97
3	0.3825	270,12	30	0.3881	279,25
4	0.3827	270,38	31	0.3879	279,24
5	0.3827	270,47	32	0.3878	279,45
6	0.383	273,35	33	0.389	276,98
7	0.3827	270,47	34	0.3883	277,08
8	0.3838	270,20	35	0.3887	277,54
9	0.3837	270,83	36	0.3888	278,50
10	0.3836	272,35	37	0.3886	278,58
11	0.3841	273,05	38	0.3884	278,91
12	0.3836	277,27	39	0.3892	279,65
13	0.3846	268,86	40	0.3906	279,11
14	0.3843	269,98	41	0.39	277,60
15	0.3844	270,84	42	0.387	272,84
16	0.3852	271,47	43	0.3873	270,61

Table 4.2. Continues

17	0.3848	271,48	44	0.3847	273,48
18	0.3847	273,41	45	0.3866	273,41
19	0.3845	273,24	46	0.3864	272,47
20	0.3855	277,71	47	0.3018	286,00
21	0.3861	279,52	48	0.3899	273,11
22	0.3869	271,77	49	0.3893	271,77
23	0.3873	276,54	50	0.3893	279,53
24	0.3866	277,17	51	0.3872	270,29
25	0.3872	275,58	52	0.3902	278,58
26	0.3875	276,86	53	0.3851	272,76
27	0.3876	277,12	54	0.3893	276,86
55	0.3867	270,59	85	0.3844	273,51
56	0.3894	282,40	86	0.3891	277,15
57	0.3853	276,66	87	0.3855	272,88
58	0.3865	273,48	88	0.3874	277,87
59	0.3859	272,03	89	0.3908	273,36
60	0.3933	279,72	90	0.3897	278,36
61	0.3858	272,54	91	0.3862	273,39
62	0.3884	277,51	92	0.3887	277,97
63	0.3897	278,08	93	0.3837	270,50
64	0.3899	278,53	94	0.3866	273,49
65	0.3876	273,31	95	0.388	276,88
66	0.3906	278,38	96	0.3861	270,69
67	0.3895	278,67	97	0.39	277,08
68	0.3895	282,87	98	0.3852	272,35
69	0.3849	270,21	99	0.3849	269,80
70	0.3842	273,36	100	0.4352	288,63
71	0.3891	276,92	101	0.385	273,16
72	0.3884	278,09	102	0.3889	276,98
73	0.3891	278,74	103	0.3856	270,63
74	0.3893	277,85	104	0.389	279,55
75	0.3895	279,25	105	0.3821	269,13
76	0.3874	277,28	106	0.3815	269,27
77	0.3878	277,61	107	0.3824	269,47
78	0.3406	294,77	108	0.3825	270,41
79	0.3848	271,41	109	0.3828	272,15
80	0.3856	270,52	110	0.3842	269,76

Table 4.3. Continues

81	0.3883	276,84	111	0.3836	270,39
82	0.385	272,65	112	0.3835	270,92
83	0.3853	272,23	113	0.384	271,22
84	0.3851	273,31	114	0.3836	271,95
115	0.3832	272,56	125	0.387	276,54
116	0.3841	272,54	126	0.3871	277,31
117	0.3833	273,23	127	0.3872	279,40
118	0.3835	273,37	128	0.3881	276,34
119	0.3838	273,53	129	0.3875	278,16
120	0.3845	273,50	130	0.3875	279,03
121	0.3847	270,55	131	0.3879	279,05
122	0.3856	278,80	132	0.3879	279,05
123	0.3864	275,65	133	0.3879	279,05
124	0.387	276,19			

As it can be seen from table, all measurement results are in the range of lab device output which is in between 0,36 IPS – 0,44 IPS and 260^{o} – 290^{o}. After, designed system is verified by this method, vibration signals on helicopter would be obtained.

4.1.2. Case 2: Result of helicopter studies

Afterwards, designed FTI system was mounted to helicopter and vibration signal measurements are taken from helicopter. In order to verify the designed FTI system, another vibration analyzer device is used for control. Experiment was conducted as follows; firstly, designed FTI system was mounted to helicopter, then helicopter had been started to run on the ground at flight RPM. After the flight RPM reached by the helicopter engines, vibration measurements are taken through the velocimeter sensors and vibration measurement results were logged for comparison. Afterwards, designed FTI system demounted from helicopter and COTS vibration analyzer device is mounted on helicopter in order to get the vibration measurements so that vibration measurements result would be compared. Measurements are taken for both horizontal and vertical vibrations. The result of the measurement and the comparison data of the COTS device is given in Table 5.2.

Table 4.4. Horizontal Vibration Measurement on Helicopter Taken from Designed FTI System

Number	Vibration Magnitude (in IPS)	Vibration Phase (in Degree)	Number	Vibration Magnitude (in IPS)	Vibration Phase (in Degree)
1	0.1603	217.51	8	0.1777	206.68
2	0.2	227.96	9	0.1763	217.72
3	0.1982	223.34	10	0.1882	225.58
4	0.1924	238.27	11	0.1355	242.95
5	0.1664	234.99	12	0.1469	239.12
6	0.2271	223.45	13	0.1582	222.11
7	0.1699	204.6	14	0.1602	240.21

Table 4.5. Horizontal Vibration Measurement Taken from COTS Device

Number	IPS	Phase
1	0.202	260
2	0.257	246

As it can be seen from the tables, both IPS and phase values of the horizontal vibration measurements of both device is very close. Measurement results of each device was not expected to be exactly same because vibration of the helicopter may vary due to whether condition. The following tables shows the vertical vibration measurement results. As it can be seen from the tables, both IPS and the Phase measurements of the vibration signal is very close to COTS device measurements.

Table 4.6. Vertical Vibration Measurement Taken from Designed FTI System

Number of measurements	Vibration Magnitude (in IPS)	Vibration Phase (in Degree)
1	0.181	41.28
2	0.172	25.48
3	0.126	48.83
4	0.16	29.58
5	0.23	91.18
6	0.152	64.16
7	0.159	66.79
8	0.117	74.72
9	0.123	51.59
10	0.103	85.98
11	0.136	57.83
12	0.12	64.5

Table 4.7. Vertical Vibration Measurement Taken from COTS Device

Number of measurements	Vibration Magnitude (in IPS)	Vibration Phase (in Degree)
1	0.157	68.5
2	0.166	82.5

4.2. Result of Machine Learning Algorithms

4.2.1. Case 1: Result of lab device studies

In order to compare the results, regression models are trained with raw data of the measurements. In order to train the models, 100 different measurements are sampled from constant vibration generator lab device. After the training was completed, sampled 33 different raw data are given to models to predict the vibration magnitude and phase. The result of the study is given below;

Table 4.8. Vibration Magnitude Results of the Trained Models

Number	Signal Processing	Matern 5/2 Gaussian Process Regression	Squarred Exponential GPR	Rational Quadratic GPR	Linear SVM	Linear Regression	Fine Gaussian SVM
1	0.385	0.3845	0.3845	0.3845	0.3832	0.3846	0.3844
2	0.3889	0.3887	0.3887	0.3887	0.3878	0.3876	0.3875
3	0.3856	0.3853	0.3853	0.3853	0.3841	0.3865	0.3845
4	0.389	0.3915	0.3915	0.3915	0.3917	0.3935	0.3874
5	0.3821	0.3855	0.3855	0.3855	0.3844	0.3841	0.3862
6	0.3815	0.3838	0.3838	0.3838	0.3829	0.3851	0.3867
7	0.3824	0.3855	0.3855	0.3855	0.3846	0.3808	0.3869
8	0.3825	0.3842	0.3842	0.3842	0.3833	0.3847	0.3868
9	0.3828	0.3868	0.3868	0.3868	0.3859	0.3868	0.3867
10	0.3842	0.3862	0.3862	0.3862	0.3847	0.3814	0.3868
11	0.3836	0.387	0.387	0.387	0.387	0.3846	0.3871
12	0.3835	0.3869	0.3869	0.3869	0.3861	0.3836	0.3865
13	0.384	0.3862	0.3862	0.3862	0.3851	0.3873	0.3868
14	0.3836	0.3868	0.3868	0.3868	0.386	0.3843	0.3864
15	0.3832	0.3859	0.3859	0.3859	0.3851	0.3847	0.3865
16	0.3841	0.3865	0.3865	0.3865	0.3854	0.3859	0.3868
17	0.3833	0.3875	0.3875	0.3875	0.3872	0.383	0.3869
18	0.3835	0.3861	0.3861	0.3861	0.385	0.3825	0.3869
19	0.3838	0.3867	0.3867	0.3867	0.3868	0.3816	0.3871
20	0.3845	0.3871	0.3871	0.3871	0.3858	0.3844	0.3868
21	0.3847	0.3854	0.3854	0.3854	0.3847	0.3836	0.3868
22	0.3856	0.3888	0.3888	0.3888	0.3876	0.3878	0.3874
23	0.3864	0.3898	0.3898	0.3898	0.3891	0.3878	0.3873
24	0.387	0.3887	0.3887	0.3887	0.3865	0.3888	0.3874
25	0.387	0.3892	0.3892	0.3892	0.3888	0.3872	0.3872
26	0.3871	0.3899	0.3899	0.3899	0.3908	0.3916	0.3878
27	0.3872	0.3889	0.3889	0.3889	0.3888	0.3869	0.3872
28	0.3881	0.3889	0.3889	0.3889	0.3875	0.3862	0.3873
29	0.3875	0.3885	0.3885	0.3885	0.3865	0.3867	0.3872
30	0.3875	0.3898	0.3898	0.3898	0.3882	0.3893	0.3877
31	0.3879	0.3901	0.3901	0.3901	0.3906	0.3897	0.3871
32	0.3879	0.3892	0.3892	0.3892	0.3875	0.3886	0.3872
33	0.3879	0.3898	0.3898	0.3898	0.3885	0.3864	0.3876

Table 4.9. Vibration Phase Results of the Trained Models

Number	Signal Processing	Exponential GPR	Squarred Exponential GPR	Rational Quadratic GPR	Matern 5/2 GPR	Medium Gaussian SVM	Ensemble Bagged Trees
1	273.1626	272.0677	271.852	271.852	271.8612	271.764	272.1001
2	276.9804	277.5151	278.3383	278.3383	278.2952	277.8863	278.8763
3	270.6296	271.7011	272.1645	272.1645	272.1169	271.6672	271.8512
4	279.5511	278.2309	278.0468	278.0468	277.9674	277.3906	277.5973
5	269.127	272.3796	272.1127	272.1127	272.065	272.1133	272.437
6	269.2714	271.6013	271.5404	271.5404	271.4342	271.0748	272.1513
7	269.4738	272.1517	271.9159	271.9159	271.8817	272.6021	274.5612
8	270.4111	272.3632	272.1138	272.1138	272.0535	271.4984	272.3901
9	272.1517	271.542	271.5396	271.5396	271.3897	271.4003	272.733
10	269.757	271.58	271.2489	271.2489	271.1412	271.8384	275.1639
11	270.3909	273.965	272.9339	272.9339	273.1164	274.2403	273.1702
12	270.9227	272.3794	272.1907	272.1907	272.1342	272.4082	273.7117
13	271.2152	271.4306	271.5516	271.5516	271.4234	271.2122	272.3331
14	271.9548	272.0812	272.0657	272.0657	271.966	271.8728	273.1894
15	272.5551	272.5851	272.4425	272.4425	272.3676	271.8668	272.4999
16	272.5441	271.5523	271.6167	271.6167	271.4895	271.6144	275.6128
17	273.2305	273.0869	272.694	272.694	272.7381	273.3504	273.2266
18	273.366	271.5446	271.5873	271.5873	271.4499	271.3047	274.5405
19	273.5273	274.1208	273.3208	273.3208	273.509	274.1132	273.7253
20	273.5038	271.6582	271.9291	271.9291	271.7778	271.3329	272.9602
21	270.5502	272.1372	272.1967	272.1967	272.0716	271.5683	272.8956
22	278.7988	276.3216	276.8981	276.8981	276.76	276.8022	278.1854
23	275.6509	276.5094	276.7086	276.7086	276.5841	276.519	277.7963
24	276.1907	276.9878	277.2623	277.2623	277.2004	276.8702	277.544
25	276.5358	276.6504	276.4354	276.4354	276.3338	276.7422	277.7938
26	277.3118	277.3081	277.4066	277.4066	277.4863	277.1829	276.9551
27	279.401	278.6897	278.2429	278.2429	278.2821	277.7171	278.6084
28	276.338	277.1326	277.5101	277.5101	277.4423	276.8235	277.6751
29	278.163	277.4387	277.9638	277.9638	277.866	277.1947	277.5127
30	279.0325	277.3911	277.2941	277.2941	277.2402	277.2633	277.9593
31	279.0475	278.4451	277.6802	277.6802	277.7391	277.7758	278.6596
32	279.0475	277.3233	278.3911	278.3911	278.2703	276.9664	278.0281
33	279.0475	277.1234	276.9896	276.9896	276.9224	277.0225	277.8487

Results show that in both methods, both magnitude and the phase of the vibration signal can be detected very precisely when predicting the lab device vibration output with the trained lab device raw data. The success of the trained models according to evaluation metrics is given below;

Validation Evaluation (Magnitude)					
Evaluation Metrics	Matern 5/2 GPR	Squared Exponential GPR	Rational Quadratic GPR	Linear SVM	Linear Regression
MSE	0.000091023	0.000091317	0.000091317	0.00011073	0.0001239
RMSE	0.0095406	0.009556	0.009556	0.0099035	0.010523
MAE	0.0022806	0.0022829	0.0022829	0.0027837	0.0035314

Test Evaluation (Magnitude)						
Evaluation Metric	Matern 5/2 GPR	Squared Exponential GPR	Rational Quadratic GPR	Linear SVM	Linear Regression	Fine Gaussian SVM
MSE	6.2E-06	6.201E-06	6.201E-06	4.1215E-06	4.2433E-06	6.59E-06
RMSE	0.00249	0.0024901	0.0024901	0.00203015	0.00205994	0.002568
MAE	0.002267	0.0022667	0.0022667	0.00176061	0.00167576	0.002097

Validation Evaluation (Phase)						
Evaluation Metrics	Exponential GPR	Squared Exponential GPR	Rational Quadratic GPR	Matern 5/2 GPR	Medium Gaussian SVN	Ensemble Bagged Trees
MSE	5.7697	6.218	6.2212	6.3466	7.0809	8.857
RMSE	2.402	2.4936	2.4942	2.5192	2.661	2.9761
MAE	1.4447	1.5436	1.5442	1.5497	1.5642	1.902

Test Evaluation (Phase)						
Evaluation Metrics	Exponential GPR	Squared Exponential GPR	Rational Quadratic GPR	Matern 5/2 GPR	Medium Gaussian SVN	Ensemble Bagged Trees
MSE	2.41014802	2.111371234	2.111371234	2.135191	2.658506	4.203126
RMSE	1.55246514	1.453055826	1.453055826	1.461229	1.630493	2.050153
MAE	1.25531515	1.237181818	1.237181818	1.240564	1.348452	1.602258

Figure 4.1. MSE, RMSE and MAE of Trained Models Case 1

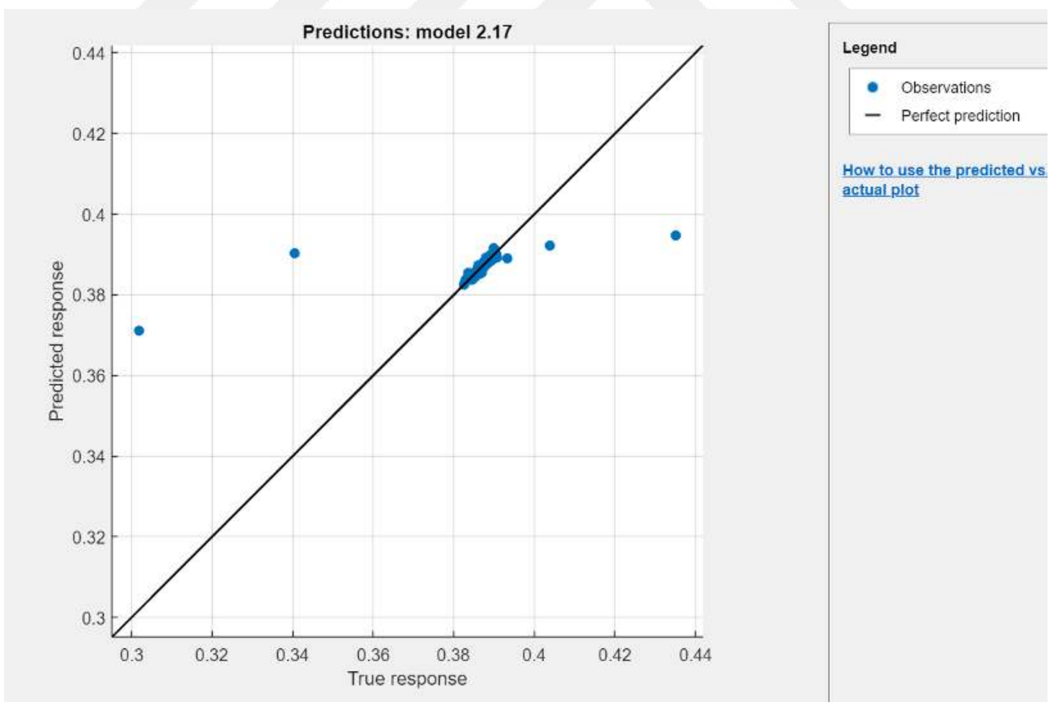

Figure 4.2. Predicted vs Actual Graph of Matern 5/2 GPR for the Trained Model of Magnitude Prediction

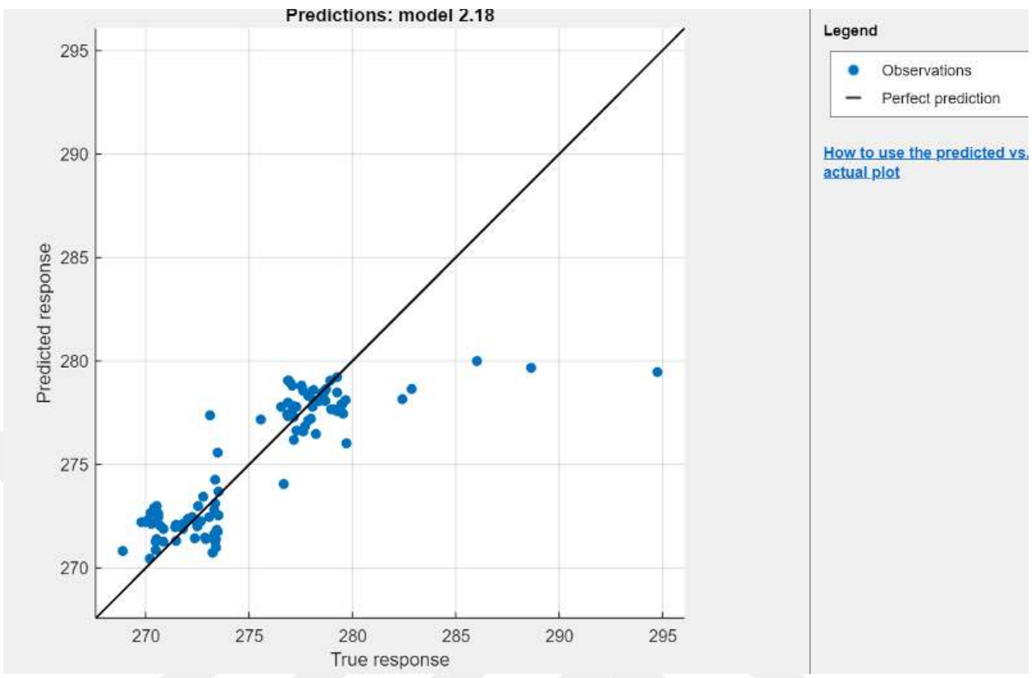

Figure 4.3. Predicted vs Actual Graph of Exponential GPR for the Trained Model of Phase Prediction

4.2.2. Case 2: Result of helicopter studies

4.2.2.1. Case 2.1: Predicting helicopter vibration data using the model trained with lab device data

The following study is done for predicting helicopter vibration data due to trained lab device data. As it can be seen from tables training with constant vibration generator data is insufficient for predicting the helicopter vibration values. This is due to lab device generating only 0,4 IPS (+/- %10) and 275^{o} (+/- 15^{o}) vibration signal and model is trained in that range.

Table 4.10. Helicopter Measurement Vibration Magnitude Results Due to Lab Device Data Training

Data Number	Signal Processing	Matern 5/2 Gaussian Process Regression	Squarred Exponential GPR	Rational Quadratic GPR	Linear SVM	Linear Regression	Fine Gaussian SVM
1	0.1603	0.335	0.3353	0.3353	0.352	0.2552	0.3871
2	0.2	0.3356	0.336	0.336	0.349	0.2121	0.3871
3	0.1982	0.331	0.3314	0.3314	0.342	0.2089	0.3871
4	0.1924	0.3395	0.3398	0.3398	0.351	0.2379	0.3871
5	0.1664	0.3463	0.3465	0.3465	0.362	0.2562	0.3871
6	0.2271	0.3332	0.3335	0.3335	0.347	0.1644	0.3871
7	0.1699	0.3287	0.3291	0.3291	0.344	0.288	0.3871
8	0.1777	0.3321	0.3325	0.3325	0.344	0.2225	0.3871
9	0.1763	0.3403	0.3406	0.3406	0.356	0.2126	0.3871
10	0.1882	0.3364	0.3368	0.3368	0.348	0.249	0.3871
11	0.1355	0.336	0.3363	0.3363	0.352	0.216	0.3871
12	0.1469	0.3397	0.34	0.34	0.354	0.268	0.3871
13	0.1582	0.3362	0.3365	0.3365	0.349	0.2841	0.3871
14	0.1602	0.3321	0.3325	0.3325	0.35	0.2422	0.3871

Table 4.11. Helicopter Measurement Vibration Phase Results Due to Lab Device Data Training

Data Number	Signal Processing	Exponential GPR	Squarred Exponential GPR	Rational Quadratic GPR	Matern 5/2 GPR	Medium Gaussian SVM	Ensemble Bagged Trees
1	217.51	281.5835	281.6043	281.6043	278.3061	279.0538	276.2309
2	227.96	281.7053	282.7767	282.7767	279.4892	279.0538	277.384
3	223.34	281.3627	282.1509	282.1509	278.862	279.0538	276.272
4	238.27	281.6442	283.5714	283.5714	280.6742	279.0538	277.7772
5	234.99	281.8797	283.7744	283.7744	280.9139	279.0538	276.8457
6	223.45	281.7704	283.6886	283.6886	280.4007	279.0538	277.7414
7	204.6	281.3327	281.8019	281.8019	277.9771	279.0538	276.0335
8	206.68	281.5704	282.9903	282.9903	279.9599	279.0538	277.2747
9	217.72	281.3713	282.4934	282.4934	278.7991	279.0538	276.9685
10	225.58	281.4698	283.5887	283.5887	279.9693	279.0538	277.5802
11	242.95	281.7613	282.5895	282.5895	279.4875	279.0538	276.876
12	239.12	281.8797	283.1841	283.1842	280.188	279.0538	277.1606
13	222.11	281.8278	283.2737	283.2737	280.3337	279.0538	276.2135
14	240.21	281.7427	283.0528	283.0528	279.5378	279.0538	275.5625

The success of the trained models according to evaluation metrics is given below;

Validation Evaluation (Magnitude)

Evaluation Metrics	Matern 5/2 GPR	Squared Exponential GPR	Rational Quadratic GPR	Linear SVM	Linear Regression
MSE	0.000091023	0.000091317	0.000091317	0.00011073	0.0001239
RMSE	0.0095406	0.009556	0.009556	0.0099035	0.010523
MAE	0.0022806	0.0022829	0.0022829	0.0027837	0.0035314

Test Evaluation (Magnitude)

Evaluation Metrics	Matern 5/2 Gaussian Process Regression	Squarred Exponential GPR	Rational Quadratic GPR	Linear SVM	Linear Regression	Fine Gaussian SVM
MSE	0.0263089	0.026415538	0.0264155	0.031071	0.0062873	0.045303
RMSE	0.1622002	0.162528576	0.1625286	0.176269	0.0792923	0.212845
MAE	0.1603429	0.160678571	0.1606786	0.174407	0.0614143	0.211579

Validation Evaluation (Phase)

Evaluation Metrics	Exponential GPR	Squared Exponential GPR	Rational Quadratic GPR	Matern 5/2 GPR	Medium Gaussian SVN	Ensemble Bagged Trees
MSE	5.7697	6.218	6.2212	6.3466	7.0809	8.857
RMSE	2.402	2.4936	2.4942	2.5192	2.661	2.9761
MAE	1.4447	1.5436	1.5442	1.5497	1.5642	1.902

Test Evaluation (Phase)

Evaluation Metrics	Exponential GPR	Squarred Exponential GPR	Rational Quadratic GPR	Matern 5/2 GPR	Medium Gaussian SVM	Ensemble Bagged Trees
MSE	3224.240385	3361.85227	3361.8529	2998.99	2946.515	2716.34
RMSE	56.78239503	57.9814821	57.981488	54.76303	54.281811	52.11852
MAE	55.60082143	56.8607643	56.860771	53.60061	53.0188	50.81648

Figure 4.4. MSE, RMSE and MAE of Trained Models Case 2.1

4.2.2.2. Case 2.2: Predicting helicopter vibration data using the model trained with both lab device and helicopter data

In order to improve the trained model, dataset for lab device is reduced to 50 and 19 more helicopter measurements are included to training data set. Therefore, training model is updated to 69 dataset including helicopter measurement data. Afterwards, new trained models are tried for predicting helicopter data. The following table shows the result of the study.

Table 4.12. Helicopter Measurement Vibration Magnitude Results Due to New Trained Model Including Helicopter Data

Data Number	Signal Processing	Rational Quadratic GPR	Squarred Exponential GPR	Exponential GPR	Matern 5/2 GPR	Linear SVM	Ensemble Bagged Trees
1	0.152	0.1538	0.1538	0.1764	0.1499	0.1373	0.1747
2	0.159	0.168	0.168	0.1781	0.1666	0.1635	0.1769
3	0.117	0.1543	0.1543	0.1713	0.1531	0.1538	0.1746
4	0.123	0.155	0.155	0.1697	0.1519	0.1491	0.1897
5	0.103	0.1684	0.1684	0.1776	0.1649	0.1557	0.1838
6	0.143	0.1269	0.1269	0.1581	0.125	0.1323	0.2023
7	0.136	0.1744	0.1744	0.1902	0.1717	0.1686	0.2017
8	0.12	0.1398	0.1398	0.1697	0.1368	0.1427	0.1861

Table 4.13. Helicopter Measurement Vibration Phase Results Due to New Trained Model Including Helicopter Data

Data Number	Signal Processing	Matern 5/2 GPR	Quadratic SVM	Squarred Exponential GPR	Rational Quadratic GPR	Linear SVM	Exponential GPR
1	64.16	96.0429	124.8237	111.7863	102.8103	130.571	83.7206
2	66.79	61.3822	77.4088	66.83	64.3869	57.4755	67.8963
3	74.72	52.1545	75.4194	53.5759	53.0118	65.2587	66.6897
4	51.59	81.443	112.0097	93.351	86.5453	120.824	81.9588
5	85.98	85.6498	124.7238	98.9884	91.4014	134.6506	84.3849
6	-2	65.4232	67.1214	68.0141	67.1388	78.8146	78.5903
7	57.83	120.4378	136.1189	135.2336	126.118	157.1943	97.8218
8	64.5	81.8943	120.9024	90.5852	85.7738	120.1917	84.845

The success of the trained models according to evaluation metrics is given below;

Validation Evaluation (Magnitude)						
Evaluation Metrics	Rational Quadratic GPR	Squarred Exponential GPR	Exponential GPR	Matern 5/2 GPR	Linear SVM	Ensemble Bagged Trees
MSE	0.00029517	0.00029517	0.0003564	0.00029696	0.00043016	0.00046417
RMSE	0.017181	0.017181	0.017233	0.018879	0.02074	0.021545
MAE	0.0075993	0.0075993	0.0088797	0.0076393	0.014697	0.010587

Test Evaluation (Magnitude)						
Evaluation Metrics	Rational Quadratic GPR	Squarred Exponential GPR	Exponential GPR	Matern 5/2 GPR	Linear SVM	Ensemble Bagged Trees
MSE	0.001112813	0.001112813	0.002161306	0.000989	0.000843	0.0034166
RMSE	0.033358844	0.033358844	0.046489851	0.03145	0.029029	0.0584521
MAE	0.027475	0.027475	0.0422625	0.025888	0.0251	0.0546

Validation Evaluation (Phase)						
Evaluation Metrics	Matern 5/2 GPR	Quadratic SVM	Squarred Exponential GPR	Rational Quadratic GPR	Linear SVM	Exponential GPR
MSE	181.41	190.06	193.07	197.97	237.02	237.45
RMSE	13.469	13.786	13.895	14.07	15.396	15.409
MAE	6.1723	6.2721	6.0433	6.2915	6.918	7.4175

Test Evaluation (Phase)						
Evaluation Metrics	Matern 5/2 GPR	Quadratic SVM	Squarred Exponential GPR	Rational Quadratic GPR	Linear SVM	Exponential GPR
MSE	1401.80778	2879.138161	2025.28347	1639.7663	3906.838	1235.14932
RMSE	37.4407235	53.65760114	45.0031496	40.494028	62.5047	35.1446913
MAE	29.6830875	46.8697625	37.1353375	32.729863	54.87025	25.198525

Figure 4.5. MSE, RMSE and MAE of Trained Models Case 2.2

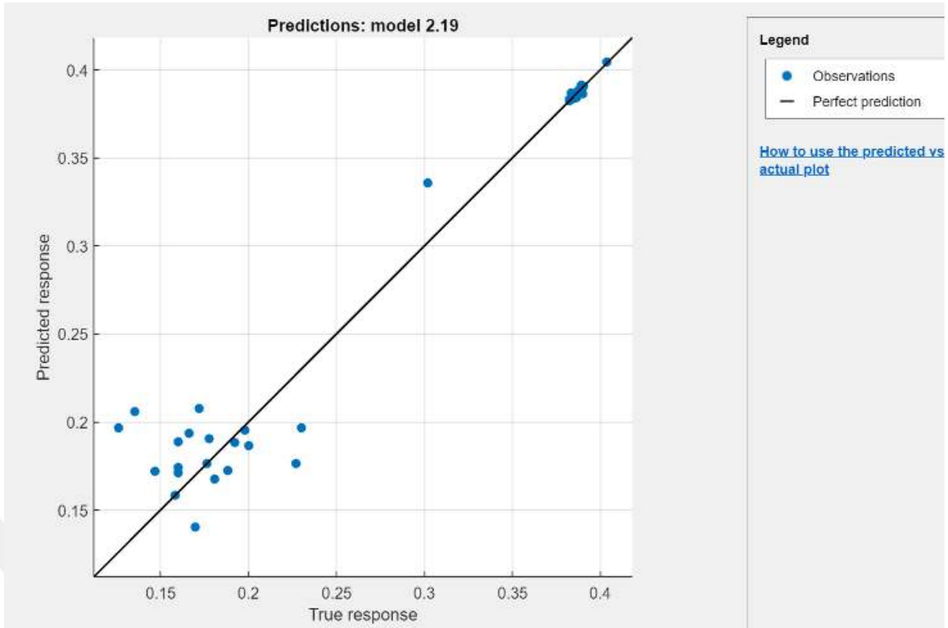

Figure 4.6. Predicted vs Actual Graph of Rational Quadratic GPR for the Trained Model of Magnitude Prediction

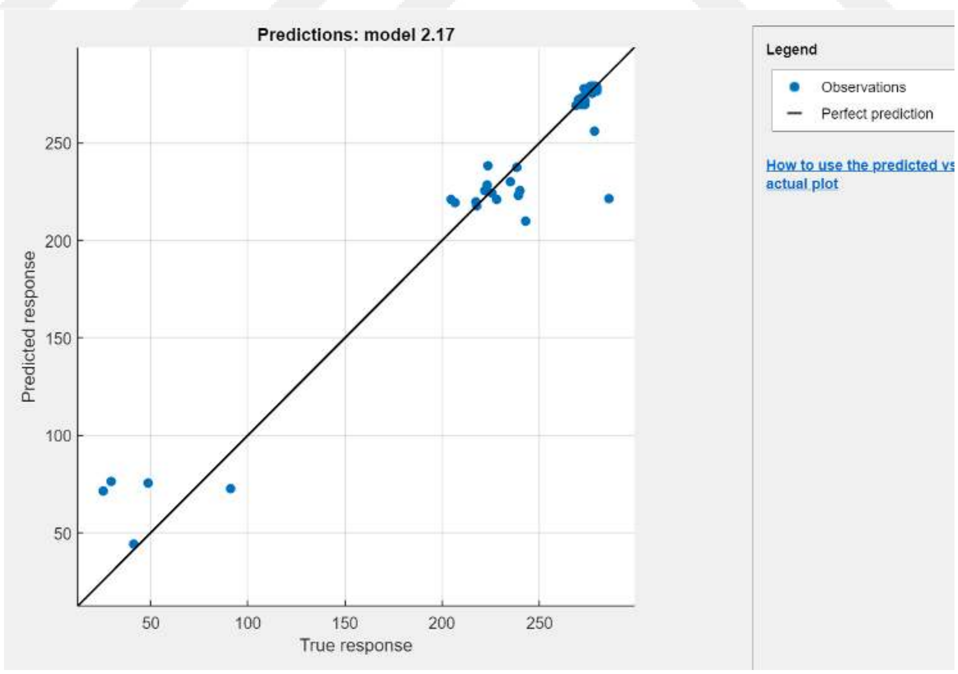

Figure 4.7. Predicted vs Actual Graph of Matern 5/2 GPR for the Trained Model of Phase Prediction

One may say that, when helicopter data is included in the training dataset, the results are improved respectively. However, the precision of the prediction still is not sufficient. In order to improve the model's precision dataset should be expanded with more helicopter vibration measurements.

The whole idea for detecting the vibration level of the system is to compensate it. In other words, eliminating the vibration out of the system. In rotating systems, vibration is caused by the tilt of the rotating system axis. This tilted axis occurs in helicopters blades when the reciprocal blade weights are mismatched. In order to get matched blade weights, balance charts are using for helicopters. This charts data is depending upon helicopter types and given by the helicopter manufacturers. Simply, charts guide technicians to decrease the vibration levels by telling to adding or removing weights to the blades, after vibration signal measurements are done. The measured vibration data are placed into balance chart graphs according to the IPS and the phase value. After the placement is done, chart axis guides technician for modification of the weight of the blade. Representative figure of helicopter balance chart is given below;

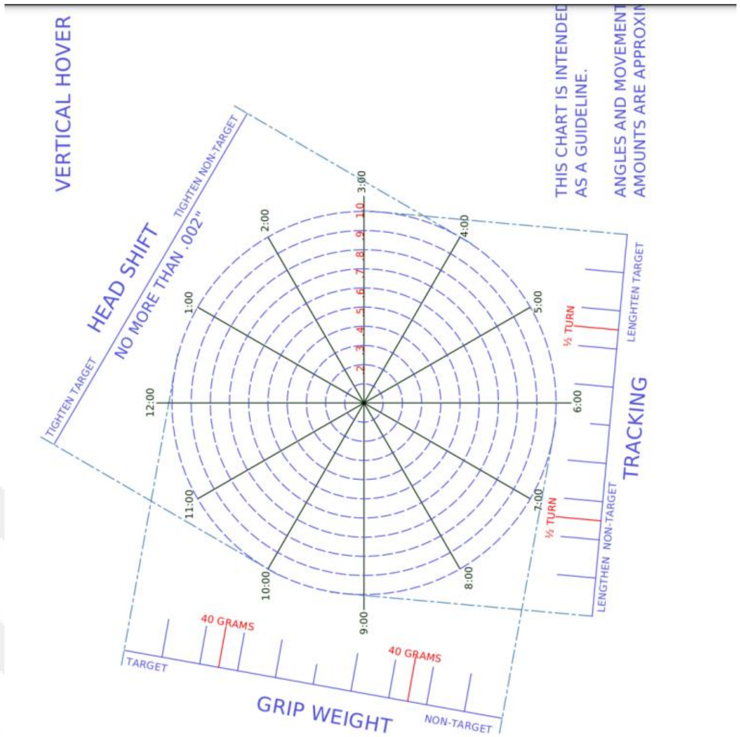

Figure 4.8. Balance Chart of a Helicopter

Finally, the comparison of several specifications between the designed FTI system and the COTS device that is used in the experimental set up is given below. After that, final designed is given figure 5.9 and 5.10.

Table 4.14. Specification Comparision Between COTS device and Designed FTI System

	Designed FTI System	COTS Device
Dimensions	25 x 10.5 x 11 cm	27.4 x 19.1 x 10.2 cm
Weight	2.275 kg	3.22 kg
Frequency Range	2 Hz - 10 kHz	3.33 Hz - 10 kHz
Memory	8GB internal, 512 GB on User PC	2 MB SRAM, 1 MB Flash EPROM
Channel	24 Channels and Extensible	36 Channels
Power Range	18-40 VDC (28 VDC Nominal)	12-28 VDC (28 VDC Nominal)
Temperature Range	(-40°C to +85°C)	(-40°C to +55°C)

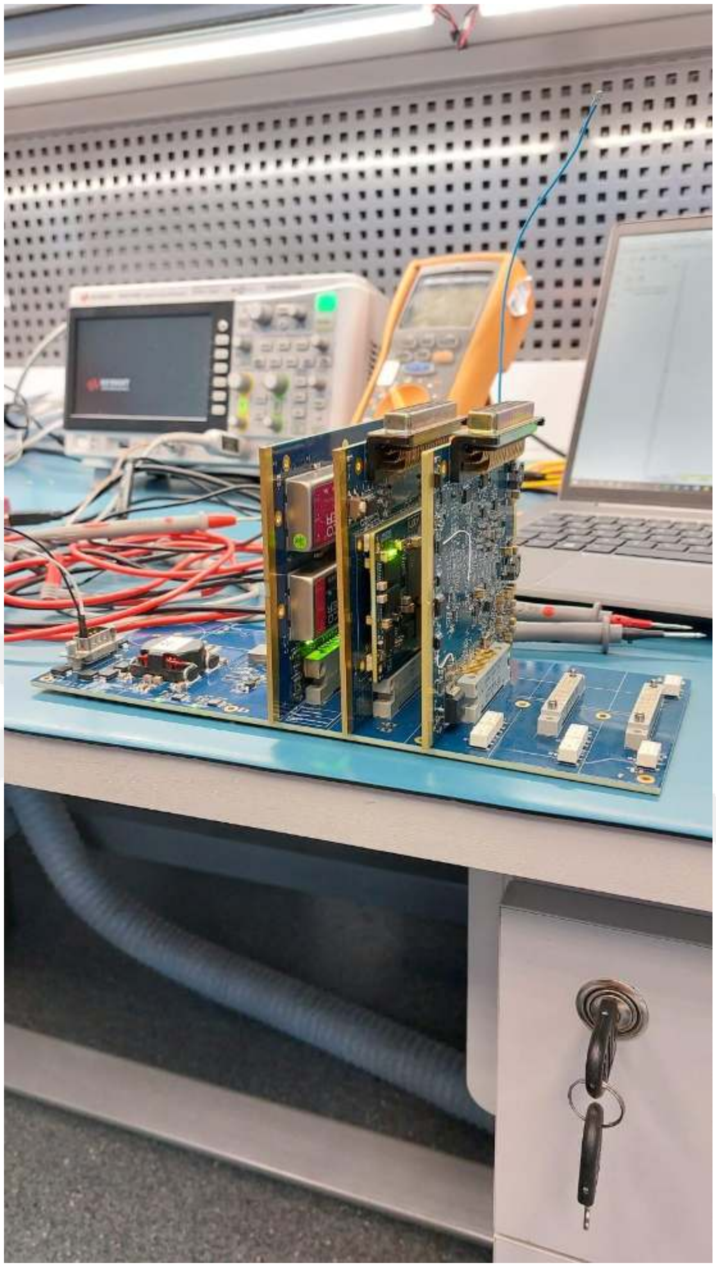

Figure 4.9. Designed FTI System

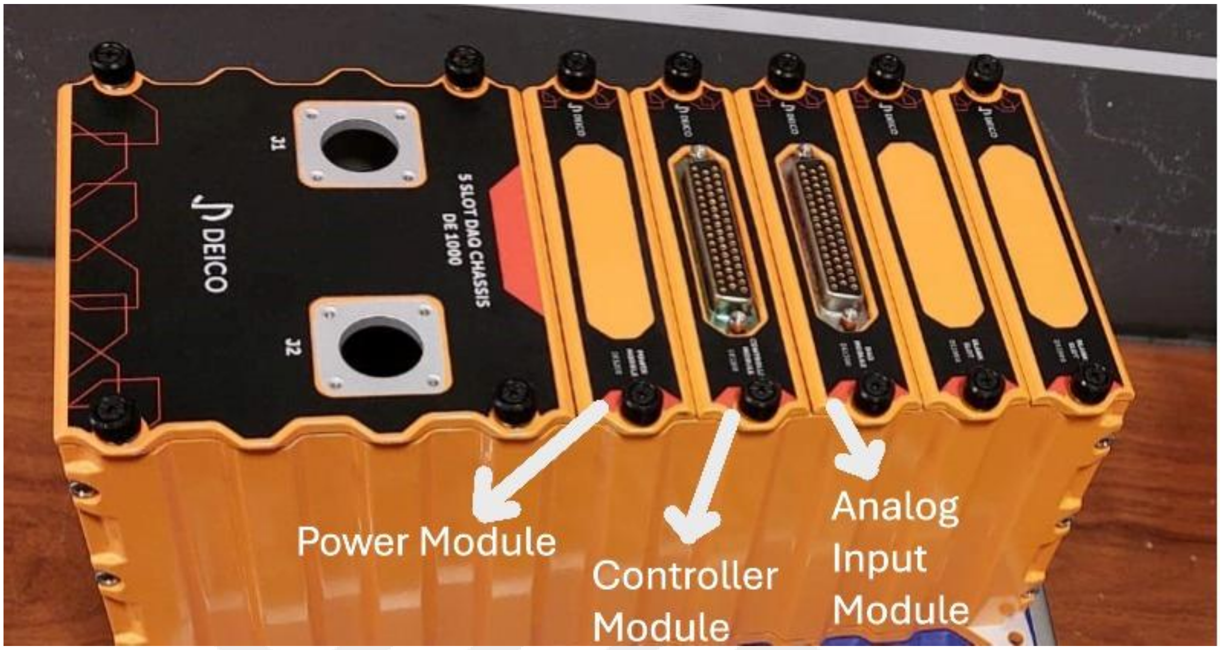

Figure 4.10. Designed FTI System Overview

5. CONCLUSION AND FUTURE WORK

Within the scope of this thesis, an FTI system is designed, the vibration signals are analyzed and the vibration level of helicopters is measured. The studies that are conducted in this context can be summarized as follows:

1) In order to design an FTI system, requirements are issued. In the light of derived requirements, an FTI system is designed that consists of modules which are a power module, controller module, analog input module and backplane module that combines all modules together.
2) A system architecture is designed for flight test instrument system to communicate analog input modules with controller module through SPI interface. Also, gigabit ethernet interface is implemented for communication with user PC. Finally, another SPI interface for used ADC and configuration modules for analog input modules is implemented in VHDL.
3) A signal processing algorithm was developed and implemented to design FTI system. In order to extract the vibration magnitude from the velocimeter measurements an FFT module is implemented to the algorithm. For the phase extraction, digital filters are designed and implemented for the noisy data. For the verification of the algorithm, a constant vibration generator device is used. After that, the algorithm and designed device are verified on a helicopter by using another COTS vibration analyzer device.
4) Regression models are trained for predicting vibration magnitude and phase values by using measurements of a constant vibration generator device. Afterwards, a trained model is used for predicting helicopter vibration data. However, the range of the trained data was limited due to constant vibration so the trained model was insufficient for predicting helicopter vibration values. In order to improve the model, helicopter measurements are included in the training dataset. Simulation results show that predictions are improved but still not very effective.

As a result, determining the vibration magnitude and phase of the helicopters with signal processing algorithms is conducted and the results of this study is promising. For the machine learning algorithms, conducted experiments show that in order to use the trained models in helicopter studies, the training datasets should be expanded with more velocimeter data that is sampled from helicopters.

For the future work, a designed FTI system can be included with different analog input modules for different types of sensors in order to monitor the different data types that are critical for the aircrafts. Because the designed system allows two more modules to implement. For the machine learning algorithms, more data should be collected from helicopters in order to improve the trained model's prediction success. Also, while models were training default values were used, in order to improve the success in future work parameters should be optimized for machine learning algorithms.

REFERENCES

[1] Donald R. Houser, "Vibration Signal Analysis Techniques" *Ohio State University* December 1973

[2] Biji Mathew, Prasun Banerjee, Muhammad Fawaz, "A Review on Vibration Analysis of Helicopter Rotor Blade," *International Journal for Research in Applied Science and Engineering Technology*, February 2022

[3] "What is Flight Test Instrumentation?" monroeaerospace.com. https://monroeaerospace.com/blog/what-is-flight-test-instrumentation/?srsltid=AfmBOopx0yarEqmqMshPY_kFrhcbay2a1Tk5bVZ7KNIJAgYAIyspCsJD (Accessed: Oct. 1, 2024)

[4] Curtiss-Wright. "Data Acquisition Systems." cutisswrightds.com https://www.curtisswrightds.com/products/flight-test/data-acquisition

[5] Mohamad Hazwan Mohd Ghazali, Wan Rahiman, "Vibration Analysis for Machine Monitoring and Diagnosis: A Systematic Review" Hindawi, *Shock and vibration*, Vol. 2021, doi: 10.1155/2021/9469318

[6] Donald R. Houser, "Vibration Signal Analysis Techniques" *Ohio State University* December 1973

[7] Jose de Jesus Rangel-Magdaleno, Rene de Jesus Romero-Troncoso, Roque Alfredo Osornio-Rios, Eduardo Cabal-Yepez, Aurelio Dominguez-Gonzalez, "FPGA-Based Vibration Analyzer for Continuous CNC Machinery Monitoring With Fused FFT-DWT Signal

Processing," *IEEE TRANSACTIONS ON INSTRUMENTATION AND MEASUREMENT*, vol. 59, no. 12, 2010

[8] Traco Power. "TEN20WIN Series, 20Watt." tracopower.com https://www.tracopower.com/ten20win-datasheet

[9] Andrew Matzik, Sohail Anwar, "Review of Electrical Filters," *International Journal of Innovative Science, Engineering & Technology*, Vol. 3 Issue 4, April 2016.

[10] Boyou Wang, "Signal Processing Based on Butterworth Filter: Properties, Design, and Applications," *Highlights in Science, Engineering and Technology*, vol. 97, 2024

[11] Boyou Wang, "Signal Processing Based on Butterworth Filter: Properties, Design, and Applications," *Highlights in Science, Engineering and Technology*, vol. 97, 2024

[12] Analog Devices. "Analog Filter Wizard." Analog.com https://tools.analog.com/en/filterwizard/

[13] Mahesh S. Chavan, Ra.Agarwala, M.D.Uplane, "Comparative Study of Chebyshev I and Chebyshev II Filter used For Noise Reduction in ECG Signal," *International Journal of circuits, Systems and Signal Processing*, Issue 1, Volume 2, 2008

[14] Khaled Younis, "Analogue Filter Design," in *Continuous Signals and Systems with MATLAB*, Boca Raton, FL, USA: Taylor & Francis Group, LLC, 2008

[15] Alan V. Oppenheim, Alan S. Willsky, S. Hamid Nawab, "Signals and Systems," 2nd ed. Upper Saddle River, New Jersey, USA: Prentice Hall, 1983

[16] Alan V. Oppenheim, Alan S. Willsky, S. Hamid Nawab, "Signals and Systems," 2nd ed. Upper Saddle River, New Jersey, USA: Prentice Hall, 1983

[17] Walt Kester. (2005). Which ADC Architecture Is Right for Your Application? Presented at analog.com [Online]. Available: https://www.analog.com/en/resources/analog-dialogue/articles/the-right-adc-architecture.html

[18] Texas Instruments. "Quad/Octal, Simultaneous Sampling, 24-Bit Analog-to-Digital Converters." ti.com https://www.ti.com/lit/ds/symlink/ads1274.pdf?ts=1737971409427&ref_url=https%253A%252F%252Fwww.google.com%252F

[19] AMD, Sunnyvale, CA, USA. DS190. (2018). Available: https://docs.amd.com/v/u/en-US/ds190-Zynq-7000-Overview

[20] Ivan W., "The Discrete Fourier Transform," in T*he Transform and Data Compression Handbook*, Boca Raton, CRC Press LLC, 2001.

[21] Zhou Wang, Alan C. Bovik, "Mean Squared Error: Love It or Leave It?," *IEEE SIGNAL PROCESSING MAGAZINE*, vol. 98, JANUARY 2009.

[22] Dulakshi Santhusitha Kumari Karunasingha, "Root mean square error or mean absolute error? Use their ratio as well," *Information Sciences*, vol. 585, March 2022.

[23] V. Jakkula, "Tutorial on Support Vector Machine (SVM)," School of EECS, Washington State University, Pullman, vol. 37, 2006.

[24] Barry de Ville, "Decision trees," *Wiley Periodicals*, Inc., vol. 5, December 2013.

[25] E. Schultz, M. Speekenbrink, A. Krause, "A tutorial on Gaussian process regression: Modelling, exploring, and exploiting functions," *Journal of Mathematical Psychology*, vol. 85, August 2018.

[26] M. Sewell, "Ensemble Learning," *UCL DEPARTMENT OF COMPUTER SCIENCE*, January 2011.